

Subcritical Water-Assisted Fractionation of Lupin Hull for Production of Cellulose Nanofiber  
Hydrogels and Aerogels

by

Deniz Ciftci

A thesis submitted in partial fulfillment of the requirements for the degree of

Doctor of Philosophy  
in  
Bioresource and Food Engineering

Department of Agricultural, Food and Nutritional Science  
University of Alberta

© Deniz Ciftci, 2017

## Abstract

In recent years, there has been a growing interest in transitioning to a bio-based economy by replacing petroleum-based products due to multiple drivers, such as growing environmental concerns, consumer demand, and the need for minimization of hazardous waste. Lignocellulosic biomass, composed of mainly cellulose, hemicellulose and lignin, has a major role in this transition, owing to its renewability, biodegradability and abundance to obtain high-value bio-based products, such as cellulose nanofibers, hydrogels and aerogels. Subcritical water technology is a promising alternative to be employed for biomass processing to minimize the use of hazardous chemicals and waste production. The objective of this thesis was to employ subcritical water technology in the enrichment of cellulose from lupin hull, a legume byproduct of the agri-food industry, and then convert the obtained cellulose to nanofiber, and form cellulose nanofiber hydrogels and aerogels by supercritical CO<sub>2</sub> (SCCO<sub>2</sub>) drying.

Non-cellulosic fractions of the lupin hull, namely, hemicellulose and lignin, were removed with subcritical water treatment, and the effects of process parameters (pressure: 50-200 bar, temperature: 160-220 °C, flow rate: 2-10 mL/min, and pH: 2-12) on lupin hull fractionation were investigated. At the optimized conditions (180 °C, 50 bar, 5 mL/min, and pH 6.2 within 40 min) for maximum hemicellulose sugar yield (85.5%) removed in the extract, a cellulose enriched residue (~80% cellulose) with increased crystallinity and thermal stability was obtained.

To compare with the traditional methods used, a combination of sodium hydroxide (NaOH) treatment (5-20%, 25-75 °C and 2-10 h) followed by acidified sodium chlorite (ASC) treatment (1.7%, 75 °C for 2-6 h) was investigated for the fractionation of lupin hull, and the treatment efficiencies were compared with those of subcritical water for the isolation of cellulose fibers. The effect of lignin content on the treatment efficiency was also examined by processing canola straw, a high-lignin biomass, in addition to lupin hull. The amount of non-cellulosics removal was higher for lupin hull (~90%) than that of canola straw (~80%) at the conditions of 15% NaOH/99 °C/6 h followed by 6 h ASC treatment, indicating that low lignin content favors the biomass fractionation. The subcritical water treatment was as efficient as the optimized NaOH treatment (15% NaOH/99 °C/4 h) that yielded a cellulose-enriched lupin hull residue of ~80% cellulose. Therefore, NaOH treatment was replaced with subcritical water treatment in the subsequent process to obtain cellulose nanofibers to reduce the use of chemicals.

Subcritical water-treated cellulose-enriched residue obtained at the optimized conditions was further purified with an ASC treatment, and then the resultant purified cellulose was fibrillated with ultrasonic treatments at varying amplitudes (20-80%) for 15-35 min to obtain cellulose nanofibers. Increasing ultrasonication amplitude and time resulted in enhanced fibrillation, with the smallest average nanofiber diameter of 15 nm at 80% amplitude and 35 min ultrasonication time.

Rheological characterization of the aqueous suspensions of cellulose nanofibers obtained by ultrasonication was conducted in the concentration range of 0.1-1.9 wt.%. All suspensions, except at 0.1 wt.% concentration, formed hydrogels. Regardless of the concentration, all samples showed a typical shear-thinning behavior. Increasing concentration of the suspension resulted in hydrogels with an increase in the dynamic moduli, forming a stronger gel network due to highly entangled structures.

Finally, highly porous (96.6-99.4% porosity) and lightweight (0.009-0.05 g/cm<sup>3</sup> density) cellulose nanofiber aerogels were formed from hydrogels with 1-2 wt.% concentration using SCCO<sub>2</sub> drying and freeze drying methods. The resulting cellulose nanofiber aerogels with the highest specific surface area of 115 m<sup>2</sup>/g, the highest porosity of 99.4% and the lowest density of 0.009 g/cm<sup>3</sup> were obtained by SCCO<sub>2</sub> drying of 1 wt.% hydrogel, which had a three-dimensional open nanoporous (~8 nm) network structure.

The results suggest that subcritical water technology is a promising method to enrich cellulose from lignocellulosic biomass, while reducing the use of chemicals. Also, lupin hull is a good cellulose source to obtain nanofibers to form hydrogels and aerogels without using chemical crosslinkers. The obtained cellulose nanofiber hydrogels and aerogels could be considered as potential candidates for many applications in food packaging, nanocomposites, paper reinforcement, coating additives, tissue engineering scaffolds, filtration media, thickening agents, rheology modifiers, and adsorbents.

## Preface

Chapter 3 of this thesis has been published as “Ciftci, D. and Saldaña, M.D.A. (2015). Hydrolysis of sweet blue lupin hull using subcritical water technology. *Bioresource Technology*, 194:75-82”. I was responsible for the experimental design, performing experiments, data collection and analysis, and drafting the manuscript. My supervisor Dr. Saldaña’s research area is subcritical water technology and she provided the topic research area, discussed the experimental design and data obtained, and revised the manuscript.

Chapter 4 of this thesis has been submitted to *Journal of Polymers and the Environment* as “Ciftci, D., Flores, R. and Saldaña, M.D.A. (2016). Cellulose fiber isolation and characterization from sweet blue lupin hull and canola straw”. Topic and experimental design were discussed with Dr. Saldaña, and completed in Dr. Flores’ laboratory in the Food Processing Center of the Department of Food Science and Technology at the University of Nebraska-Lincoln in the United States. I was responsible for the experimental design, performing experiments, data collection and analysis, and drafting the manuscript. Dr. Saldaña also helped with data discussion, and revision of the manuscript.

Chapter 5 of this thesis has been submitted to *Food and Bioprocess Technology* as “Ciftci, D., Flores, R. and Saldaña, M.D.A. (2016). Cellulose nanofibers of lupin hull obtained by processing with subcritical water and ultrasonication”. Research that started in Dr. Saldaña’s laboratory was completed in Dr. Flores’ lab. I was responsible for the experimental design, performing experiments, data collection and analysis, and drafting the manuscript. Topic and

experimental design were discussed with Dr. Saldaña, and she helped with data discussion and revised the manuscript.

Chapter 6 of this thesis has been submitted to *Fibers and Polymers* as “Ciftci, D., Flores, R. and Saldaña, M.D.A. (2016). Characterization of aqueous suspensions of cellulose nanofibers from lupin hull”. Research was completed in Dr. Flores’ laboratory. I was responsible for the experimental design, performing experiments, data collection and analysis, and drafting the manuscript. Dr. Saldaña helped with the experimental design, data discussion, and revised the manuscript.

Chapter 7 of this thesis has been submitted to *The Journal of Supercritical Fluids* as “Ciftci, D., Ubeyitogullari, A., Razera Huerta, R., Ciftci, O.N., Flores, R. and Saldaña, M.D.A. (2016). Lupin cellulose nanofiber aerogel preparation by supercritical CO<sub>2</sub> drying and freeze drying”. Research that started in Dr. Saldaña’s laboratory was completed in Dr. Flores’ lab. I was responsible for the experimental design, performing experiments, data collection and analysis, and drafting the manuscript. Dr. Saldaña helped with the experimental design, data discussion and revised the manuscript. Mr. Ubeyitogullari and Dr. Ciftci helped with some analysis of supercritical CO<sub>2</sub>-dried aerogels. Ms. Razera Huerta assisted in subcritical water sample generation.

*To Ozan & Kayra Deniz...*

## **Acknowledgements**

I would like to express my gratitude to my supervisor, Dr. Marleny D.A. Saldaña, for her encouragement and guidance throughout my research in this PhD thesis. I gained lots of knowledge and priceless experiences as her student.

I would like to thank Dr. Feral Temelli and Dr. Thava Vasanthan for being in my supervisory committee, providing me with valuable critiques and helpful advice during my PhD program.

Special thanks to Dr. Rolando Flores from the Department of Food Science and Technology at the University of Nebraska-Lincoln in the United States for his support and guidance during my stay as a visiting student in his lab.

I would also like to thank to Dr. Mark Martinez from the Department of Chemical and Biological Engineering of the University of British Columbia for accepting to be my external examiner.

I would also like to thank my lab mates at the University of Alberta and friends for their helpful support during my PhD program. Special thanks to the technical staff at the Chromatography lab at the AFNS department at the University of Alberta, and scientists at the Nebraska Center for Materials and Nanoscience, Center of Microscopy, and Proteomics and Metabolomics Facility at the University of Nebraska-Lincoln for training me and helping me with sample characterizations. I would like to express my thanks to Alberta Innovates Technology Futures and the Natural Sciences and Engineering Research Council of Canada (NSERC) for their financial support.

I would like to truly express my deepest gratitude to my parents, Fatma and Selahaddin, my grandmother, Emine, my sister, Lacin and my family in-law, Emine, Israfil, AYTEK, Kezban for their endless support throughout my PhD study and my life in general.

Special thanks to my cousin, Cem and my aunt Hacer for their cheerful support and positive feelings over these years.

Last but not the least, I would like to thank my husband, Ozan and my son, Kayra for being my source of happiness and motivation at the most difficult times, and for being the meaning of my life.

## Table of Contents

|   |           |
|---|-----------|
| <b>Chapter 1. Introduction and thesis objectives.....</b>   | <b>1</b>  |
| 1.1. Introduction.....  | 1         |
| 1.2. Hypothesis.....  | 4         |
| 1.3. Thesis objectives.....   | 5         |
| <br>  |           |
| <b>Chapter 2. Literature review.....</b>  | <b>7</b>  |
| 2.1. Lignocellulosic biomass matrix.....  | 7         |
| 2.2. Fractionation methods of lignocellulosic biomass.....  | 14        |
| 2.2.1. Biological methods.....  | 17        |
| 2.2.2. Physical methods.....  | 17        |
| 2.2.3. Chemical methods.....  | 18        |
| 2.2.4. Physico-chemical methods.....  | 21        |
| 2.2.4.1. Subcritical water technology.....  | 25        |
| 2.2.4.1.1. Extraction and reaction mechanisms of lignocellulosic<br>biomass in subcritical water..... | 30        |
| 2.3. Nanocelluloses.....  | 32        |
| 2.3.1. Production methods of cellulose nanofibers.....  | 34        |
| 2.3.2. Gelation behavior of cellulose nanofiber suspensions.....                                      | 39        |
| 2.3.2.1. Cellulose nanofiber aerogels.....  | 41        |
| 2.4. Conclusions.....   | 47        |
| <br>  |           |
| <b>Chapter 3. Hydrolysis of sweet blue lupin hull using subcritical water<br/>technology.....</b>     | <b>48</b> |
| 3.1. Introduction.....  | 48        |
| 3.2. Materials and methods.....   | 50        |
| 3.2.1. Raw material.....  | 50        |
| 3.2.2. Proximate compositional analysis.....  | 51        |
| 3.2.3. Hydrolysis in subcritical water.....   | 52        |
| 3.2.4. Analytical methods.....  | 53        |

|   |           |
|---|-----------|
| 3.2.4.1. Total phenolic content.....  | 53        |
| 3.2.4.2. Total organic carbon analysis.....                                 | 53        |
| 3.2.4.3. Hemicellulose, cellulose and lignin analysis.....                  | 54        |
| 3.2.5. Characterization of the solid residues.....                          | 55        |
| 3.2.5.1. X-ray Diffraction analysis.....                                    | 55        |
| 3.2.5.2. Thermo-gravometric analysis.....                                   | 56        |
| 3.2.5.3. Scanning Electron Microscopy analysis.....                         | 56        |
| 3.2.6. Statistical analysis.....  | 56        |
| 3.3. Results and discussion.....  | 57        |
| 3.3.1. Proximate compositional analysis.....                                | 57        |
| 3.3.2. Hydrolysis in subcritical water - Effects of process parameters....  | 59        |
| 3.3.2.1. Extracts.....  | 59        |
| 3.3.2.2. Solid residue.....   | 65        |
| 3.3.3. Characterization of the solid residues.....                          | 71        |
| 3.3.3.1. X-ray Diffraction analysis.....                                    | 71        |
| 3.3.3.2. Thermo-gravimetric analysis.....                                   | 73        |
| 3.3.3.3. Scanning Electron Microscopy analysis.....                         | 75        |
| 3.4. Conclusions.....   | 76        |
| <br>  |           |
| <b>Chapter 4. Cellulose fiber isolation and characterization from sweet</b> |           |
| <b>blue lupin hull and canola straw.....</b>                                | <b>77</b> |
| 4.1. Introduction.....  | 77        |
| 4.2. Materials and methods.....   | 80        |
| 4.2.1. Materials.....   | 80        |
| 4.2.2. Cellulose isolation.....   | 80        |
| 4.2.3. Characterization.....  | 81        |
| 4.2.3.1. Chemical composition.....  | 81        |
| 4.2.3.2. X-ray diffraction analysis.....                                    | 82        |
| 4.2.3.3. Thermo-gravimetric analysis.....                                   | 82        |
| 4.2.3.4. Scanning Electron Microscopy analysis.....                         | 82        |
| 4.2.4. Statistical analysis.....  | 83        |

|   |            |
|---|------------|
| 4.3. Results and discussion.....  | 83         |
| 4.3.1. Chemical composition.....  | 83         |
| 4.3.2. Crystallinity.....   | 91         |
| 4.3.3. Thermal behavior.....  | 94         |
| 4.3.4. Morphology.....  | 97         |
| 4.4. Conclusions.....   | 99         |
| <br>  |            |
| <b>Chapter 5. Cellulose nanofibers of lupin hull obtained by processing<br/>with subcritical water and ultrasonication.....</b> | <b>100</b> |
| 5.1. Introduction.....  | 100        |
| 5.2. Experimental.....  | 103        |
| 5.2.1. Materials.....   | 103        |
| 5.2.2. Preparation of cellulose fibers.....   | 103        |
| 5.2.3. Preparation of cellulose nanofibers.....   | 103        |
| 5.2.4. Determination of lignin content.....   | 104        |
| 5.2.5. Water retention value.....   | 104        |
| 5.2.6. Microscopic analysis.....  | 105        |
| 5.2.7. Fourier Transform Infrared Spectroscopy analysis.....  | 105        |
| 5.2.8. X-ray Diffraction analysis.....  | 106        |
| 5.2.9. Statistical analysis.....  | 106        |
| 5.3. Results and discussion.....  | 106        |
| 5.3.1. Water retention value.....   | 107        |
| 5.3.2. Morphology and size.....   | 109        |
| 5.3.3. Attenuated Total Reflectance - Fourier Transform Infrared<br>Spectroscopy.....   | 114        |
| 5.3.4. Crystallinity.....   | 116        |
| 5.4. Conclusions.....   | 118        |
| <br>  |            |
| <b>Chapter 6. Characterization of aqueous suspensions of cellulose<br/>nanofibers from lupin hull.....</b>                      | <b>119</b> |
| 6.1. Introduction.....  | 119        |

|   |            |
|---|------------|
| 6.2. Materials and methods.....   | 121        |
| 6.2.1. Materials.....   | 121        |
| 6.2.2. Preparation of cellulose nanofiber suspensions/hydrogel.....   | 122        |
| 6.2.3. Microscopic analysis.....  | 123        |
| 6.2.4. X-ray Diffraction analysis.....  | 123        |
| 6.2.5. Thermo-gravimetric analysis.....   | 123        |
| 6.2.6. Rheological behavior.....  | 123        |
| 6.2.7. Statistical analysis.....  | 123        |
| 6.3. Results and discussion.....  | 124        |
| 6.3.1. Morphology and structure.....  | 124        |
| 6.3.2. Rheological properties.....  | 127        |
| 6.4. Conclusions.....   | 131        |
| <br>  |            |
| <b>Chapter 7. Lupin cellulose nanofiber aerogel preparation by<br/>supercritical CO<sub>2</sub> drying and freeze drying.....</b> | <b>132</b> |
| 7.1. Introduction.....  | 132        |
| 7.2. Materials and methods.....   | 135        |
| 7.2.1. Materials.....   | 135        |
| 7.2.2. Preparation of cellulose nanofiber hydrogels.....  | 135        |
| 7.2.3. Preparation of cellulose nanofiber aerogels by freeze drying.....  | 136        |
| 7.2.4. Preparation of cellulose nanofiber aerogels by supercritical<br>carbon dioxide drying.....                                 | 136        |
| 7.2.5. Characterization of the aerogels.....  | 138        |
| 7.2.5.1. Bulk density and porosity.....   | 138        |
| 7.2.5.2. Specific surface area and pore size.....   | 138        |
| 7.2.5.3. Microscopic analysis.....  | 139        |
| 7.2.5.4. X-ray diffraction analysis.....  | 140        |
| 7.2.5.5. Thermo-gravimetric analysis.....   | 140        |
| 7.2.6. Statistical analysis.....  | 140        |
| 7.3. Results and discussion.....  | 140        |
| 7.3.1. Aerogel properties.....  | 140        |

|  |            |
|--|------------|
| 7.3.2. Morphology.....   | 144        |
| 7.3.2.1. Cellulose nanofiber hydrogels.....                      | 144        |
| 7.3.2.2. Supercritical carbon dioxide-dried aerogels.....        | 146        |
| 7.3.2.3. Freeze-dried aerogels.....                              | 148        |
| 7.3.3. Crystallinity.....  | 151        |
| 7.3.4. Thermal stability.....                                    | 153        |
| 7.4. Conclusions.....  | 154        |
| <b>Chapter 8. Summary, conclusions, and recommendations.....</b> | <b>156</b> |
| 8.1. Summary and conclusions.....                                | 156        |
| 8.2. Recommendations.....  | 162        |
| <b>References.....</b>   | <b>165</b> |
| <b>Appendix A.....</b>   | <b>189</b> |
| <b>Appendix B.....</b>   | <b>193</b> |
| <b>Appendix C.....</b>   | <b>196</b> |
| <b>Appendix D.....</b>   | <b>198</b> |
| <b>Appendix E.....</b>   | <b>199</b> |

## List of Tables

|  |     |
|--|-----|
| <b>Table 2-1.</b> Composition of lignocellulosic biomass.....  | 13  |
| <b>Table 2-2.</b> Methods for lignocellulosic biomass fractionation (Adapted from Kumar et al., 2009).....                                   | 15  |
| <b>Table 2-3.</b> Physico-chemical properties of water at different temperatures (L: liquid, G: gas) (Adapted from Moller et al., 2011)..... | 27  |
| <b>Table 2-4.</b> Examples of production methods of cellulose nanofibers.....  | 35  |
| <b>Table 3-1.</b> Composition of lupin hull used in this study.....  | 58  |
| <b>Table 3-2.</b> Effect of temperature on total organic content of lupin hull extracts at 50 bar.....                                       | 70  |
| <b>Table 4-1.</b> Chemical composition of lupin hull and canola straw before and after different treatments.....                             | 85  |
| <b>Table 7-1.</b> Comparison of cellulose nanofiber aerogel properties obtained by different dryings.....                                    | 142 |

## List of Figures

|  |    |
|--|----|
| <b>Figure 2-1.</b> Structure of lignocellulosic biomass (Adapted from Lee et al., 2013).....   | 7  |
| <b>Figure 2-2.</b> Chemical structure of cellulose.....  | 8  |
| <b>Figure 2-3.</b> Crystalline and amorphous regions in cellulose microfibrils   | 9  |
| <b>Figure 2-4.</b> Example of hemicellulose structure: xylan.....  | 11 |
| <b>Figure 2-5.</b> Major building blocks of lignin.....  | 12 |
| <b>Figure 2-6.</b> Phase diagram of water (Adapted from Murphy and Koop, 2005).....  | 25 |
| <b>Figure 2-7.</b> Dielectric constant of water as a function of temperature at 200 bar. Solid circles on the plot are the values corresponding to different organic solvents at 25 °C and 1 bar (values given in parentheses) (Adapted from Delgado-Zamarreno et al., 2009).....  | 28 |
| <b>Figure 3-1.</b> Effect of process parameters on total hemicellulose sugar yield (sum of xylose, galactose, arabinose, and mannose) in the extracts. a) Temperature and pressure (5 mL/min, pH 6.2); b) flow rate (180 °C, 50 bar, pH 6.2); c) pH (180 °C, 50 bar, 5 mL/min).....  | 60 |
| <b>Figure 3-2.</b> Effect of process parameters on cellulose and lignin contents in the solid residues. a) Temperature (50 bar, 5 mL/min, pH 6.2); b) flow rate (180 °C, 50 bar, pH 6.2); c) pH (180 °C, 50 bar, 5 mL/min). Means within the same group of biomass fraction with different letters are significantly different at $p < 0.05$ ..... | 66 |
| <b>Figure 3-3.</b> Effect of temperature and pressure on total phenolic content of lupin hulls.....  | 69 |
| <b>Figure 3-4.</b> X-ray diffraction (XRD) patterns of untreated lupin hulls and subcritical water treated lupin hulls at optimum conditions of 180 °C, 50 bar, 5mL/min, and pH of 6.2.....  | 72 |

|  |    |
|--|----|
| <b>Figure 3-5.</b> Thermo-gravimetric (TG) curves of untreated lupin hulls and subcritical water treated lupin hulls at optimum conditions of 180 °C, 50 bar, 5 mL/min, and pH of 6.2.....   | 74 |
| <b>Figure 3-6.</b> Scanning electron microscopy (SEM) images of lupin hulls: a), b), and c) untreated hulls, d), e), and f) subcritical water treated hulls at optimum conditions (180 °C, 50 bar, 5mL/min, pH 6.2).....   | 75 |
| <b>Figure 4-1.</b> Effect of NaOH concentration and time on hemicellulose and lignin removal of (a, b) lupin hull, and (c, d) canola straw. Means with different letters within each temperature are different from each other at $p < 0.05$ .....   | 88 |
| <b>Figure 4-2.</b> Effect of ASC treatment (1.7%/75 °C) time (2, 4 and 6 h) on cellulose, hemicellulose, and lignin recovery of (a) lupin hull and (b) canola straw treated at optimum NaOH conditions (15% NaOH/99 °C/6h). Means with different letters within each biomass fraction are different from each other at $p < 0.05$ .....  | 90 |
| <b>Figure 4-3.</b> X-ray diffraction (XRD) patterns of untreated, NaOH (15%/99 °C/6h) and NaOH-ASC (ASC: 1.7%/75 °C/6h) treated (a) lupin hull, and (b) canola straw, and their crystallinity index (CI) values.....   | 92 |
| <b>Figure 4-4.</b> Thermo-gravimetric (TG) curves of untreated, NaOH (15%/99 °C/6h) and NaOH-ASC (ASC: 1.7%/75 °C/6h) treated (a) lupin hull, and (b) canola straw.....  | 96 |
| <b>Figure 4-5.</b> Scanning electron microscopy (SEM) images of (a) untreated lupin hull, (b,c) untreated canola straw, (d-f) NaOH treated lupin hull, (g-i) NaOH treated canola straw, (j) NaOH-ASC treated lupin hull, (k,l) NaOH-ASC treated canola straw at the optimized conditions (NaOH: 15%/99 °C/6h, and ASC: 1.7%/75 °C/6h), (m-o) lignin from lupin hull, and (p-s) lignin from canola straw after NaOH treatment (15%/99 °C/6h)..... | 98 |

|  |     |
|--|-----|
| <b>Figure 5-1.</b> Water retention value (WRV) of untreated and ultrasonicated lupin hull cellulose at different amplitudes (20, 50 and 80%) for varying time (15, 25 and 35 min). Means with different letters within all amplitudes are different from each other at $p < 0.05$ .....  | 108 |
| <b>Figure 5-2.</b> Transmission electron microscopy (TEM) images and diameter size distribution of ultrasonicated lupin hull cellulose at different conditions: (a) 50% amplitude for 25 min, (b) 50% amplitude for 35 min, (c) 80% amplitude for 25 min, and (d) 80% amplitude for 35 min.....  | 110 |
| <b>Figure 5-3.</b> Effect of WRV values on the average diameter size at 50-80% amplitude for 25-35 min.....  | 112 |
| <b>Figure 5-4.</b> Scanning electron microscopy (SEM) images of (a) purified lupin hull cellulose microfibrils, (b) isolated cellulose nanofibers (80% amplitude for 35 min); oven dried at 40 °C for 48 h, and (c) freeze dried at -45 °C for 48 h.....   | 114 |
| <b>Figure 5-5.</b> Attenuated Total Reflectance Fourier Transform Infrared Spectroscopy (ATR-FTIR) spectra of untreated lupin hull, purified lupin hull cellulose and isolated cellulose nanofibers (80% amplitude for 35 min).....  | 115 |
| <b>Figure 5-6.</b> X-ray diffraction (XRD) patterns of ultrasonicated lupin hull cellulose at different conditions: 50% amplitude for 25 min, 50% amplitude for 35 min, 80% amplitude for 25 min, and 80% amplitude for 35 min.....  | 117 |
| <b>Figure 6-1.</b> Morphology and structural characteristics of cellulose nanofibers at different concentrations: TEM images of (a) 0.1 wt.%, (b) 0.7 wt.%, (c) 1.6 wt.%, and (d) 1.9 wt.%, (e) XRD patterns, (f) TG curves.....   | 125 |
| <b>Figure 6-2.</b> Rheological properties of cellulose nanofiber suspensions at different concentrations: (a) Steady-state viscosity, (b) strain sweep test, (c) $G'$ (0.1-1.9 wt.%), (d) $G''$ (0.1-1.9 wt.%), (e) $G'$ and $G''$ (0.1 wt.%), (f) $G'$ and $G''$ (0.4 wt.%), (g) $G'$ and $G''$ (1.0 wt.%), (h) loss tangent (0.1, 0.4 and 1.0 wt.%). ..... | 128 |

|   |     |
|---|-----|
| <b>Figure 7-1.</b> Transmission electron microscopy (TEM) images of the cellulose nanofiber hydrogels (1, 1.5, and 2 wt.%) and the appearance of the resultant aerogels at macroscopic level.....                   | 146 |
| <b>Figure 7-2.</b> The morphologies of supercritical carbon dioxide (SCCO <sub>2</sub> )-dried aerogels as a function of the initial hydrogel concentration ((a-c) 1 wt.%, (d-f) 1.5 wt.%, and (g-i) 2 wt.%).....   | 147 |
| <b>Figure 7-3.</b> The morphologies of freeze-dried aerogels as a function of the initial hydrogel concentration ((a and b) 1 wt.%, (c and d) 1.5 wt.%, and (e and f) 2 wt.%).....                                  | 149 |
| <b>Figure 7-4.</b> The morphologies of freeze-dried aerogels with rapid freezing using (a and b) liquid nitrogen and with (c and d) slow freezing using regular freezer at a hydrogel concentration of 1 wt.%...... | 151 |
| <b>Figure 7-5.</b> X-ray diffraction (XRD) patterns of aerogels with different concentrations.....  | 152 |
| <b>Figure 7-6.</b> Thermo-gravimetric (TG) curves of aerogels with different concentrations.....  | 154 |

## List of abbreviations

|           |  |
|-----------|--|
| AFEX      | Ammonia fiber explosion                      |
| ARP       | Ammonia recycle percolation                  |
| ASC       | Acidified sodium chlorite                    |
| ATR       | Attenuated total reflectance                 |
| BET       | Brunauer–Emmett–Teller                       |
| BJH       | Barrett-Joyner-Halenda                       |
| CI        | Crystallinity index                          |
| FE-SEM    | Field emission scanning electron microscopy  |
| FTIR      | Fourier transform infrared spectrometer      |
| $G''$     | Loss modulus                                 |
| $G'$      | Storage modulus                              |
| $H_2SO_4$ | Sulfuric acid                                |
| HCl       | Hydrochloric acid                            |
| HMF       | Hydroxymethyl furfural                       |
| HPLC      | High performance liquid chromatograph        |
| NaOH      | Sodium hydroxide                             |
| $NaClO_2$ | Sodium chlorite                              |
| NREL      | National Renewable Energy Laboratory         |
| $P$       | Porosity                                     |
| $SCCO_2$  | Supercritical carbon dioxide                 |
| SEM       | Scanning electron microscopy                 |
| TEM       | Transmission electron microscopy             |
| TEMPO     | 2,2,6,6-tetramethylpiperidine-1-oxyl radical |
| TGA       | Thermo-gravimetric analysis                  |
| TOC       | Total organic carbon                         |
| UV        | Ultraviolet                                  |
| WRV       | Water retention values                       |
| XRD       | X-ray diffraction                            |

## **Chapter 1. Introduction and thesis objectives**

### **1.1. Introduction**

As overdependence on petroleum products has increased and depletion of resources has become evident, the development of sustainable technologies and the use of renewable biomass resources are critical to meet the growing environmental concerns regarding pollution and waste generation, and the high demand for petroleum-based materials. Consequently, much attention has been focused on the utilization of lignocellulosic biomass as a raw material to produce biomaterials, chemicals and energy. Lignocellulosic biomass consists mainly of cellulose (30-50%), hemicellulose (15-35%), lignin (10-30%), and other minor components (protein, soluble nonstructural sugars, nitrogenous material, chlorophyll, and waxes) (Mosier et al., 2005). Cellulose and hemicellulose are sugar polymers with chains of multiple sugars wrapped in a lignin sheet (Wyman et al., 2005). Lignin is a highly complex material that provides strength to plant. There are vast biomass sources, such as agro-industrial by-products from cultivation (e.g. straw) and industrial processing (e.g. hull) that are particularly suitable for the production of value-added materials since they do not compete with the food sector (Knauf and Moniruzzaman, 2004). It is estimated that there are  $1 \times 10^{10}$  metric tons of lignocellulosic biomass grown worldwide every year (Smichi et al., 2014). Therefore, an efficient utilization of such resources is of great importance not only to minimize the environmental impact, but also to obtain high value-added products.

Isolation of cellulose nanofibers from lignocellulosic biomass for use in food formulations, composite materials, packaging, cosmetics, and electronics to improve strength and stiffness combined with low weight, biodegradability and renewability is a promising way of adding value to biomass (Agarwal et al., 2006; Hubbe et al., 2008). Cellulose nanofiber is a network of interconnected microfibrils with little order on the nanometer scale, which is typically in the range of 10-80 nm in diameter with length of several microns (Abdul Khalil et al., 2012). The entangled network structure of nanofibers with a high aspect ratio and high specific surface area allow formation of hydrogels via physical crosslinking. The hydrogel structure permits formation of aerogel, which is an advanced material with high porosity and surface area.

Recently, preparation of highly porous and lightweight aerogels based on cellulose nanofibers has received great attention due to a number of desirable characteristics of nanofibers, such as high aspect ratio, low thermal expansion, good mechanical and optical properties, low weight, low density and biodegradability (Syverud and Stenius, 2009; Yano and Nakahara, 2004). Freeze drying is a widely-used method for aerogel formation where water is removed by sublimation; however, supercritical carbon dioxide (SCCO<sub>2</sub>) drying has been accepted as a new method for forming aerogels with improved properties such as higher surface area and porosity due to the lack of surface tension and liquid-vapor interfaces in the pores (Pierre and Pajonk, 2002). This class of cellulose aerogels based on nanofibers offer new application areas in medical and pharmaceutical fields, where biocompatibility and biodegradability is needed

(Aulin et al., 2010), as well as in environmentally friendly packaging, and high performance and biodegradable nanocomposites (Pääkkö et al., 2008).

Cellulose nanofiber production from lignocellulosic biomass include fractionation of cellulose fibers with various treatments, such as acid, alkaline and organosolv treatments and then fibrillation of the purified cellulose fibers using mechanical approaches, such as high pressure homogenization, microfluidizers, super grinding/refiner-type treatments, and high intensity ultrasonication (Alemdar and Sain, 2008; Dufresne et al., 2000; Herrick et al., 1983; Iwamoto et al., 2007; Taniguchi and Okamura, 1998; Wang, et al., 2016) alone or in various combinations. Some researchers have also employed additional chemical pre-treatments, such as surface modifications of cellulose fibers with TEMPO (2,2,6,6-tetramethylpiperidine-1-oxyl radical)-mediated oxidation, and carboxymethylation with chloroacetic acid, to achieve better fibrillation (Besbes et al., 2011; Hubbe et al., 2008; Wågberg et al., 2008). However, these conventional processes use hazardous chemicals and solvents, and generate large amounts of waste streams that may require intensive waste treatment, raising environmental concerns besides the additional processing costs.

In recent years, there is a growing demand for environmentally friendly methods due to growing environmental concerns, government measures, and social perception. Therefore, there is a critical need for alternative methods that eliminate or reduce the use of hazardous chemicals and solvents and waste generation from biomass processing. Subcritical water technology has received attention as an environmentally friendly alternative technology for biomass

conversion because water is an inexpensive, abundant, non-toxic and environmentally benign solvent (Brunner, 2009; Saldaña and Valdivieso-Ramirez, 2015). Under subcritical water conditions, the properties of water are modified by increasing the temperature to below 374 °C and keeping the pressure high enough to maintain the water in the liquid state. Subcritical water has unique properties of dielectric constant, ionic product, density, viscosity, diffusivity, electric conductance, and solvent ability. An increase in the ionic product and a decrease in the dielectric constant, viscosity, and density of water in the subcritical region makes it an excellent medium for fast, homogeneous and efficient reactions (Kruse and Dinjus, 2007). Thus, subcritical water technology offers a promising way to eliminate non-cellulosics components of biomass, such as hemicellulose and lignin, and to create increased surface area of cellulosic fibers making it accessible for further treatments to obtain nanofibers.

## **1.2. Hypothesis**

Subcritical water technology can be used as an alternative technology for the isolation of cellulose fibers from lignocellulosic biomass to produce cellulose nanofibers. It was also hypothesized that cellulose nanofiber can be used to form hydrogels and these hydrogels might be converted into aerogels using SCCO<sub>2</sub> drying.

### 1.3. Thesis objectives

The main objective of this thesis was to develop an environmentally friendly approach based on subcritical water technology to produce cellulose nanofibers and to obtain cellulose nanofiber aerogels using SCCO<sub>2</sub> drying and freeze drying.

The specific objectives were:

- to optimize the process parameters of subcritical water treatment, such as pressure, temperature, flow rate and pH for the removal of hemicellulose and lignin from lupin hull and, to determine the effects of treatment conditions on the structure (Chapter 3),
- to optimize the treatment conditions of combined alkaline treatment, and bleaching, such as concentration, temperature, and time for maximum cellulose recovery from lupin hull and canola straw and, to investigate the effect of lignin content of the starting materials on the treatment efficiency, and to compare the efficiencies of the employed treatments with that of Chapter 3 (Chapter 4),
- to investigate the production of cellulose nanofibers with ultrasonic fibrillation of lupin hull cellulose isolated with the subcritical water-assisted approach (Chapter 3), and to evaluate the effects of ultrasonication parameters, such as applied amplitude and time on the fibrillation process of cellulose fibers (Chapter 5),

- to characterize the aqueous cellulose nanofiber suspensions/hydrogels of lupin hull at varying concentrations in terms of morphology, structure, and rheological behavior (Chapter 6), and
- to investigate the effects of SCCO<sub>2</sub> drying and freeze drying, and the concentration of cellulose nanofibers of lupin hull on the formation of aerogels (Chapter 7).

## Chapter 2. Literature review

### 2.1. Lignocellulosic biomass

Lignocellulosic biomass is the most abundant non-food biomass with a worldwide annual production of  $1 \times 10^{10}$  metric tons (Smichi et al., 2014). Lignocellulose is a generic term used for describing the main constituents in most plants, namely cellulose, hemicelluloses, and lignin.

Figure 2-1 shows the chemical structure of a typical lignocellulosic biomass. Cellulose and hemicelluloses are the main sugar polymers, and together with lignin, represent the key constituents of plant cell walls. It also contains smaller amounts of pectin, protein, extractives (soluble non-structural materials, such as non-structural sugars, nitrogenous material, chlorophyll, and waxes), and ash (Chakraborty et al., 2005).

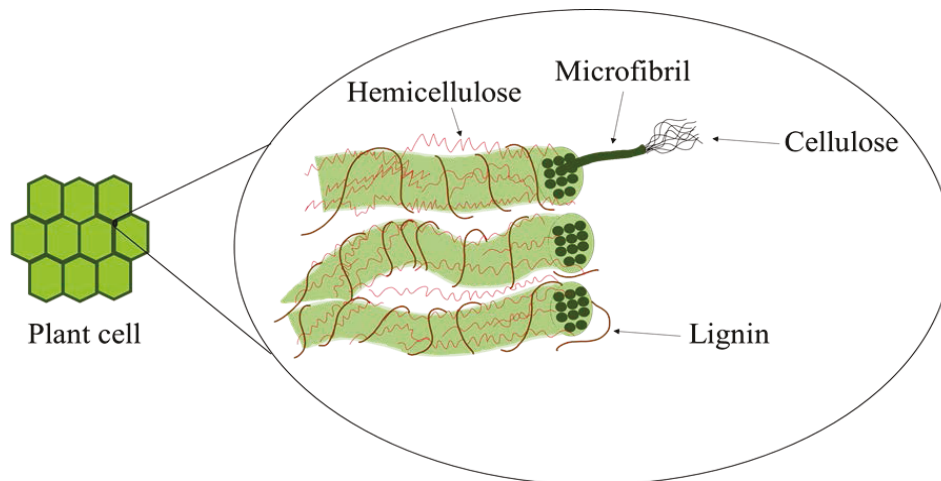


**Figure 2-1.** Structure of lignocellulosic biomass (Adapted from Lee et al., 2014).

Inside the lignocellulosic biomass, cellulose appears to be the core of the complex and is found in an organized fibrous structure. Hemicellulose is placed both both the micro- and the macro-fibrils of cellulose. Lignin provides a structural role to the matrix in which cellulose and hemicellulose are embedded (Shevchenko et al., 1999).

Cellulose is the most abundant biopolymer on earth, existing in a variety of living species, such as plant, animals, bacteria, and some amoebas (Perez and Samain, 2010). Cellulose is a linear homopolymer composed of glucose units linked together by  $\beta$ -1,4-glycosidic bonds with cellobiose (consists of two molecules of glucose) residues as the repeating unit at different degrees of polymerization (Fig. 2-2). The chemical formula of cellulose is  $(C_6H_{10}O_5)_n$ , where  $n$ , degree of polymerization, depends on the cellulose source material. Typically, 10,000 to 15,000 repeat units form a single cellulose chain (O' Sullivan, 1997).

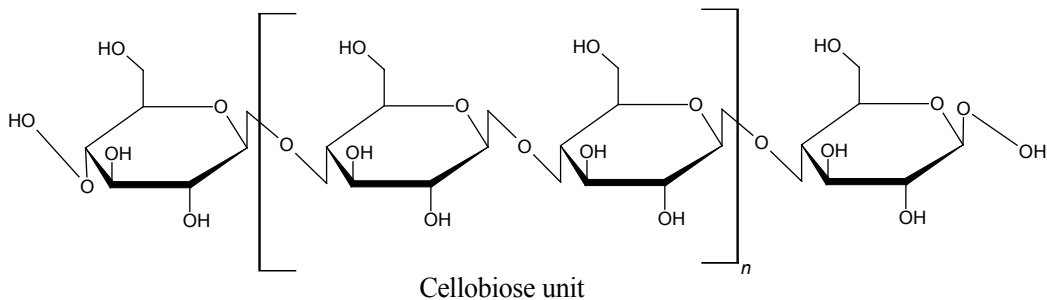


**Figure 2-2.** Chemical structure of cellulose.

There are three hydroxyl groups per repeating unit, so cellulose macromolecules are likely to be involved in a number of intra- and inter-

molecular hydrogen bonds, which govern the physical properties of cellulose (Zimmerman et al., 2004). Each repeating unit is rotated 180°, creating a high degree of symmetry since each side has the same number of hydroxyl groups. This organization leads to a high degree of hydrogen bonding between adjacent molecules of cellulose, creating highly crystalline regions, which makes cellulose a relatively stable polymer. Thus, cellulose does not readily dissolve in typical aqueous solvents. Cellulose swells but is unable to dissolve in water (melting point: 260-270 °C) (Raymond, 1986).

During cellulose formation, van der Waals and intermolecular hydrogen bonds between hydroxyl groups and oxygens of adjacent molecules promote aggregation of multiple cellulose chains, forming fibrils which are packed into larger microfibrils with 5-50 nm in diameter and several micrometers in length (Moon et al., 2011). As shown in Figure 2-3, these microfibrils have highly ordered (crystalline) regions where the cellulose chains are arranged in a highly ordered crystalline structure and disordered (amorphous) regions that are in low order distributed along the microfibrils (Klemm et al., 2005).

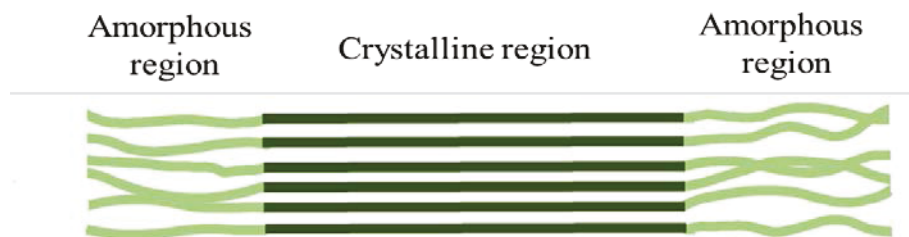


**Figure 2-3.** Crystalline and amorphous regions in cellulose microfibrils.

Several types of interchangeable cellulose polymorphs (I, II, III, IV, V and VI) have been identified depending on the inter- and intramolecular interactions and molecular orientations present, or the treatments applied for isolation. Native cellulose type I displays the best mechanical properties, which is subdivided into two phases ( $I_\alpha$  and  $I_\beta$ ) (Sugiyama et al., 1991). Thermodynamically, the  $I_\beta$  is more stable than the  $I_\alpha$ . It has been reported that cellulose  $I_\alpha$  was converted to  $I_\beta$  by hydrothermal annealing at above 200 °C in a number of different acidic or basic solvent media (Yamamoto et al., 1989; Yamamoto and Horii, 1993).

Hemicellulose is a complex carbohydrate structure that is composed of a linear as well as branched polymers of pentosans (e.g. xylose and arabinose) and hexosans (e.g. mannose, glucose, and galactose), and sugar acids (e.g. galactouronic acid) (Fengel and Wegener, 1984). The backbone of hemicellulose is either a homopolymer or a heteropolymer with branches with short lateral chains linked by  $\beta$ -1,4-glycosidic bonds and occasionally  $\beta$ -1,3-glycosidic bonds (Kuhad et al., 1997). Unlike cellulose, hemicelluloses are lacking crystalline structure, mainly due to the highly-branched structure, and the presence of acetyl groups connected to the polymer chain. They have lower molecular weight (150-165 g/mol) than cellulose (180.16 g/mol) (Sjöström, 1981). The hemicellulose content of hardwoods and softwoods are different because hemicelluloses from hardwood are mainly composed of xylans, whereas the dominant component of hemicelluloses from softwood is glucomannans. In herbaceous plants including crop byproducts, hemicellulose fractions are formed by a wide variety of sugar residues, such as xylose, arabinose, glucose, galactose and mannose, depending

upon the source (Fengel and Wegener, 1984; Saha, 2003). The structure of a typical hemicellulose chain can be seen in Figure 2-4.

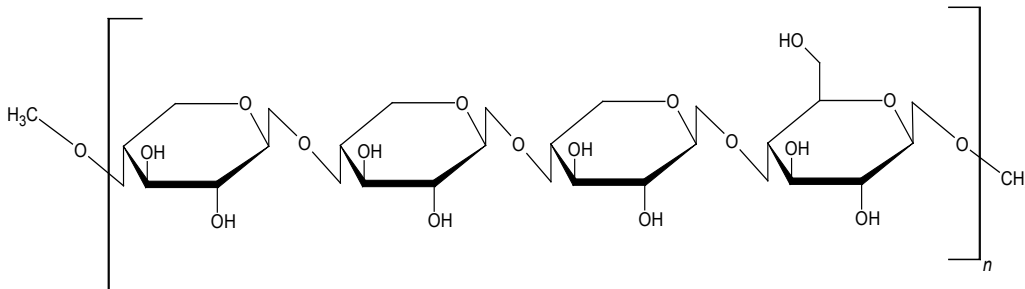


**Figure 2-4.** Example of hemicellulose structure: xylan.

Lignin is the third most abundant organic polymer present in nature after cellulose and hemicelluloses (Buranov and Mazza, 2008). It is an amorphous three-dimensional hydrophobic polymer. In the plant cell wall, lignin protects plants, imparting structural support, impermeability, and resistance against microbial attack (Sánchez, 2009). Composition and structure of lignin vary depending on its origin. Herbaceous plants, such as grasses and cereal straws, have the lowest contents of lignin, whereas softwoods have the highest lignin contents.

Lignin molecules are made up of three phenylpropane monomers: *p*-coumaryl alcohol (*p*-hydroxyphenyl propanol), coniferyl alcohol (guaiacyl propanol), and synapyl alcohol (syringyl alcohol) (Pérez et al., 2002; Sánchez, 2009) (Fig. 2-5). These monomers also known as monolignols are polymerized by a radical coupling process that links them by carbon-carbon (C-C) and ether bonds (C-O-C). The existence of strong C-C and C-O-C linkages in the lignin affects its susceptibility to chemical disruption (Harkin, 1973). Covalent linking also exists between lignin and polysaccharides, which strongly enhances the

adhesive bond strength and acts as the “glue” that connects cellulose and hemicellulose (Kumar et al., 2009).

There are three main types of lignin units, which are guaiacyl (with one methoxyl group in the phenol ring), syringyl (with two methoxyl groups) and *p*-hydroxyphenylpropane. The lignin from softwood is mainly composed of guaiacyl units, the lignin from hardwoods contains both guaiacyl and syringyl units, whereas the lignin of herbaceous plants, such as grasses and cereal straws contain all three units in significant amounts at different ratios (Brodeur et al., 2011).

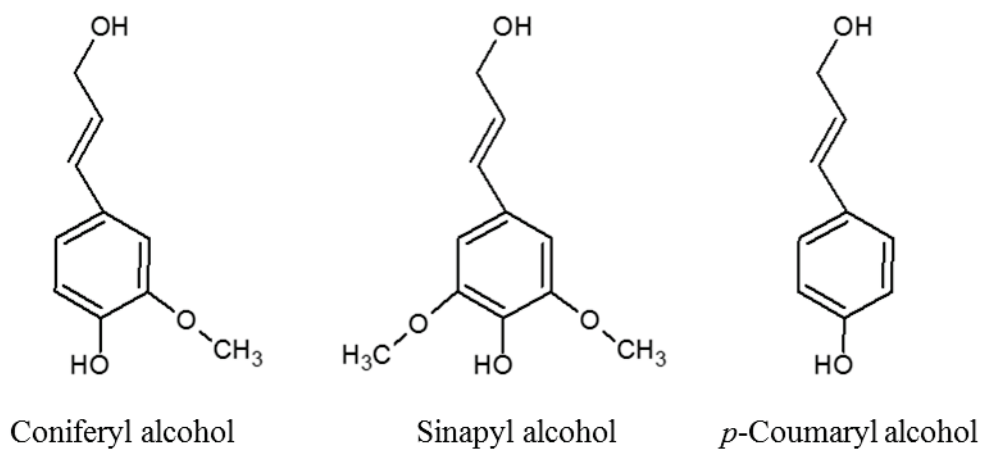


**Figure 2-5.** Major building blocks of lignin.

The fraction of each component in lignocellulosic biomass varies, depending on the types of plants and regions as shown in Table 2-1. Even though the total amount of hemicellulose and cellulose in such biomass usually accounts for more than 60%, their lignin contents may vary depending on the biomass. For example, softwood has greater amount of lignin compared to that of agro-industrial by-products, such as cereal/oilseed straws and hulls.

Among the agro-industrial by-products, lupin hull is the one of the lowest lignin feedstocks. Lupin is a legume crop with 450 species mainly cultivated in Australia. Lupin seeds contain high levels of protein and are used as valuable ingredients mainly in bakery products as well as in dietary and functional food products. Recently, the use of lupin seeds as a food source is increasing due to its many health benefits. They are gluten-free, high in antioxidants, and considered to be prebiotic. The hulls comprise about 25% of the seed weight and predominantly contain structural polysaccharides, cellulose and hemicelluloses (Bailey et al., 1974).

**Table 2-1.** Composition of lignocellulosic biomass.

| Source       | Composition (wt.%) |               |        |                           |
|--------------|--------------------|---------------|--------|---------------------------|
|              | Cellulose          | Hemicellulose | Lignin | Ref.                      |
| Hardwood     | 40-55              | 24-40         | 18-25  | Sun and Cheng (2002)      |
| Softwood     | 45-50              | 24-35         | 25-35  | Sun and Cheng (2002)      |
| Switchgrass  | 31-45              | 24-31         | 12-23  | Howard et al. (2003)      |
| Oat straw    | 31-35              | 20-26         | 10-15  | Rowell (1992)             |
| Wheat straw  | 35-40              | 21-27         | 15-25  | Prasad et al. (2007)      |
| Canola straw | 32                 | 21            | 19     | Pronky and Mazza (2012)   |
| Soy hull     | 56                 | 13            | 18     | Alemdar and Sain (2008)   |
| Lupin hull   | 45                 | 25            | 8      | Ciftci and Saldaña (2015) |
| Bagasse      | 41-50              | 25-30         | 18-25  | Guo et al. (2009)         |
| Corn stover  | 27-48              | 13-27         | 14-31  | Van et al. (2011)         |
| Corn cob     | 34                 | 34            | 18     | Van Dongen et al. (2011)  |
| Coconut husk | 44                 | 12            | 33     | Goh et al. (2010)         |
| Rice husk    | 29-36              | 12-29         | 15-20  | Allen et al. (2001)       |

At present, some bread manufacturers use lupin hull flour in high fiber bread making; however, huge amounts of lupin hulls are left as waste. Owing to a unique aspect of its low lignin content, lupin hull is a promising candidate to obtain high value added products, which needs less demanding delignification processes. Thus, lupin hull can be used as an ideal feedstock to yield a wide range of valuable products that can replace oil-derived products. Similarly, tons of unused cereal and oilseed straws are generated every year, with only a small percentage being used in applications such as feedstock and energy production. For example, canola seed is one of the main oilseeds used for the production of edible oil; however, it has been reported that high volume of canola straw (3 tons/ha) is annually ploughed into the ground or burnt (Yousefi, 2009). In addition, there has been an increased interest in the use of triticale, which produces more straw than other cereal crops (Pronyk and Mazza, 2010). Thus triticale straws could be available for use as a renewable feedstock.

## **2.2. Fractionation methods of lignocellulosic biomass**

The recalcitrance of lignocellulosic biomass is the main challenge to overcome to use it as a renewable source for the production of chemicals and fuels (Elander et al., 2009). The separation of the three main components of lignocellulosic biomass is limited by many factors, such as lignin content, cellulose crystallinity, water content and available surface area.

**Table 2-2.** Methods for lignocellulosic biomass fractionation (Adapted from Kumar et al., 2009).

| <b>Treatment</b>             | <b>Conditions</b>   | <b>Advantages</b>  | <b>Disadvantages</b>                                  |
|------------------------------|---|--|---|
| <b>Biological</b>            |   |  |   |
|                              | Several fungi (brown-, white- and soft-rot fungi)   | Degrades lignin and hemicelluloses; low energy requirements                  | Slow hydrolysis rates                                 |
| <b>Physical</b>              |   |  |   |
| Chipping<br>Milling          | Room temperature<br>Energy input < 30 kW per ton biomass  | Reduces cellulose crystallinity  | Power consumption higher than inherent biomass energy |
| <b>Chemical</b>              |   |  |   |
| Acid hydrolysis: dilute-acid | Type I: T>160°C, continuous-flow process for low solid loading (5-10%)-<br>Type II: T<160°C, batch process for high solid loadings (10-40%) | Hydrolyzes hemicellulose to xylose and other sugars; alters lignin structure | Equipment corrosion; formation of toxic compounds     |
| Alkaline hydrolysis          | Low temperature; long process time; concentration of the base   | Removes hemicelluloses and lignin; increases accessible surface area         | Residual salts in biomass                             |
| Organosolv                   | 150-200 °C with or without catalysts (oxalic, salicylic, and acetylsalicylic acid)  | Hydrolyzes lignin and hemicelluloses   | High costs due to solvent recovery                    |

**Table 2-2. (Continued)**

| <b>Treatment</b>                         | <b>Conditions</b>                               | <b>Advantages</b>  | <b>Disadvantages</b>   |
|--|---|--|--|
| Steam explosion                          | 160-260°C (6.9-48 bar) for 5-15 min             | Hemicellulose hydrolysis and lignin transformation; cost-effective for hardwood and agricultural residues                  | Destruction of a portion of the xylan fraction; incomplete disruption of the lignin-carbohydrate matrix; generation of high inhibitory compounds |
| Ammonia fiber explosion method (AFEX)    | 90°C for 30 min. 1-2 kg ammonia /kg dry biomass | Increases accessible surface area, removes lignin and hemicellulose  | Do not modify lignin neither hydrolyzes hemicellulose  |
| Ammonia recycle percolation method (ARP) | 150-170°C for 14 min. Fluid velocity 1cm/min    | Increases accessible surface area, removes lignin and hemicellulose  | Do not modify lignin neither hydrolyzes hemicellulose  |
| Ozonolysis                               | Room temperature                                | Reduce lignin content; no toxic residue  | Expensive for the ozone required   |
| Wet oxidation                            | 148-200°C for 10-30 min                         | Efficient removal of lignin; low formation of inhibitors; low energy demand  | High cost of oxygen and alkaline catalyst  |
| Subcritical water                        | 100-374°C for 221 bar 10-30 min                 | Environmentally friendly; increased reaction rate due to enhanced mass and heat transfer; removes lignin and hemicellulose | Lignin recondensation  |

T: Temperature

Lignocellulosic biomass fractionation involves many different technologies usually classified into biological, physical, chemical, and physico-chemical (Kumar et al., 2009) (Table 2-2). The main goal of fractionation is to deconstruct the cell wall matrix to remove or alter the lignin and hemicellulose structures, and to increase the porosity of the cellulose fibers.

### **2.2.1. Biological methods**

In this treatment, microorganisms, such as white, brown and soft rot-fungi are used to degrade hemicellulose and lignin but leave cellulose intact (Sánchez, 2009). This method has some advantages, such as mild operation conditions and low energy requirements; however, the rate of biological hydrolysis is very low. Thus, it requires long processing times of 3-10 days compared to other technologies (Sun and Cheng, 2002). Current efforts are to use biological treatments in combination with chemical treatments.

### **2.2.2. Physical methods**

Various types of physical processes, such as milling, chipping, and extrusion are commonly used to reduce the size and thereby increase the accessible surface area. The energy requirements of these physical treatments are relatively high and depend on the final particle size and biomass characteristics (Brodeur et al., 2011). These methods are too expensive, and they are employed in combination with chemical treatments to improve the process efficiency (Kumar et al., 2009).

### **2.2.3. Chemical methods**

#### ***Acid treatment***

Acid treatment involves the use of concentrated and diluted acids to break the complex structure of the lignocellulosic biomass. However, concentrated acids are toxic, hazardous, highly corrosive and generate waste streams, which makes the process very costly due to the corrosion of equipment and the need for recovery of the acid after the treatment (Sun and Cheng, 2002). Thus, the most widely employed acid is dilute acid to improve the economic feasibility. Dilute sulphuric acid has been commercially used for a wide variety of lignocellulosic biomass, including corn stover (Xu et al., 2009), spruce (Shuai et al., 2010) and switchgrass (Digman et al., 2010) to remove hemicellulose. Other acids have also been applied, such as hydrochloric acid (Wang et al., 2010), phosphoric acid (Zhang et al., 2007), and nitric acid (Himmel et al., 1997). Also, organic acids such as maleic and oxalic acid have been used (Mosier et al., 2001).

Dilute acids often solubilize hemicellulose without affecting lignin and cellulose. Typically, the process employs 0.4-2% (w/v) of acid (mainly sulfuric acid) at temperatures of 130-220 °C to recover hemicelluloses. The hydrolysis might occur from a few minutes to some hours (Esteghlalian et al., 1997; Nguyen et al., 2000; Silverstein et al., 2007). Dilute acid treatment of lignocellulosic biomass results in the production of chemical compounds, such as acetic acid, furfural, or 5-hydroxymethylfurfural (5-HMF) and oligomeric and/or monomeric sugars to be used in the production of bioethanol, depending on the processing conditions (Almazán et al., 2001; Ramos, 2003; Um and van Walsum, 2009). In

addition, acid-soluble lignin could be released from the cell wall matrix into the hydrolysates, which quickly condensate and precipitate in acidic environments (Liu and Wyman, 2003; Shevchenko et al., 1999). The optimum conditions for the treatment depend highly on the targeted sugars and the purpose of the treatment. Acid hydrolysis alone is not enough to obtain relatively pure cellulose, thus, it is generally followed by alkali treatments for removal of lignin.

### ***Alkaline treatment***

Alkaline treatment is used to break the bonds between lignin and carbohydrates (cellulose and hemicellulose) and disrupt the lignin structure. Alkaline solutions (0.05-0.15 g alkali/g lignocellulosic biomass), such as sodium hydroxide, calcium hydroxide (lime) or ammonia are added in batch mode directly to lignocellulosic biomass (Wyman et al., 2005), and as a subsequent treatment to acid hydrolyzed lignocellulosic biomass (Moldes et al., 2002) or before an acid hydrolysis (Parajó et al., 1996) to remove lignin and part of hemicellulose and to efficiently increase the accessibility to cellulose. Alkali treatments can be carried out at ambient conditions with long processing times in the order of hours or days rather than minutes or seconds (Zheng et al., 2009).

Use of an alkali causes swelling, leading to increase the internal surface area, a decrease in the degree of polymerization, and crystallinity with a consequent separation of structural linkages between lignin and carbohydrates and disruption of lignin structure (Carvalho et al., 2008). Then, it is followed by saponification of intermolecular ester bonds crosslinking hemicelluloses and other

components, such as lignin and hemicelluloses (Sun and Cheng, 2002). The effect of the treatment depends on the lignin content of the raw material (McMillan, 1994). In contrast to acid treatments, alkaline-based methods are more effective for lignin solubilization, exhibiting only minor cellulose solubilization (Carvalho et al., 2008).

Sun et al. (1995) studied the effects of different alkaline solutions for the removal of lignin and hemicellulose from wheat straw. They obtained that the optimum condition to remove 60% of lignin and 80% of hemicellulose was using 1.5% sodium hydroxide for 144 h at 20 °C. Xylose was the major component of the hemicellulose fraction obtained in the hydrolysates. Kim and Holtzaple (2005) used lime to treat corn stover in order to remove lignin. Maximum lignin removal of 87.5% was achieved at 55 °C for four weeks with aeration.

### ***Organosolv treatment***

Organosolv processes use an organic or aqueous organic solvent mixture with or without an acid catalyst (HCl or H<sub>2</sub>SO<sub>4</sub>) to break the internal lignin and hemicellulose bonds (Pan et al., 2007; Taherzadeh and Karimi, 2008) to fractionate lignocellulosic biomass. The organic solvents commonly used for this process are ethanol, methanol, acetone, ethylene glycol, triethylene glycol, tetrahydrofurfuryl alcohol, glycerol, aqueous phenol and aqueous *n*-butanol (Chum et al, 1988; Thring et al., 1990). The main benefit of organosolv treatment is that relatively pure lignin (organosolv lignin) can be recovered as a by-product (Hu et al., 2008). However, it is a complex and costly treatment because organic

solvents are expensive and their use requires high pressure equipment due to organic solvents high volatility (Brodeur et al., 2011). Ethanol and methanol have usually been preferred due to their cheaper price compared to other solvents. Solvent recovery is necessary after the treatment to reduce operation costs. Operation temperature is in the range of 150-200 °C. It has been reported that a more selective lignin removal can be achieved when a catalyst is used and less degraded lignin is obtained for further applications (Kin, 1990; Vázquez et al., 1992). However, Aziz and Sarkanen (1989) indicated that no catalyst was required for satisfactory delignification at temperatures above 185 °C.

#### **2.2.4. Physico-chemical methods**

##### ***Steam explosion***

Steam explosion is one of the most common methods for lignocellulosic biomass fractionation. In this process, biomass is heated using high pressure saturated steam in the temperature range of 160-260 °C at corresponding pressures of 6.9-48.3 bar for several seconds to a few minutes, and then the pressure is suddenly released, which makes the materials undergo an explosive decompression, leading to hemicellulose degradation and lignin matrix disruption (Kurabi et al., 2005; Ruiz et al., 2006). The process parameters that affect the steam explosion are residence time, temperature, particle size and moisture content of the lignocellulosic biomass (Sun and Cheng, 2002). Addition of catalysts, such as acid or alkali, have been reported to improve the fractionation (Stenberg et al., 1998, Zimbardi et al., 2007).

During steam explosion, hemicellulose is hydrolyzed by organic acids, such as acetic acids and other acid formed from breaking of acetyl groups or other functional groups, released from lignocellulosic biomass. The acidic nature of water at high temperatures promotes further hydrolysis of the hemicellulose as well (Weil et al., 1997; Cantarella et al., 2006). Degradation of sugars also occur during steam explosion, generating aldehydes like furfural (Garcia-Aparicio et al., 2006).

There are several studies applying steam explosion to lignocellulosic biomass. Lawther et al. (1996) reported that low pressure steam treatment (2 bar, 120 °C, and residence times of up to 300 min) had no detrimental effect on the composition of wheat straw. Varga et al. (2004) applied steam explosion treatment to corn stover and investigated the influence of different processing conditions of temperature (185-195 °C), residence time (5-15 min), and concentration of H<sub>2</sub>SO<sub>4</sub> (2-36.5%, w/w) on sugar yield. They found that steam treatment at 190 °C for 5 min with 2% sulfuric acid resulted in the highest overall yield of sugars, 56 g from 100 g of untreated material, corresponding to 73% of the theoretical amount calculated using equations. However, studies without a catalyst reported sugar recoveries between 45-65% (Heitz et al., 1991). Although steam explosion can effectively open up the lignocellulosic biomass structure, leading to the reduction of particle size and increased pore volume, it leads to low hemicellulose sugar yield along with low lignin removal (Excoffier et al., 1991).

### ***Ammonia fiber explosion (AFEX) and ammonia recycle percolation (ARP)***

The AFEX treatment is conceptually similar to the steam explosion, which can be presented as a combination of steam explosion and alkaline treatment. In this process, lignocellulosic biomass is exposed to liquid ammonia at high temperature and pressure for a period of time, and then the pressure is suddenly released (Teymouri et al., 2005). Typically, an AFEX treatment is performed with 1-2 kg ammonia/kg dry biomass at 90 °C for around 30 min. It simultaneously reduces the lignin content and solubilizes some hemicellulose; however, it does not significantly remove hemicellulose as the acid treatments (Mes-Hartree et al., 1988; Mosier et al., 2005).

The ARP is a flow-through process in which aqueous ammonia is sent through a packed bed reactor, containing the biomass at a certain flow rate. Process parameters are as follows: ammonia concentration, 2.5-20% (typically, 10-15%); reaction time, up to 90 min; solid concentration, 15-30% (w/w); temperature, 140-170 °C; and percolation rate, 5 mL/min (Carvalho et al., 2008). The main advantage of this treatment compared to the AFEX treatment is its ability to remove the majority of the lignin (75-85%) and more than half of the hemicellulose (50-60%) from lignocellulosic biomass (Kim and Lee, 2005). Iyer et al. (1996) used ARP treatment for some herbaceous biomass and indicated the removal of 60-80% and 65-85% lignin from corn stover and switchgrass, respectively. The disadvantage of the AFEX and ARP treatments is that these processes are expensive due to the cost of ammonia and its recovery process (Holtzapfel et al., 1991).

### ***Ozonolysis***

Ozone can be used to fractionate lignocellulosic biomass, especially to remove lignin by attacking and cleaving the aromatic ring structures, while hemicellulose and cellulose are hardly decomposed. It is a powerful oxidant, soluble in water and readily available. Treatments are carried out at room temperature and normal pressure. It has been applied to many lignocellulosic biomass, such as wheat straw (Ben-Ghedalia and Miron, 1981), cotton straw (Ben-Ghedalia and Shefet, 1983), bagasse, green hay, and pine (Neely, 1984). Vidal and Molinier (1988) reported that lignin content of poplar sawdust decreased from 29% to 8% after ozonolysis treatment. A drawback of ozonolysis is that a large amount of ozone is required, which makes the process costly. Morrison and Akin (1990) applied ozone to grasses and identified caproic, levulinic, *p*-hydroxybenzoic, vanillic, azelaic, and malonic acids and aldehydes, such as *p*-hydroxybenzaldehyde, vanillin, and hydroquinone in the hydrolysates.

### ***Wet oxidation***

Wet oxidation utilizes oxygen or air as an oxidizer in combination with water at elevated temperature and pressure (Bjerre et al., 1996). In this treatment, water is added at a ratio of 1 L to 6 g biomass. A pressure of ~12 bar is reached by pumping air into the vessel. In general, the process is carried out at 148-200 °C for 10-30 min (Pedersen and Meyer, 2009). Na<sub>2</sub>CO<sub>3</sub> can be added to the mixture to reduce by-product formation. During treatment, lignin is decomposed to carbon dioxide, water, and carboxylic acids (Banerjee et al., 2009). Lignin removal

ranges from 50% to 70%, depending on the processing conditions of wet oxidation (Brodeur et al., 2011).

#### 2.2.4.1. Subcritical water technology

Subcritical water is a unique and sustainable reaction medium. Recently, there has been a growing interest in using subcritical water as a solvent and reaction medium for lignocellulosic biomass fractionation. Subcritical water is water above its boiling point at ambient pressure ( $>100\text{ }^{\circ}\text{C}$  and 1 bar) and below its critical point of  $374\text{ }^{\circ}\text{C}$  at 221 bar (Murphy and Koop, 2005; Saldaña and Valdivieso-Ramirez, 2015) (Fig. 2-6). Water above its critical point is known as supercritical water. Under these conditions, physical and chemical properties (density, viscosity, dielectric constant, and ionic product etc) of water changes dramatically.

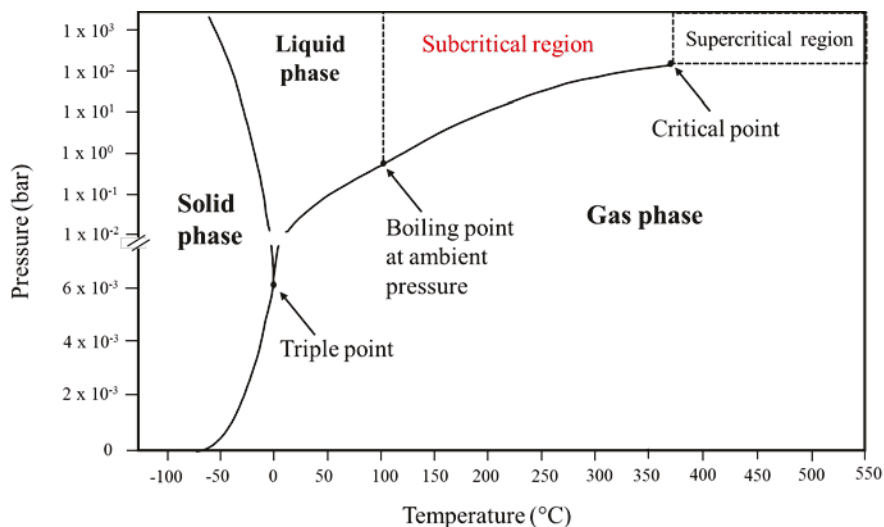


**Figure 2-6.** Phase diagram of water (Adapted from Murphy and Koop, 2005).

Table 2-3 summarizes some physical and chemical properties of sub- and supercritical water different from water at ambient conditions. Sub and supercritical water behave more similar to gases than liquids due to their high diffusion coefficient, thermal conductivity and low viscosity (Table 2-3) (Brunner, 2009; Weingartner and Franck, 2005). Thus, water in the subcritical region makes it an excellent medium for fast, homogeneous and efficient reactions due to its low viscosity, low density and high solubility of organic substances (Kruse and Dinjus, 2007). Decreasing the solvent viscosity leads to an enhanced mass transfer, accelerating any mass transfer-limited chemical reaction. The diffusivity increases by roughly an order of magnitude with the change in density from 1 to 0.1 g/cm<sup>3</sup> (Akiya and Savage, 2002).

Water is a highly polar solvent with a high dielectric constant ( $\epsilon$ ) at room temperature and atmospheric pressure due to the presence of an extensive of hydrogen bonded structure. The dielectric constant ( $\epsilon$ , measure of polarity) of water decreases from 78.5 (25 °C, 1 bar) to 27.1 (250 °C, 50 bar) and 18.2 (330 °C, 300 bar) due to the weakening of hydrogen bonds with increasing temperature, thereby attaining solvent polarities normally associated with polar organic solvents.

**Table 2-3.** Physico-chemical properties of water at different temperatures (L: liquid, G: gas) (Adapted from Moller et al., 2011).

|   | <b>Ambient water</b>                                       | <b>Subcritical water</b>  | <b>Supercritical water</b>  |
|---|--|---|---|
| <b>Temperature (°C)</b>   | 0-100  | 100-374   | >374  |
| <b>Vapor pressure (bar)</b>   | 0.03 (24 °C)   | 1 (100 °C)-221 (374 °C)   | >221  |
| <b>Aggregate state</b>  | Liquid   | Liquid  | no phase separation between gas-like and liquid-like densities, for example, 0.252 (410 °C/300 bar)                           |
| <b>Density (g/cm<sup>3</sup>)</b>                                   | 0.997 (25 °C)  | 0.958 (101 °C/1.1 bar)<br>0.692 (330 °C/300 bar)                        |   |
| <b>Viscosity (mPa s)</b>  | L: 884, G: 9.9 (25 °C)                                     | L: 277, G: 12.3 (101 °C)<br>L: 50.4, G: 30.7 (371 °C)                   | Low   |
| <b>Heat capacity, C<sub>p</sub> (J/g °C)</b>                        | L: 4.2, G: 2.0 (25 °C)                                     | L: 4.2, G: 2.1 (101 °C)<br>L: 69, G: 145 (371 °C)                       | 1300 (400 °C/250 bar)   |
| <b>Dielectric constant, ε</b>                                       | 78.5 (25 °C/1 bar)   | 27.1 (250 °C/50 bar)<br>18.2 (330 °C/300 bar)                           | 5.9 (400 °C/250 bar)<br>10.5 (400 °C/500 bar)   |
| <b>Compressibility</b>  | No   | Slightly increased, but still a liquid at 370 °C                        | Yes   |
| <b>Ionic product, K<sub>w</sub> (mol<sup>2</sup>/L<sup>2</sup>)</b> | 10 <sup>-14</sup> increased to 10 <sup>-12</sup> at 100 °C | Increases from 10 <sup>-12</sup> (100 °C) to 10 <sup>-11</sup> (300 °C) | Strongly decreasing to below 10 <sup>-20</sup> (400 °C) and below 10 <sup>-23</sup> (550 °C); increases slightly with density |

As observed in Figure 2-7, the dielectric constant values of subcritical water resemble those of other less polar solvents at room temperature, such as methanol ( $\epsilon= 32.6$ ) and 1-butanol ( $\epsilon= 17.8$ ) at 25 °C and 1 bar. Thus, under these conditions, water could be used as an environmentally friendly alternative to dissolve medium-polarity and even non-polar organic compounds compared to petrochemical solvents, which are often toxic. In addition, solvent removal is expensive and time-consuming. Water, on the other hand, is ubiquitous, non-toxic and has low disposal cost (Curren and King, 2009).

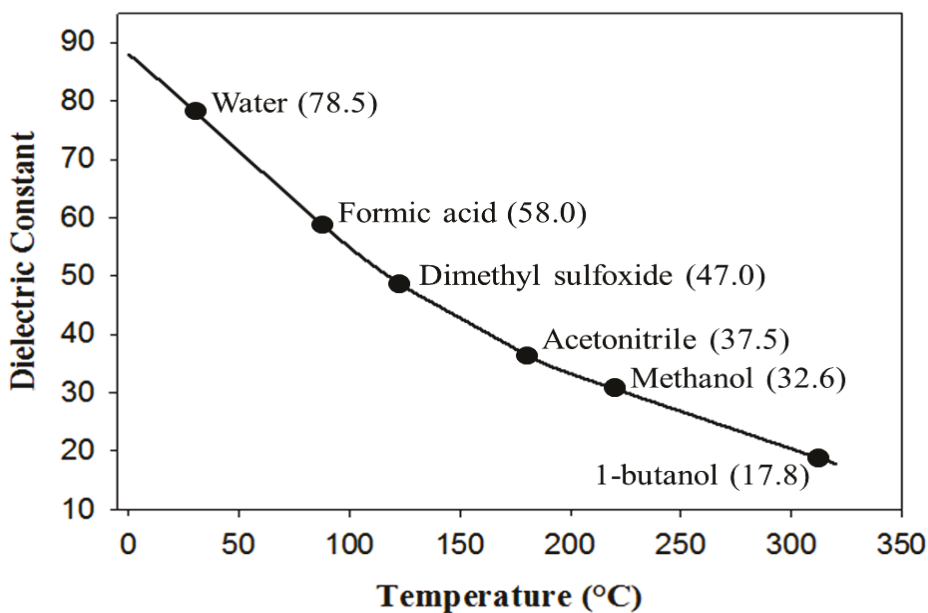


**Figure 2-7.** Dielectric constant of water as a function of temperature at 200 bar. Solid circles on the plot are the values corresponding to different organic solvents at 25 °C and 1 bar (values given in parentheses) (Adapted from Delgado-Zamarreno et al., 2009).

The ionic product ( $K_w$ ) of subcritical water increases with temperature and is 2-3 orders of magnitude ( $10^{-11}$  at 300 °C and 221 bar) greater than that at ambient temperature ( $10^{-14}$ ). The high concentrations of the  $H^+$  and  $OH^-$  ions, resulting from the high  $K_w$  of water facilitate acid- or base-catalyzed reactions in subcritical water, such as hydrolysis of ether and/or ester bonds, and also the extraction of low-molecular-mass products (Kruse and Dinjus, 2007). At temperatures above 300 °C, it starts to decrease with a further increase in temperature. For instance, at a temperature of 400 °C and a pressure of >221 bar,  $K_w$  becomes  $10^{-20}$ . Above the critical temperature (374 °C), the ionic product sharply decreases due to decreasing ion solvation with decreasing density.

Subcritical water differs not only from ambient water but also in some aspects from supercritical water. Supercritical water is compressible, and the properties strongly depend on the pressure. It is miscible with light gases and small organic compounds (Kruse and Gawlik, 2003). Dominant reaction mechanisms shift from those of free radicals to those of ionic through manipulating the water density, which varies greatly with temperature and pressure (Watanabe et al., 2004). The compressibility is still rather low in subcritical water despite the high temperature. The relatively high density combined with the high dissociation constant of subcritical water favors ionic reactions, such as dehydration of carbohydrates and alcohols and aldol splitting reactions (Akiya and Savage, 2002). However, radical reactions dominate at the supercritical region, resulting in gasification (Kruse and Dinjus, 2007).

#### **2.2.4.1.1. Extraction and reaction mechanisms of lignocellulosic biomass in subcritical water**

Hemicelluloses are hydrolyzed much faster than cellulose. Hemicelluloses are easily solubilized and hydrolyzed in subcritical water at temperatures above 180 °C while cellulose decomposition starts at temperatures over 230 °C and 98 bar (Bobleter, 1994). When the process is performed under suitable conditions (temperature, pressure, flow rate and time), the hydronium ions (from water auto-ionization and from *in situ* generated acids) catalyze the breakdown of hemicellulosic polysaccharides, resulting in a number of effects. The cleavage of *O*-acetyl and uronic acid substitutions from hemicellulose produces acetic acid and other organic acids, which help catalyze the hydrolysis of polysaccharide, such as hemicellulose into soluble oligosaccharides first, and then produce monomeric sugars. Under acidic conditions, these monomeric sugars are subsequently partially degraded to aldehydes, such as furfural and 5-HMF.

Subcritical water treatments have been reported to have the potential to increase cellulose digestibility, sugar extraction, and pentose recovery, with the advantage of producing hydrolysates, containing little or no inhibitor (such as furfural and 5-HMF) of sugar fermentation (Kim et al., 2009). Many researchers have attempted to fractionate hemicellulose and lignin from various lignocellulosic biomass with subcritical water technology. Mok and Antal (1992) found that almost 100% of the hemicellulose of various wood and herbaceous plants was hydrolyzed at 230 °C, 2 min and 345 bar using subcritical water treatment. Around 90% of hemicelluloses were recovered as monomeric sugars.

Perez et al. (2008) applied subcritical water to treat wheat straw and obtained maximum hemicellulose-derived sugar recovery and minimum degradation products. After optimization of process variables, such as temperature and residence time, 80% xylose recovery was achieved at 188 °C and 40 min (Perez et al., 2008). Pronky and Mazza (2010) optimized the fractionation of triticale straw using subcritical water technology to maximize hemicellulose and lignin yields, producing also a cellulose rich fraction. They reported that subcritical water was successful in removing 73-78% of the hemicellulose, leaving a cellulose-rich residue of 65% glucose concentration. Lignin was equally distributed between the solid residues and the extracts. The optimum reaction conditions for hemicellulose yield were determined to be 165 °C, with a flow rate of 115 mL/min, and a water-to-solid ratio of 60 mL/g. At these optimum conditions, they fractionated straws from five cereals (triticale, durum wheat, CPS wheat, feed barley, and oats) and two oilseeds (canola, and mustard) with subcritical water technology using a flow-through reactor in another study (Pronk and Mazza, 2012). More than 90% of the xylan and nearly 50% of the lignin were extracted and there was no effect on the yield due to crop species.

Vrije et al. (2002) reported that lignin hydrolysis is catalyzed by alkaline pH. Various phenols and methoxy phenols are formed by hydrolysis of ether-bonds during hydrothermal degradation of lignin. These products can also degrade further by hydrolysis of methoxy groups. Wahyudiono et al. (2007) studied the hydrothermal breakdown of pure lignin at 350-400 °C. The main compounds identified were catechol, phenols, and cresols, which resulted from

the secondary hydrolysis of methoxy groups. Karagoz et al. (2005) also obtained phenolic compounds (2-methoxy-phenol, 1,2-benzenediol, 4-methyl-1,2-benzenediol, 3-methyl-1,2-benzenediol and phenol) from subcritical water treatment of commercial lignin at 280 °C for 15 min.

### **2.3. Nanocelluloses**

The term nanocelulose generally describes the cellulosic materials in which at least one of the dimensions of the fiber is on the nanoscale. There are basically two main classifications of nanocelluloses obtained from lignocellulosic biomass, depending on the basis of their dimensions, functions, and production methods: cellulose nanofibers and nanocrystals. Different terminologies are interchangeably used in the literature to describe these cellulose nanoparticles.

As the world's most abundant renewable resource, lignocellulosic biomass has a great potential for sustainable nanocellulose production. Therefore, cellulose isolation from lignocellulosic biomass to prepare nanocelluloses has attracted recent attention due to a number of desirable characteristics of nanocelluloses. These characteristics include high aspect ratio (length to diameter ratio), low thermal expansion, good mechanical and optical properties, low weight, low density and biodegradability, which may lead to many applications in nanocomposites, paper reinforcement, coating additives, food packaging, tissue engineering scaffolds, filtration media, thickening agents, rheology modifiers, adsorbents, etc (Fukuzimi et al., 2009; Nakagaito et al., 2010; Belbekhouche et al., 2011; Abdul Khalil et al., 2012; Brinchi et al., 2013).

Being the smallest structural unit of plant fiber, cellulose nanofibers, otherwise known as cellulose nanofibrils, microfibrillated cellulose or nanofibrillated cellulose, are formed by a bundle of stretched cellulose chain molecules composed of crystalline and amorphous domains (Sakurada et al., 1962) with long, flexible and entangled cellulose nanofibers. They are typically in the range of 5-100 nm diameter and have lengths of a few microns since nanofibers usually consists of aggregates of cellulose microfibrils (Svagan et al., 2007). However, the structure of cellulose nanocrystals, otherwise known as cellulose nanowhiskers, nanocrystalline cellulose or crystal of cellulose, is characterized by primarily crystalline domains of cellulose chains produced by chemical treatments such as acid hydrolysis (e.g. sulfuric acid or hydrochloric acid) and range from 2 to 20 nm in diameter, with a length of 100 nm to several micrometers. They have low aspect ratio (length/diameter) and limited flexibility due to the absence of amorphous regions (Chakraborty et al., 2006).

Cellulose nanofibers can generally be produced by the combination of different methods. In general, lignocellulosic biomass is treated by various physical, chemical, and/or physico-chemical methods before mechanical treatments to remove matrix components, such as hemicellulose and lignin, and to obtain purified cellulose as described previously in Section 2.2. The treatments need to be carefully controlled to avoid undesirable cellulose degradation (Wang and Sain, 2007).

### **2.3.1. Production methods of cellulose nanofibers**

#### ***Mechanical treatments***

The production of nanofibers by fibrillation of cellulose fibers into nano-sized elements requires intensive mechanical treatments. Many different mechanical approaches have been developed, such as high pressure homogenization, the use of microfluidizers, super grinding/refiner-type treatments, combinations of beating, rubbing, cryogenic crushing, and high intensity ultrasonication in various combinations (Table 2-4).

High pressure homogenization has been the most widely used method to obtain cellulose nanofibers. Such materials were first obtained by Herrick et al. (1983) and Turbak et al. (1983) using high pressure homogenization. Their method includes passing cellulosic wood pulp suspensions through a high pressure homogenizer at 550 bar. The resulting gels consisted of strongly entangled and disordered networks of nanofibers.

During the homogenization process, the dilute slurries of cellulose fibers are pumped at high pressure into a vessel through a very small nozzle (Frone et al., 2011). Subjecting cellulose fibers to a large pressure drop with shearing and impact forces promotes high degree of fibrillation of the fibers and results in the release of nanofibers (Siro and Plackett, 2010). Zhang et al. (2012) obtained cellulose nanofibers from bleached kraft bamboo pulp using chemical pretreatment and high pressure homogenization.

**Table 2-4.** Examples of production methods of cellulose nanofibers.

| <b>Raw material</b>          | <b>Treatment</b>  | <b>Mechanical treatment</b>  | <b>Width (nm)</b> | <b>Reference</b>              |
|------------------------------|---|--|-------------------|-------------------------------|
| Bleached kraft pulp          | Enzymatic (by fungus OS1)   | High shear refining, cryocrushing/disintegrator                        | 10-75             | Janardhnan and Sain (2006)    |
| Softwood pulp                | Enzymatic (endoglucanase)/TEMPO-mediated oxidation                                    | High shear refining/high pressure homogenization                       | 5-20              | Pääkkö et al. (2007)          |
| Soybean stock                | Alkaline (NaOH)/acid (HCl)  | Cryocrushing/high pressure defibrillation                              | 50-100            | Wang and Sain (2007)          |
| Wheat straw and soy hulls    | Alkaline (NaOH)/acid (HCl)  | Cryocrushing/high pressure defibrillation/high pressure homogenization | 30-40             | Alemdar and Sain (2008)       |
| Wheat straw                  | Alkaline (NaOH)/acid (HCl)/bleaching (H <sub>2</sub> O <sub>2</sub> )/steam explosion | High pressure homogenization   | 10-50             | Kaushik and Sing (2011)       |
| Poplar wood                  | Alkaline (KOH)/bleaching (acidified NaClO <sub>2</sub> )                              | Ultrasonication  | 5-20              | Chen et al. (2012)            |
| Softwood bleached kraft pulp | Alkaline (NaOH)/bleaching (acidified NaClO <sub>2</sub> )/TEMPO-mediated oxidation    | Ultrasonication  | ~3                | Tanaka et al. (2014)          |
| Banana rachis                | Alkaline (KOH)  | Grinding/ High pressure homogenization                                 | 10-40             | Velásquez-Cocka et al. (2016) |
| Bamboo parenchymal cells     | Alkaline (KOH)/bleaching (acidified NaClO <sub>2</sub> )                              | Ultrasonication  | 30-50             | Wang et al. (2016)            |

TEMPO: 2,2,6,6-Tetramethylpiperidin-1-yl)oxyl

Zhang et al. (2012) studied the effect of sodium hydroxide dosage and homogenization times on water retention value (WRV) of nanofibers. Their results revealed that there was a linear relationship between the dosage of sodium hydroxide and the WRV of nanofibers. It was found that the WRV and the degree of fibrillation of fiber was increased when the number of high pressure homogenization treatments was increased. Kaushik and Sing (2011) isolated cellulose nanofibers from wheat straw using alkaline steam explosion followed by chemical and high shear homogenization. They obtained nanofibers of 30-50 nm in width with improved thermal stability. Degree of polymerization decreased from 2609.7 for steam exploded wheat straw to 266.9 for cellulose nanofibers. Homogenizers were widely used by other researchers as well to obtain nanofibers (Besbes et al., 2011; Dufresne et al., 2000; Hassan et al., 2011; Henriksson et al., 2007; Iwamoto et al., 2005; Liimatainen et al., 2014; Nakagaito and Yano, 2004). However, the main issue of homogenization is the clogging of the system, which is a challenge for upscaling such a process (Spence et al., 2011).

Some researchers have used commercial grinders with specially designed disks to isolate cellulose nanofibers. In such equipment, the cellulose slurry is passed between a static grind stone and a rotating grind stone, revolving at ~1500 rpm. The process consists of breaking the cellulose wall structure due to shear forces generated by the grinding stones. Thereby, cellulose nanofibers are individualized from the pulp (Taniguchi and Okamura, 1998). Iwamoto et al. (2007) obtained nanofibers of 50-100 nm in diameter from softwood by treating homogenized cellulosic pulp in a grinder up to 10 repetitions.

Cryocrushing is another process for the preparation of nanofibers in which cellulose fibers are frozen using liquid nitrogen and then crushed by applying high shear forces (Chakraborty et al., 2005). Rupturing of cell walls and releasing of nanofibers occur by the application of high impact forces to the frozen cellulosic fibers due to the exerted pressure by ice crystals (Wang and Sain, 2007). Alemdar and Sain (2008) isolated nanofibers from wheat straw and soy hulls via chemo-mechanical treatments, involving cryocrushing followed by fibrillation and subsequent homogenization. Their results indicated that almost 60% of the nanofibers had a diameter within a range of 30-40 nm and lengths of several thousand nanometers. In another study, nanofibers having a diameter in the range of 50-100 nm were produced from soybean stock using cryocrushing method by Wang and Sain (2007).

Recently, an ultrasonication method has been successfully applied for the fibrillation of cellulose fibers into nanoscale by a number of researchers (Chen et al., 2011; Cheng et al., 2007; Cheng et al., 2009; Wang and Cheng, 2009; Wang, et al., 2016). This treatment consists in exposing a liquid to ultrasonic waves (>20 kHz), which results in the vibration of exposed fibers as they experience high-pressure and low-pressure cycles, creating microscopic vacuum bubbles or voids in the liquid (cavitation) (Cheng et al., 2009). Such hydrodynamic shear forces lead to disruption of molecular interactions of cellulose fibers and individualization of microfiber bundles into the solution. Chen et al. (2012) obtained cellulose nanofibers from poplar wood using chemical pretreatments and high intensity ultrasonication. They found that the diameter distributions of the

resulting nanofibers were dependent on the output power of the ultrasonic treatment. Cellulose nanofibers that are 5-20 nm in width and several microns in length were obtained when the output power of the ultrasonication was greater than 1000 W. Wang et al. (2016) isolated cellulose nanofibers via an ultrasonication process of chemically (acid/alkali) pretreated parenchymal cells of bamboo. The effect of time on fibrillation was studied in the range of 10-80 min (19.5–20.5 kHz, energy supply was below 30% of the maximum power output). Films of cellulose nanofibers were produced with vacuum filtration and air-drying of nanofiber suspensions and their mechanical properties were evaluated. Optimum ultrasonication time of 40 min was reported to obtain high-quality films. The results demonstrated that ultrasonication route is promising for easy fibrillation of parenchymal cells of bamboo and for energy saving during production of high quality nanofibers at large scale.

### ***Surface modification of cellulose***

To achieve better fibrillation during mechanical treatments, surface modifications of cellulose fibers, such as oxidation and carboxymethylation, have been employed by some researchers to add ionic groups on the surface of fibers (Besbes et al., 2011; Hubbe et al., 2008; Wagberg et al., 2008). These processes make the fibers highly charged and easier to liberate during mechanical fibrillations. In the oxidation process, cellulose fiber suspension is oxidized by 2,2,6,6-tetramethylpiperidine-1-oxyl radical (TEMPO) with NaClO as a primary oxidant and NaBr as an additional catalyst at a pH of 10-11. This method

selectively introduces carboxyl (acidic) groups at the C6 of the glucose unit (Saito et al., 2006). Besbes et al. (2011) used TEMPO oxidation under neutral conditions for cellulose fibers of alfa alfa, pine and eucalyptus with the carboxyl content up to 500  $\mu\text{mol/g}$  and cellulose nanofibers with diameters in the range of 5-20 nm. In the carboxymethylation process, the surface of cellulose fibers was negatively charged promoting the formation of stable suspension from carboxymethylated fibers and improving the degree of fibrillation into nanosize (Hubbe et al., 2008). Cellulose nanofibers with diameters of 5-15 nm were obtained by passing carboxymethylated cellulose fibers through a high pressure homogenizer (Wagberg et al., 2008). The procedure involves a step of solvent exchange from water to ethanol, impregnation of monochloroacetic acid by sodium hydroxide addition to the mixture of methanol and isopropanol. Thus, the main drawback is the use of organic solvents due to environmental concerns.

### **2.3.2. Gelation behavior of cellulose nanofiber suspensions**

Cellulose nanofibers are usually produced in the form of aqueous suspensions. As native cellulose has a highly hydrophilic nature, cellulose nanofibers are able to retain a large amount of water. Thus, aqueous suspensions of cellulose nanofiber are known to exhibit gel-like properties due to the formation of an entangled network structure attributed to the high aspect ratio and the high specific surface area of the nanofibers (Lasseguette et al., 2008; Pääkkö et al., 2007). Characteristics of the suspensions might vary depending on the production methods of cellulose nanofibers.

The rheological behavior is one of the key characteristics of cellulose nanofibers suspensions, which can influence various processes, such as pumping, mixing or coating. Regardless of the pretreatment and/or fibrillation methods, all types of cellulose nanofibers suspension exhibit shear thinning properties, i.e., their viscosity decreases while shear rate increases. They also show thixotropic behavior (time-dependent shear thinning property). When a steady shear rate is applied, their viscosity decreases, reaching an equilibrium level, and viscosity recovers when the shear rate is reduced to zero.

Cellulose nanofibers in water easily form hydrogel structures, i.e., materials composed mainly by water that is contained in a hydrophilic polymeric network (Hoffman, 2002). Such hydrogels have a great potential for applications in such fields as tissue engineering, including scaffolds to store human cells, drug delivery, sorbents, sensors, contact lenses and water purification (Dong et al., 2013; Klouda and Mikos, 2008; Lee and Mooney, 2001).

Self-standing cellulose nanofiber hydrogels were reported by some researchers with the treatment of cellulose nanofiber suspensions with acid (Saito et al., 2011) and alkaline media (Abe and Yano, 2011), or using cross-linking agents like metal cations (silver nanoparticles) (Dong et al., 2013). Saito et al. (2011) reported the formation of hydrogels from TEMPO-oxidized cellulose nanofibers by lowering the pH to  $\sim 2$  with the addition of dilute hydrochloric acid (0.1 M) to the suspensions at concentrations of 0.4 wt.%. Lowering of pH to low values induced higher interfibrillar interactions due to the reduction of electrostatic repulsion between fibers with the protonization of the carboxylate

groups. Two self-standing hydrogel types with different crystal forms, namely cellulose I and cellulose II, were produced by Abe and Yano (2011) from mechanically disintegrated cellulose nanofiber suspensions using alkali treatments followed by neutralization. They reported that formation of cellulose II hydrogel using above 12 wt.% sodium hydroxide solution was due to the cellulose shrinkage and coalescence as a result of mercerization. However, hydrogel formation at lower concentrations before mercerization threshold was attributed to the swelling of the fibers, thus the improvement of cellulose nanofiber entanglement and, some aggregation as well.

Such cellulose nanofiber suspensions/hydrogels can be further converted to other cellulose nanofiber forms like aerogels via suitable drying methods.

#### **2.3.2.1. Cellulose nanofiber aerogels**

Aerogels are ultralight and highly porous materials typically produced by drying the wet gel to remove the trapped liquid without collapsing the network (Hüsing and Schubert, 1998). As a result of such unique microstructures, aerogel materials exhibit many attractive properties, such as high porosity, high specific surface area, ultra-low density, low thermal conductivity, low dielectric permittivity and excellent shock absorption capacity. As their porosities, densities and specific surface areas vary greatly depending on the starting material, they have a wide range of applications in different fields, such as aeronautics, biomedicine, construction, agriculture and environmental remediation (Akimov, 2003).

The first aerogel made of silicon dioxide was fabricated by Kistler in 1931 (Kistler, 1931). Since then, many different kinds of aerogel materials have been prepared from silica, metal oxides, polymers and pyrolyzed polymers (carbon aerogels) (Pierre and Pajonk, 2002). The most common aerogels have been inorganic that are prepared by sol-gel polymerization of metal oxides (Meng et al., 1997; Pierre et al., 1999). Even though they have a high compressive strength, a typical problem has been their fragility. Various types of organic aerogels have also been formed with the resorcinol/formaldehyde and melamine/formaldehyde, which are the most common precursor mixtures for forming the organic network (Gross and Fricke, 1992; Nguyen and Dao, 1998).

Recently, aerogels based on cellulose nanofibers have received great attention due to the renewability, biodegradability, biocompatibility and abundance of cellulose. As a result of high modulus and high strength of native cellulose I structure combined with high aspect ratio and high surface area of nanofibers, they offer the advantage of increased flexibility and ductility compared to traditional aerogels. Furthermore, such materials are of special interest for medical, cosmetic, pharmaceutical, and other applications where biocompatibility and biodegradability are needed (Aulin et al., 2010; Pääkkö et al., 2008).

Aerogel processing starts with the formation of a gel from an aqueous solution (i.e., a hydrogel). Generally, a cross linker, which can be of chemical (a cross linker compound such as sodium trimetaphosphate and calcium chloride) or physical (pH, temperature, etc.) nature, is required to induce gel formation.

Crosslinkers are not required in the gelation of cellulose nanofiber suspensions. The aqueous cellulose nanofiber gel is formed due to the intramolecular hydrogen bonding and the long and entangled nanofiber network. Then, “sponge-like” aerogels are developed by replacing the liquid in the gel by air via suitable drying method without collapsing the network structure.

Freeze-drying is one route for the preparation of cellulose nanofiber aerogels, where the solvent in the gel is removed without entering the liquid state. Basically, the process involves two major steps, which are growth of ice crystals (freezing) and sublimation of the water molecules in a temperature range from -20 °C to -50 °C at a lower pressure than that of the triple point of the water (Vorona et al., 2012).

The first report on aerogels based on cellulose nanofibers was made by Pääkkö et al. (2008), who investigated the influence of the two different freeze-drying methods, cryogenic and vacuum, on the formation of aerogels from 2 wt.% aqueous cellulose nanofiber suspension, which were obtained by enzymatic pretreatment and fibrillation of softwood pulp. Aerogels with a density of 0.02 g/cm<sup>3</sup> and porosity of 98-98.7% were obtained. Cryogenic freeze-drying gave a specific surface area of 70 m<sup>2</sup>/g, while the vacuum freeze-drying resulted in a lower value of 20 m<sup>2</sup>/g. Similar freeze-drying methods have been applied to obtain cellulose nanofiber aerogels by a number of researchers (Aulin et al., 2010; Chen et al., 2011, Sehaqui et al., 2010). Aerogels from carboxymethylated cellulose nanofiber suspensions of various concentrations (0.0031-3.13 wt.%) were prepared by Aulin et al. (2010). Specific surface areas of 11 and 15 m<sup>2</sup>/g

were reported for the cellulose nanofiber aerogels with densities of 0.030 and 0.020 g/cm<sup>3</sup>, respectively, after complete water removal through freeze-drying.

Ultralight and highly flexible cellulose nanofiber aerogels were obtained by freeze-drying of hydrogels of cellulose nanofibers isolated from wood with high water uptake behavior. The density of aerogels obtained from 0.1 to 1.5% cellulose nanofiber hydrogels varied between  $1.3 \times 10^{-3}$  and  $17.0 \times 10^{-3}$  g/cm<sup>3</sup>, with the water uptake capability ranging from 155 to 54.

Sehaqui et al. (2011) carried out solvent exchange to *tert*-butanol prior to freeze drying to reduce the extent of cellulose nanofiber aggregation during sublimation of water. Aerogels based on wood pulp cellulose nanofibers (1 wt.% cellulose nanofiber in aqueous suspension) were prepared with the specific surface area as high as 153-284 m<sup>2</sup>/g. Saito et al. (2011) proposed another route where aqueous suspensions of wood cellulose nanofibers were converted to self-standing hydrogels, which involved addition of 0.1 M HCl onto an aqueous cellulose nanofiber dispersion (until reaching pH ~2) and adsorption of toluidine blue. Then, cellulose nanofiber aerogels were prepared by freeze drying of cellulose nanofiber hydrogels (0.4-0.8 wt.%) after solvent exchange with *tert*-butanol. They obtained very large surface areas of 338-349 m<sup>2</sup>/g compared to previous studies and ultra-low densities of 0.0051-0.0097 g/cm<sup>3</sup> with elastic moduli of 64-135 kPa and yield stresses of 7-20 kPa, which were comparable to those reported for tough cellulose aerogels (Sehaqui et al., 2010). Wan et al. (2015) also used *tert*-butanol freeze drying to obtain hydrophobic cellulose nanofiber aerogels isolated from coconut shell, which included chemical

treatment and ultrasonic isolation. The low bulk density of  $0.00084 \text{ g/cm}^3$  was achieved with a much lower specific surface area of  $9.1 \text{ m}^2/\text{g}$  and pore volume of  $0.025 \text{ cm}^3/\text{g}$ . After the hydrophobic modification by methyl trichlorosilane, the cellulose nanofiber aerogels showed high water repellency properties, an ultra-strong oil adsorption capacity and superior oil-water separation performance. The absorption capabilities of the hydrophobic cellulose nanofiber aerogels were as high as 296-669 times their own weights for various organic solvents and oil, which might find application to deal with chemical leaks and oil spills.

Supercritical drying has been the most widely used method for the preparation of aerogels, providing high porosity and superior textural properties of the wet gel in a dry form. For supercritical drying of polysaccharide based aerogels, supercritical carbon dioxide ( $\text{SCCO}_2$ ) is the most appropriate fluid due to its mild critical point conditions ( $74 \text{ bar}$  and  $31 \text{ }^\circ\text{C}$ ).  $\text{SCCO}_2$  drying avoids the formation of a surface tension and shrinkage of the material as the formation of liquid-vapor interfaces in the pores of the material is prevented during drying (Pierre and Pajonk, 2002).

Aerogel formation with  $\text{SCCO}_2$  drying of the hydrogel starts with a solvent exchange step. Due to the low affinity of water to  $\text{SCCO}_2$ , the solvent exchange step, which is the replacement of the water contained in the pores of the hydrogel with a suitable liquid solvent, is required (Diamond and Akinfiev, 2003). The solvent exchange can be conducted by either one step soaking via placing the gel directly in the new solvent (with high solubility in  $\text{CO}_2$ ) or by following multi-step soaking in different water-to-new solvent mixtures with increasing

concentration of the new solvent after a certain time with each step (Robitzer et al., 2008). Thereby, an ‘alcogel’ is formed after the solvent (usually ethanol or acetone) exchange step. Then, the alcohol is extracted from the gel by SCCO<sub>2</sub> drying forming the aerogel structure.

SCCO<sub>2</sub> drying has been successfully applied for the preparation of polysaccharide-based aerogels, such as starch (Kenar et al., 2014; Mehling et al., 2009),  $\beta$ -glucan (Comin et al., 2012), agar (Brown et al., 2010), pectin (García-González et al., 2015), chitin (Tsiptsias et al., 2009), chitosan (Robitzer et al., 2011) and cellulose (Ayadi et al., 2016; Gavillon and Budtova, 2011) with the specific surface area of 100-600 m<sup>2</sup>/g, density of 0.001-0.5 g/cm<sup>3</sup> and porosity of 86-99%. However, there are only a few studies that reported the production of cellulose nanofiber aerogels using SCCO<sub>2</sub> drying (Korhonen et al. 2011; Sehaqui et al., 2011). Korhonen et al. (2011) obtained cellulose nanofiber aerogels (from never-dried hardwood kraft pulp with 1.7 wt.% aqueous suspension) either by freeze-drying in liquid nitrogen or liquid propane or by SCCO<sub>2</sub> drying to prepare aerogel templates with the purpose of producing inorganic hollow nanotube aerogels by atomic layer deposition onto such templates. The values of properties of aerogels like density and specific surface area have not been reported; however, they reported that, in contrast to freeze-drying, SCCO<sub>2</sub> drying produces aerogels without major interfibrillar aggregation.

In summary, cellulose nanofiber aerogels offer a superior alternative to traditional aerogels in terms of renewability and mechanical properties. Understanding the effects of the different variables involved in the formation of

the aerogels (such as the drying method, the source and/or surface charge of cellulose nanofibers, the solvent used to replace water and the concentration of the starting suspensions) provides better control on the final aerogel properties including density, morphology, specific surface area and porosity, and influence its final application.

#### **2.4. Conclusions**

Lignocellulosic biomass has a great potential for sustainable cellulose nanofiber production, owing to its renewability, biodegradability, and abundance. Fractionation of lignocellulosic biomass using subcritical water technology offers an environmentally friendly alternative to isolate cellulose fibers, which then can be fibrillated into nanofibers using mechanical treatments. Conversion of cellulose nanofiber suspensions/hydrogels to other cellulose nanofiber forms like aerogels via suitable drying methods is a promising alternative to traditional aerogels with a wide range of applications in different fields, such as aeronautics, biomedicine, construction, agriculture, and environmental remediation.

## **Chapter 3. Hydrolysis of sweet blue lupin hull using subcritical water technology\***

### **3.1. Introduction**

Lignocellulosic biomass refinery approach is currently gaining significant prominence not only for the minimization of environmental impact, but also for the rational utilization of natural biomass resources. This implies the fractionation of major lignocellulosic biomass components (cellulose, hemicellulose, and lignin) to yield a wide range of valuable products that can replace petroleum-derived products. Among the major components, the separation of the hemicellulose fraction, which may find broader use for chemicals, fuel, and food applications has been proposed as the first stage of lignocellulosic biomass refineries.

Hemicelluloses are branched polysaccharides, associated in plant cell walls with cellulose and lignin. They are comprised of a wide variety of sugar residues, such as xylose, arabinose, glucose, galactose, and mannose depending upon the source. The expanding range of hemicellulosic sugar applications includes products for the food industry and the pharmaceutical industry as novel sweeteners, prebiotics, gels, films, coatings, adhesives, and stabilizing and viscosity-enhancing additives (Ebringerova, 2005). Bioconversion of hemicelluloses into ethanol by fermentation is another valuable application (Krishna et al., 2000). Several processes have been developed to fractionate hemicellulose from lignocellulosic biomass. These processes include dilute acid

---

\*A version of this chapter has been published. Ciftci, D. and Saldaña, M.D.A. (2015). Hydrolysis of sweet blue lupin hull using subcritical water technology. *Bioresource Technology*, 194:75-82.

hydrolysis, alkaline treatment, organosolv process, steam explosion, and subcritical water treatment.

Subcritical water treatment is attracting considerable attention as an environmentally friendly technology because it avoids the use of toxic chemicals and neutralization of high volumes of sludges (Brunner, 2009). Subcritical water has unique properties as described in Chapter 2, Section 2.2.4.1. Many researchers have attempted to fractionate hemicellulose from various lignocellulosic biomass with subcritical water technology (Mok and Antal, 1992; Perez et al. 2008; Pronky and Mazza, 2010; 2012). Mok and Antal (1992) found that almost 100% of the hemicellulose of various wood and herbaceous plants was hydrolyzed at 230 °C and 345 bar for 20 min using subcritical water treatment. Perez et al. (2008) applied subcritical water at 188 °C, 1/10 solid-to-liquid ratio and 40 min in a batch system to treat wheat straw and obtained maximum hemicellulose-derived sugar recovery of 80%, with minimum sugar degradation products like furfural. Pronky and Mazza (2010) studied optimization of the fractionation of triticale straw using subcritical water technology to obtain a cellulose-rich fraction. They reported that subcritical water was successful in removing 73-78% of the hemicellulose, leaving a cellulose rich residue (65% glucose concentration). The optimum reaction conditions for efficient hemicellulose yield were determined to be 165 °C, with a flow rate of 115 mL/min, and a solvent-to-solid ratio of 60 mL/g. At these optimum conditions, they fractionated five cereals (triticale, durum wheat, CPS wheat, feed barley, and oats) and two oilseeds (canola and mustard) straws with subcritical water using a flow-through reactor (Pronky and

Mazza, 2012). More than 90% of the xylan was extracted, and there was no significant effect on the yield due to crop species utilized.

Sweet blue lupin (*Lupinus angustifolius*) is a high-protein legume finding applications mainly in bakery products as well as in dietary and functional food products as a valuable ingredient. One unique aspect of lupin hull is its low lignin content, which facilitates access to the hemicellulose fraction (Bailey et al., 1974). Thus, lupin hull can be used as an ideal feedstock for hemicellulosic sugar production. To the best of the authors's knowledge, there is no reported study on the hydrolysis of lupin hull using subcritical water technology. Research on the fractionation of lupin hulls is needed for their exploitation according to the lignocellulosic biomass refinery concept. Therefore, the main objective of this study was to optimize the process conditions for maximum hemicellulosic sugar yield from lupin hull using subcritical water technology. The effects of process parameters, such as pressure (50-200 bar), temperature (160-220 °C), flow rate (2-10 mL/min) and pH (2-12) on hemicellulose removal were studied. X-ray diffraction (XRD), thermo-gravimetric (TG) and scanning electron microscopy (SEM) analyses of subcritical water treated lupin hulls at optimum conditions were performed to investigate the impact of treatment on the structure.

## **3.2. Materials and methods**

### **3.2.1. Raw material**

Sweet blue lupin hulls were kindly provided by Ceapro Inc. (Edmonton, AB, Canada). Hulls were ground in a centrifugal mill (Retsch, Haan, Germany) to

obtain a powder with maximum particle size of 1.0 mm, then vacuum packed and stored at -20 °C. The particle size range was selected based on the National Renewable Energy Laboratory (NREL) procedure (Sluiter et al., 2008) as deviation to a smaller particle size could result in a low bias in carbohydrate content due to excessive sugar degradation. On the other hand, deviation to a larger particle size may also result in a low bias in carbohydrate content because of incomplete hydrolysis of polymeric sugars.

All sugar standards (D(+)glucose, D(+)xylose, D(+)galactose, L(+)arabinose, and D(+)mannose with a purity of  $\geq 96\%$ ) were obtained from Sigma Aldrich (St. Louis, MO, USA). All other chemicals and solvents, including sulfuric acid were of analytical grade and obtained from Fisher Scientific (Fair Lawn, NJ, USA).

### **3.2.2. Proximate compositional analysis**

Moisture content was determined gravimetrically by drying the hulls in an air oven at 105 °C for 16 h. The ash content of the hulls was determined according to the NREL procedure at a muffle furnace set to  $575 \pm 25$  °C (Sluiter et al., 2005). The protein content was determined using a Leco nitrogen analyzer (Model FP-428, Leco instruments Ltd., Mississauga, ON, Canada). The protein content was calculated using a conversion factor of 6.25. The fat content was determined by Soxhlet extraction using a Goldfish extraction unit (Labconco Co., Kansas, MO, USA) with hexane for 6 h.

### 3.2.3. Hydrolysis in subcritical water

A semi-continuous flow type subcritical water system similar to the one reported by Singh and Saldaña (2011) was used in this study. The system consisted of a high performance liquid chromatograph (HPLC) pump (Gilson 307, Villiers-le-Bel, France), a pre-heater, a stainless steel high pressure vessel, a digital pressure gauge, a cooling system (Swagelok, Solon, Ohio, USA), an oven (Binder, Bohemia, NY, USA) and a back pressure regulator (Tescom, Elk River, MN, USA). Distilled water was first degassed and then delivered with the HPLC pump at varying flow rates to the preheating section. Then, it was passed through the vessel (2.54 cm ID x 10 cm length, capped with a 20  $\mu\text{m}$  stainless steel frit at the inlet and outlet) preloaded with the mixed sample (3 g) and glass beads (39 g). The pressure of the system was maintained constant using the back pressure regulator. The system was heated by the oven and its temperature was monitored by a digital thermometer. The extracts (200 mL) were collected in vials after flowing through the cooler placed after the vessel. Solvent to feed ratio (200/3, mL/g) was determined based on a preliminary study. The experiments were conducted at temperatures of 160-220  $^{\circ}\text{C}$ , pressures of 50-200 bar, flow rates of 2-10 mL/min, and initial pH levels of 2-12. The desired initial pH of water supply was achieved by addition of small amounts of acetic acid or sodium hydroxide for the acidic or basic pH conditions, respectively. The changes in pH values after treatments were also recorded. All experiments were performed at least in duplicates. The solid residue left in the high pressure vessel after each experiment

was dried in an oven at 40 °C. Liquid extracts and solid residues were then stored at -20 °C for further analysis.

### **3.2.4. Analytical methods**

#### **3.2.4.1. Total phenolic content**

Total phenolic content of extracts was determined by Folin-Ciocalteu method (Singleton and Rossi, 1965) that measures the capacity of a compound to reduce the Folin reagent. Briefly, 40 µL of sample was mixed with 3.1 mL of water. Then, 200 µL of Folin-Ciocalteu reagent was added and allowed to withstand for 5 min. Sodium carbonate (20% w/v; 600 µL) was then added to the mixture. After shaking, the mixture was incubated for 90 min in dark at room temperature (21 °C). The absorbance of the samples at 765 nm was measured against the blank using a spectrophotometer (Genova MK3, New Malden, Surrey, UK). The total phenolic content was determined using a gallic acid standard calibration curve. The results were expressed as milligrams of gallic acid equivalent per gram of hull.

#### **3.2.4.2. Total organic carbon analysis**

Total organic carbon (TOC) contents of the extracts were analyzed using a TOC-V instrument (Shimadzu, Columbia, MD, USA). In TOC analysis, the samples were ignited at 720 °C on a platinum based catalyst, and the carbon dioxide formed was swept by pure oxygen through a non-dispersive infrared detector. Samples were flash combusted under helium in the presence of oxygen

and the resulting carbon dioxide gas was separated by chromatography and detected quantitatively by thermal conductivity detector.

### **3.2.4.3. Hemicellulose, cellulose and lignin analysis**

Raw material and solid residues were analyzed for lignin and structural carbohydrates (hemicellulose and cellulose) according to the NREL standard analytical procedures (Sluiter et al., 2008). Acid insoluble lignin and acid soluble lignin contents were determined by treating samples with 72% sulfuric acid for 1 h in a water bath at 30 °C, and then diluting to 4% sulfuric acid and autoclaving at 121 °C for 1 h. Acid insoluble lignin was determined gravimetrically after the filtration of the hydrolysate. Acid soluble lignin in the hydrolysate was determined by the spectrophotometric method at 320 nm. The results for lignin content of the samples were reported as the sum of the acid insoluble lignin and acid soluble lignin.

Total hemicellulosic sugars (xylose, galactose, arabinose, and mannose) and cellulosic sugar (glucose) in the hydrolysate were determined using an HPLC system consisted of a Shimadzu LC-20AT pump (Shimadzu Co., Kyoto, Japan) equipped with an autosampler (SIL-9A), an ultraviolet (UV) detector (Waters 486, Milford, MA, USA) and a Shodex sugar SP0810 column (300 mm×8 mm; Phenomenex, Torrance, CA, USA) operated at 80 °C. HPLC grade water was used as the mobile phase at a flow rate of 0.6 mL/min. The sugar concentrations were determined by comparison against a set of known sugar standards.

Liquid extracts obtained from subcritical water treatment were analysed for total hemicellulosic sugars (xylose, galactose, arabinose, and mannose) following the NREL standard analytical procedures (Sluiter et al., 2006). Total hemicellulosic sugars were determined after post acid hydrolysis with 4% sulfuric acid at 121 °C for 1 h. Neutralized and filtered samples were analyzed by HPLC as described before. Separately, a subsample (20 µL) of each subcritical water extract was used for HPLC determination for sugar monomers after neutralization with calcium carbonate and filtration. The total hemicellulosic sugar content for the samples were expressed as sum of the hydrolysed oligomers from post-acid hydrolysis and the monomers from direct HPLC injection. The yield of hemicellulosic sugars in the extracts was calculated as follows: yield = [(sugars in the extract/initial sugars in the substrate) x 100%].

### **3.2.5. Characterization of the solid residues**

#### **3.2.5.1. X-ray diffraction analysis**

The solid residues left in the reactor were analyzed by an X-ray diffractometer (XRD); Rigaku Ultima IV with a D/Tex detector using a Fe filter, over the  $2\theta$  range of 10-45 degrees. The XRD apparatus was equipped with a Cobalt tube and the tube's conditions were 40 kV and 40 mA. The scanning speed was 0.6 degrees  $2\theta$  per minute with a 0.01 step size. The crystallinity index (CI) of samples was calculated based on the diffraction intensities of crystalline area and amorphous regions by making use of the following equation (Segal, 1959):

$$CI (\%) = \frac{I_{002} - I_{am}}{I_{002}} * 100 \quad (3.1)$$

where,  $I_{002}$  is the intensity of the crystalline portion of biomass (cellulose) at  $2\theta = 22.5^\circ$  and  $I_{am}$  is the intensity of amorphous region at  $2\theta = 18.5^\circ$ .

### **3.2.5.2. Thermo-gravimetric analysis**

The non-isothermal thermo-gravimetric (TG) analyses curves of solid residues were obtained using a TG analyzer (TGA) Q50 (TA Instruments, New Castle, DE, USA). Approximately 10-15 mg of sample was loaded into the open platinum pan, and then heated from 30 °C to 600 °C at a 10 °C/min heating rate under 40 mL/min of dry nitrogen flow. Data were analyzed by the TA Universal analysis software (Version 4.5A, TA Instruments, New Castle, DE, USA).

### **3.2.5.3. Scanning Electron Microscopy analysis**

The morphology of the untreated lupin hull and the solid residues were analyzed using field emission SEM (FE-SEM) (JEOL 6301 FXV, Peabody, MA, USA). For SEM analysis, a thin layer of the sample was applied to a sample mount using double-sided carbon tape, and sputter coated with gold using a Xenusput XE200 (Edwards High Vacuum, Crawley, UK).

### **3.2.6. Statistical analysis**

Data were presented as mean  $\pm$  standard deviation based on at least duplicate experiments and analyses. Analysis of variance (one-way and two-way) of the results was performed using the SPSS software package (version 17.0, SPSS Inc., Chicago, IL, USA). Multiple comparison of the means was carried out

by a Duncan's test. Differences were considered to be statistically significant at 95% confidence interval ( $p < 0.05$ ). A t-test was performed for the comparison of only 2 means ( $p < 0.05$ ) using the SigmaPlot software (version 11.0, Jandel Scientific, San Francisco, CA, USA).

### **3.3. Results and discussion**

#### **3.3.1. Proximate compositional analysis**

The chemical composition of lupin hulls used in this study is summarized in Table 3-1. Values were determined for the extractive (nonstructural sugars, organic acids, inorganic material, nitrogenous material, chlorophyll, waxes, and other minor components) - free material as specified by the NREL laboratory procedure. Samples were extracted with toluene-ethanol (2:1, v/v) for 8 h at 80 °C in a Soxhlet apparatus.

The extractive-free lupin hull had 45.2% of cellulose (estimated as glucan content) and 25.4% of hemicellulosic sugars. Xylose (12.8%) and galactose (6.7%) were the most abundant sugars in the hemicellulose fraction, indicating the presence of xylan and galactan as the main polysaccharides followed by arabinose (4.1%) and mannose (1.8%). Acid insoluble lignin and acid soluble lignin accounted for 6.4% and 1.2%, respectively.

**Table 3-1.** Composition of lupin hull used in this study.

| <b>Component</b>      | <b>Content (wt.%)<sup>*</sup></b> |
|-----------------------|-----------------------------------|
| Cellulose             | 45.2±2.1                          |
| Hemicellulose         | 25.4±1.4                          |
| Xylose                | 12.8±1.7                          |
| Galactose             | 6.7±1.1                           |
| Arabinose             | 4.1±0.1                           |
| Mannose               | 1.8±0.2                           |
| Lignin                | 7.6±1.2                           |
| Acid soluble lignin   | 1.2±0.1                           |
| Acid insoluble lignin | 6.4±0.8                           |
| Protein               | 6.7±0.5                           |
| Fat                   | 1.8±0.1                           |
| Ash                   | 4.2±0.4                           |
| Moisture              | 5.8±0.6                           |
| Others                | 1.3                               |

<sup>\*</sup>Values are reported as the mean ± standard deviation based on triplicate analyses.

Bailey et al. (1974) determined the composition of sweet blue lupin hull. They reported cellulose, hemicellulose and lignin contents of 50.9, 12.7, and 0.4%, respectively. Hemicellulose and lignin contents reported by these authors were lower compared to this study, which may be attributed to the use of different cultivars. The substantial amount of hemicellulose and low lignin content of lupin hull indicates its suitability as a source for sugar removal.

### 3.3.2. Hydrolysis in subcritical water - Effects of process parameters

#### 3.3.2.1. Extracts

Using subcritical water treatment, water acts as a weak acid, releasing the hydronium ion from water auto-ionization and from *in situ* generated acids, which causes depolymerization of hemicellulose by selective hydrolysis of glycosidic linkages, liberating *O*-acetyl group and other acid moieties from hemicellulose, forming acetic and uronic acids. The release of these acids catalyzes the hydrolysis of hemicelluloses and oligosaccharides from hemicellulosic material (Alvarez et al., 2014).

Effects of temperature (160-220 °C) and pressure (50-200 bar) on hemicellulose removal from lupin hulls were studied at constant flow rate (5 mL/min), pH (6.2) and solvent to solid ratio (66.7) to find optimum temperature and pressure conditions. Figure 3-1a shows the effect of temperature and pressure on total hemicellulosic sugar (mainly sum of xylose, galactose, arabinose, and mannose) yield in the extracts. Pressure effect on hemicellulose decomposition was not significant in the range of 50-150 bar.

The yield of hemicellulosic sugars in the extracts slightly decreased from 79.5% to 76.5% as the pressure increased from 150 bar to 200 bar (200 °C). However, the yield in the extracts was strongly affected by temperature. Increasing temperature from 160 to 180 °C resulted in increased hemicellulose yield from 60.8-64.2% to 81.5-85.5%. The highest yield of 85.5% was achieved at 180 °C and 50 bar. However, the yield decreased sharply at elevated temperatures of 200 and 220 °C.

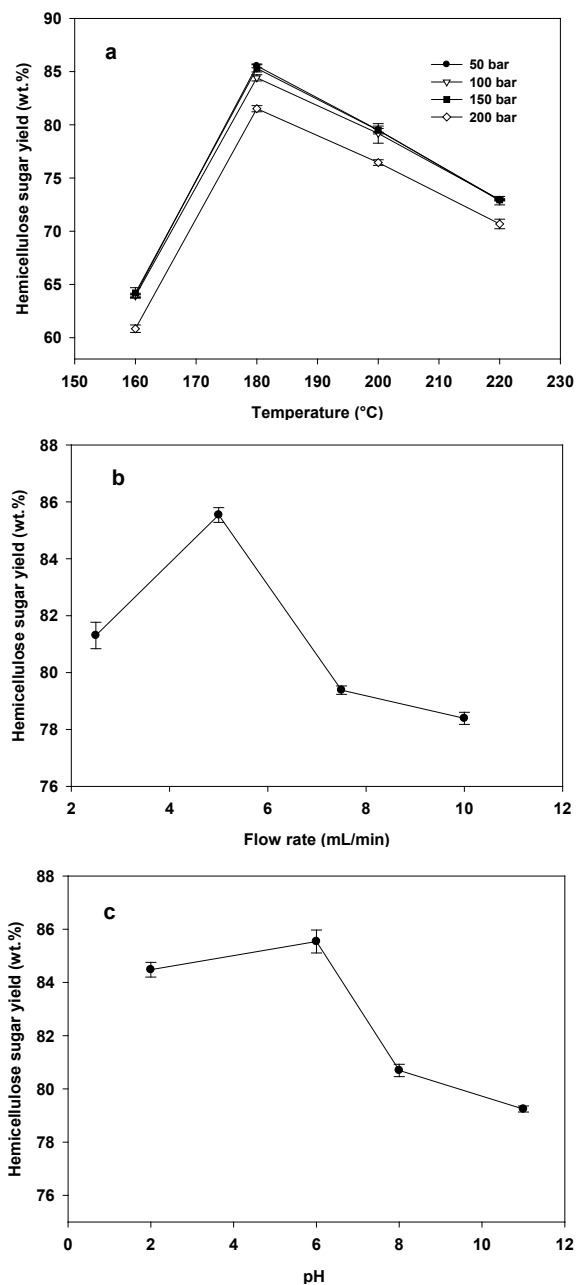


**Figure 3-1.** Effect of process parameters on total hemicellulosic sugar yield (sum of xylose, galactose, arabinose, and mannose) in the extracts. a) Temperature and pressure (5 mL/min, pH 6.2); b) flow rate (180 °C, 50 bar, pH 6.2); c) pH (180 °C, 50 bar, 5 mL/min).

When the treatment temperature was increased to 220 °C, corresponding hemicellulosic sugar yield decreased significantly to the range of 70.7-73%. These results are consistent with the findings obtained by Yu et al. (2013). They reported that total xylose concentration in the extracts during subcritical water treatment of sugarcane bagasse firstly increased with the temperature and then decreased sharply above 180 °C, the peak appeared at 160 °C with the total xylose recovery of 41.9%. In addition, the removal rate of xylose increased with the temperature from 8.4% at 140 °C to 100% at 200 °C.

Decrease in the yield of hemicellulosic sugars in the extracts at temperatures above 180 °C could indicate that substantial amount of hemicellulosic sugars were decomposed at those temperatures to secondary products, such as furfural and hydroxymethyl furfural (HMF) that were not measured in this study. During subcritical water treatment under severe treatment conditions, hemicellulosic sugars could degrade into furan derivatives, which are furfural and HMF obtained from the dehydration of pentoses and hexoses, respectively. Such hemicellulosic sugar degradation was reported at temperatures higher than 180 °C (Hongdan et al. 2013; Pronky and Mazza, 2010; Weiqi et al. 2013). Weiqi et al. (2013) reported that when the treatment temperature was raised from 160 to 180 °C, corresponding yield of total xylose in the subcritical water extracts of eucalyptus increased from 30.8 to 85.0%. Then, the yield of total xylose in the extracts rapidly decreased with further increase in temperature, which was attributed to the degradation of xylose into furfural as a result of severe treatment conditions. Furfural content was increased from 0.24 to 3.29 g/L by

raising temperature from 160 to 200 °C, which indicates that more xylose decomposed. Similar decrease of hemicellulosic sugar trend in the extract was observed by Hongdan et al. (2013) when the temperature increased above 180 °C during subcritical water treatment of sugarcane bagasse in a batch system at a solid to liquid ratio of 1/20 (w/v) with a reaction time of 40 min, which was attributed to the degradation of xylose and arabinose into furfural, and galactose into 5-HMF. They reported that the amounts of furan compounds increased with the increase in treatment temperature and time. Maximum concentration was obtained at 220 °C and 20 min residence time, and measured as 0.11 g/L and 2.42 g/L for HMF and furfural, respectively. In another study, Pronky and Mazza (2010) reported 67-73% yield of hemicellulose from triticale straw in the extracts at 170 °C, 110 bar and a solvent-to-solid ratio of 60 mL/g and only 9-10% of the hemicellulose remained in the solid residue, which implies a theoretical yield of hemicellulose close to 90%. These results indicated that almost 20% of the extracted hemicellulose was converted into degradation products at these processing conditions.

Effects of four different flow rates (2.5, 5, 7.5, and 10 mL/min) on hemicellulose removal from lupin hulls were investigated in this study at optimum temperature and pressure of 180 °C and 50 bar, respectively, and at constant pH of 6.2 and solvent to solid ratio of 66.7 to find optimum flow rate for maximum yield. As seen in Figure 3-1b, hemicellulosic sugar yield in the extracts first increased as the flow rate increased with the highest yield occurring at 5 mL/min. When the flow rate increased from 2.5 to 5 mL/min, the amount of

hemicellulosic sugars obtained increased significantly from 81.3 to 85.5%, and then gradually decreased to 78.4% with further increase in flow rate.

The decrease in hemicellulose yield at higher flow rates of 7.5 and 10 mL/min can be explained by reduced residence time, thus lowering the contact time of material with liberated acids in the reactor during subcritical water treatment, which catalyzes hemicellulose hydrolysis as described earlier; consequently, lower hydrolysis rate can be expected. Similarly, increased hemicellulose yields with decreasing flow rate were obtained by Pronky and Mazza (2011) for triticale straw using a flow-through subcritical water equipment at a solvent to solid ratio of 60. They reported that decreasing flow rate from 200 mL/min to 100 mL/min increased the hemicellulose yield by an average of 14% at 130 °C and 170 °C, and 24% increase was achieved with decreasing flow rate from 234.1 mL/min to 65.9 mL/min at 150 °C. Similar increasing yield trend was reported by Kim and Lee (2006) for xylan removal from corn stover treated using a subcritical water flow-through reactor.

Even though improved yields were reported at lower flow rates, in some cases long residence time may increase the chance of degradation before the hemicellulosic sugars exit (Liu and Wyman, 2003; Buranov and Mazza, 2007). It was reported that decreasing flow rate increased the removal of hemicellulose during fractionation of flax shives (92.2%), but also increased degradation from 13.3 to 17.3% (Buranov and Mazza, 2007). On the contrary, Liu and Wyman (2003) reported that xylose yield from corn stover processed in a subcritical water flow through reactor increased to 97% when the flow rate was increased to 10

mL/min at 220 °C. They hypothesized that increasing flow rate leads to reducing the thickness of a liquid film surrounding biomass particles, thus improving mass transfer of hydronium ions into the hydrophobic biomass surface, which accelerates the hydrolysis of hemicellulose. However, they observed a decreased yield when temperature decreased to 180 °C at the same flow rate, which was attributed to the removal of dissolved xylose and oligomers before they can degrade at temperatures above 220 °C.

Effect of four different pH levels (2.6, 6.2, 8.5, and 11.7) on hemicellulose removal from lupin hulls were studied at a constant solvent to solid ratio of 66.7 and, at optimum temperature, pressure, and flow rate (180 °C, 50 bar, and 5 mL/min) to find optimum pH. At low and medium, pH values of 2.6 and 6.2, respectively, hemicellulosic sugar yield in the extracts increased noticeably. Treating lupin hull with subcritical water at an acidic pH of 2.6 yielded 84.5% hemicellulosic sugars. When water at pH 6.2 was used, 85.5% of yield was obtained. However, when the pH of water was increased to 11.7, the hemicellulosic sugar yield decreased significantly to 79.2 %.

Hemicelluloses contain acetyl and uronic acid groups, which can be liberated during subcritical water treatment as discussed earlier. Consistently, it was observed that pH values of the subcritical water extracts decreased from an initial pH of 6.2 to around pH of 2-3 in the range of temperatures and pressures studied. These acidic conditions promoted the hydrolysis of the hemicellulose fraction. As expected, hemicellulose hydrolysis was maximized at acidic conditions. However, increasing acidity further did not improve hemicellulosic

sugar yield, which may be attributed to the degradation of sugars under severe conditions. This is in agreement with the findings reported by Phaiboonsilpa and Saka (2011). They studied the effect of acetic acid addition on chemical conversion of Japanese beech in a flow reactor with subcritical water and observed that the additional acetic acid did not show any significant effect on improving the hydrolysis of hemicelluloses from Japanese beech.

#### **3.3.2.2. Solid residue**

Subcritical water treatment of lupin hulls led to cellulose enriched residues. There were trace amounts of hemicellulose in the solid residues treated at 180 °C, while it was completely decomposed and undetectable at 200 and 220 °C based on HPLC analysis. Figure 3-2 demonstrates the effect of process parameters on cellulose and lignin contents of the solid residues left after subcritical water treatment. Pressure had no significant influence in the range of 50-200 bar (data not shown). In general, the main role of pressure in subcritical water systems is to maintain water in the liquid state.

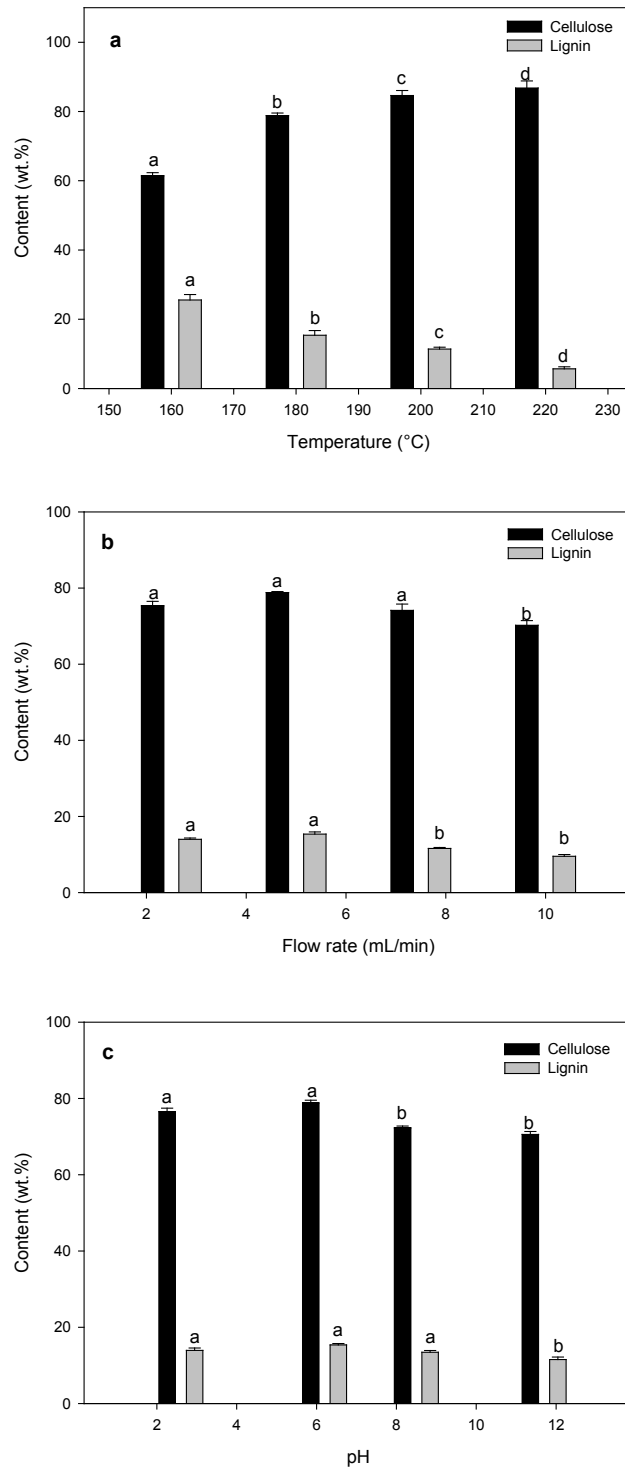


**Figure 3-2.** Effect of process parameters on cellulose and lignin contents in the solid residues. a) Temperature (50 bar, 5 mL/min, pH 6.2); b) flow rate (180 °C, 50 bar, pH 6.2); c) pH (180 °C, 50 bar, 5 mL/min). Means within the same group of biomass fraction with different letters are significantly different at  $p < 0.05$ .

In some cases, high pressures may have a physical effect, causing mechanical deconstruction of biomass material, and improving hydrolysis reactions during subcritical water treatment (Hanim et al., 2012). Temperature had a pronounced effect on cellulose and lignin contents of the solid residues. As the treatment temperature increases, density of water decreases from 0.997 g/cm<sup>3</sup> (25 °C/1 bar) to 0.843 g/cm<sup>3</sup> (220 °C/50 bar) (NIST Chemistry Webbook). With the change in density from 1 to 0.1 g/cm<sup>3</sup>, the diffusivity increases by roughly an order of magnitude (Akiya and Savage, 2002).

On the other hand, the dielectric constant ( $\epsilon$ , measure of polarity) of water decreases from 78.5 (25 °C/1 bar) to 31.7 (220 °C/50 bar) (Uematsu, 1980) due to the weakening of hydrogen bonds with increasing temperature, thereby attaining solvent polarities normally associated with polar organic solvents, such as ethanol or methanol. Therefore, water becomes more non-polar and an excellent solvent for organic compounds.

Increasing treatment temperature from 160 to 220 °C resulted in cellulose enriched residues. The cellulose content increased from 61.4% (160 °C/50 bar) to 86.8% (220 °C/50 bar) when compared with the initial percentage of 45.2%, and the lignin content varied from 25.6% (160 °C/50 bar) to 5.7% (220 °C/50 bar) (Fig. 3-2a). On the other hand, effect of flow rate and pH on cellulose and lignin contents of the solid residues was not pronounced (Fig. 3-2b and 3-2c).

These results implied that the cellulose and lignin did not decompose as readily as hemicellulose under subcritical water treatment. Hemicellulose is more

susceptible to hydrolysis than cellulose and lignin because of its branched structure and lower degree of polymerization (Bobleter, 1994).

Hemicellulose and cellulose are both natural polymers made up of sugar units. Unlike hemicellulose, cellulose is a linear homopolymer without branches composed of glucose units linked together by strong  $\beta$ -1,4-glycosidic bonds, its regular structure provides it a greater thermal stability than hemicellulose (John and Thomas, 2008). Therefore, cellulose requires more severe processing conditions than hemicellulose to decompose. Decomposition of hemicellulose starts at a lower temperature than that of cellulose using subcritical water. Total xylose of 85% from the hemicellulose fraction was generated in the extracts, whereas limited amounts of glucose and gluco-oligosaccharides from the cellulose fraction were released (< 2%) at 180 °C and 20 min of residence time during subcritical water treatment of eucalyptus biomass in a laboratory scale stirred autoclave (Weiqi et al., 2013). Kim and Lee (2006) found almost no reduction in the cellulose content of the subcritical water treated corn stover at temperatures of 170-220 °C and flow rates of 2.5-5.0 mL/min. Cellulose was shown to start to decompose at temperatures above 230 °C by Ando et al. (2000) in a model system study using commercial cellulose. Mok and Antal (1992) obtained 4-22% of the cellulose in the extracts from subcritical water treatment of a variety of woody and herbaceous biomass species at 200-230 °C and 345 bar.

On the other hand, lignin is a three-dimensional hydrophobic polymer made up of three phenylpropane monomers polymerized by a radical coupling process that links them by carbon-carbon (C-C) and ether bonds (C-O-C). The

presence of strong C-C and C-O-C linkages in the lignin affects its susceptibility to chemical disruption (Harkin, 1973). In lignocellulosic biomass, lignin is covalently bonded to hemicelluloses via ether and ester-linked phenolic compounds, such as ferulic acid. Subcritical water treatment causes breaking of such bonds, increasing total phenolic content in the extracts. As shown in Figure 3-3, increasing temperature resulted in increased phenolic content of ten times from 0.07 mg gallic acid/g lupin hull at 160°C/200 bar to 0.72 mg gallic acid/g lupin hull at 220°C/200 bar which implies that higher temperatures facilitated breaking of strong interactions between carbohydrates and lignin.

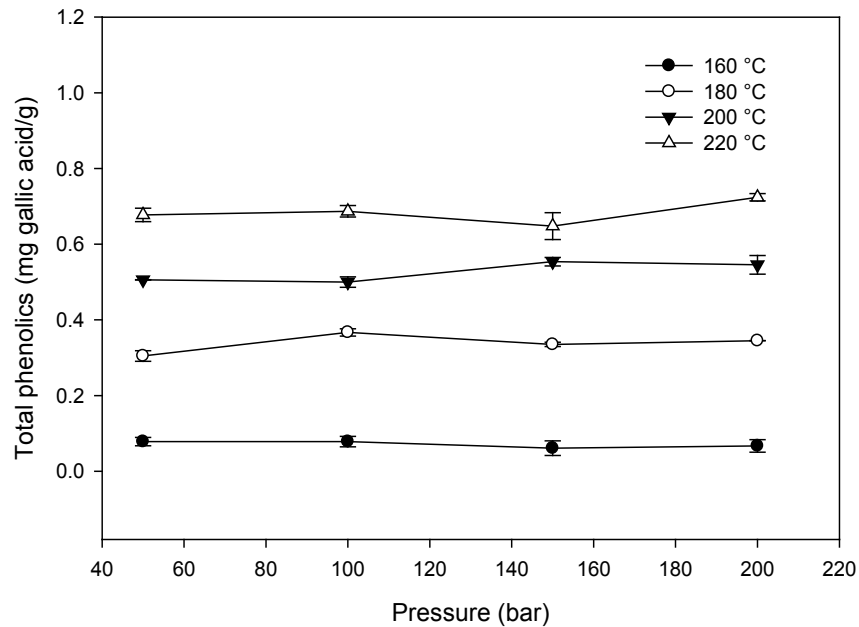


**Figure 3-3.** Effect of temperature and pressure on total phenolic content of lupin hulls.

As expected, pressure had no significant effect on total phenolic content ( $p < 0.05$ ). Consistently, it was shown that TOC amount of extracts increased as treatment temperature increased, which can be the result of a greater release of major hemicellulosic sugars and other lignocellulosic biomass components into the water (Table 3-2). It was likely that the hydrolysis of hulls to water soluble saccharides and the degradation products progressed more rapidly at higher temperatures.

**Table 3-2.** Effect of temperature on total organic content of lupin hull extracts at 50 bar.

| Temperature (°C) | Total organic content (mg/L)* |
|------------------|-------------------------------|
| 160              | 4088±27                       |
| 180              | 5020±15                       |
| 200              | 5277±32                       |
| 220              | 5640±54                       |

\* Values are reported as the mean  $\pm$  standard deviation based on triplicate analyses.

The amount of TOC was dramatically increased from 4088 to 5640 mg/L when temperature was increased from 160 to 220 °C at 50 bar as hemicellulose was actively started to separate in this temperature range. The aim of this study was to determine the hemicellulosic sugar yield in the extracts, degradation products from hemicellulose and lignin were not determined.

### 3.3.3. Characterization of the solid residues

#### 3.3.3.1. X-ray diffraction analysis

Figure 3-4 shows comparison of the diffraction patterns of the solid residue treated at optimum conditions with that of untreated lupin hull. Untreated lupin hull showed a broad diffraction pattern (softly rising and decreasing backgrounds). However, the pattern of untreated sample changed remarkably after subcritical water treatment (three peaks clearly visualized) displaying similar diffraction patterns with that of native cellulose. This may be explained by the removal of hemicellulose and some amount of lignin from lupin hulls, leading to a cellulose enriched residue. Typical native cellulose structure (cellulose I) presents three well-defined crystalline peaks at around  $2\theta = 16.5^\circ$ ,  $22.5^\circ$  and  $34.5^\circ$  (Nishiyama et al., 2002).

The CI of the samples investigated was determined using Eq. (3.1) from the XRD spectra obtained in Figure 3-4. The CI of the untreated lupin hull was 38.2% due to the existence of a large amount of amorphous substances, including hemicellulose and lignin. After subcritical water treatment at optimum conditions, the CI value of solid residue increased to 58.6%, suggesting that there was a remarkable increase in the relative amount of crystalline part of the lupin hull, implying an effective removal of amorphous moieties of the cell wall, such as hemicellulose and/or lignin.

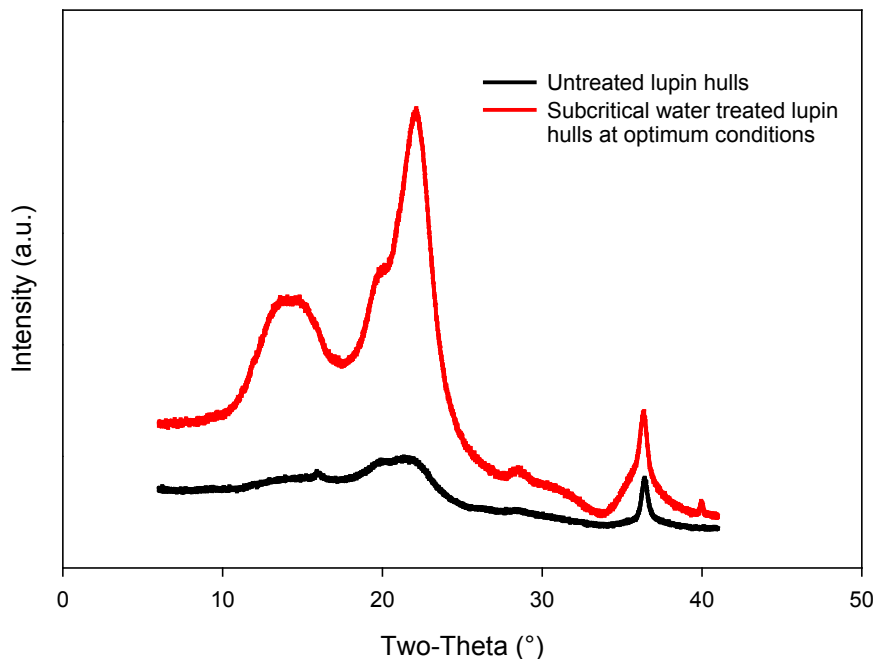


**Figure 3-4.** X-ray diffraction (XRD) patterns of untreated lupin hulls and subcritical water treated lupin hulls at optimum conditions of 180 °C, 50 bar, 5mL/min, and pH of 6.2.

Ozturk et al. (2010) determined the CI of subcritical water treated kenaf samples as 74.2% at 200 °C in a batch system. However, they observed a substantial CI decline to 19.4% at 250 °C treated sample which was associated with cellulose decrystallization at 200 and 250 °C, leaving behind a relatively degraded material. Similar trend was reported by Lu and Saka (2010) where the crystalline structure of cellulose in Japanese beech was destroyed at 230 °C when treated using subcritical water in a batch type system. However, they reported that crystalline structure was maintained even at 250 °C in a semi-flow type subcritical water system, which disappeared completely with further increase in temperature to 270 °C.

### 3.3.3.2. Thermo-gravimetric analysis

TG analysis is one of the most convenient methods to determine general degradation characteristics of materials under combustion. Thermal degradation characteristics of lignocellulosic biomass are strongly affected by their chemical composition, implying that the differences in the proportions of cellulose, hemicellulose and lignin contribute to the thermal characteristics of the sample. Comparing to other lignocellulosic biomass components, hemicellulose was found to be less stable than cellulose and lignin during pyrolysis. It has been determined that the lignocellulosic biomass pyrolysis process can be divided into the following 4 ranges: <220 °C, moisture evolution; 220-315 °C, predominantly hemicelluloses decomposition; 315-400 °C, cellulose decomposition; and >400 °C, mainly lignin decomposition (Yang et al., 2006).

Figure 3-5 shows the TG data of untreated and subcritical water treated lupin hulls at optimum conditions for maximum hemicellulosic sugar yield. Treated hulls showed higher thermal stability compared to untreated hulls as seen from the weight losses obtained from the TG curves during pyrolysis.

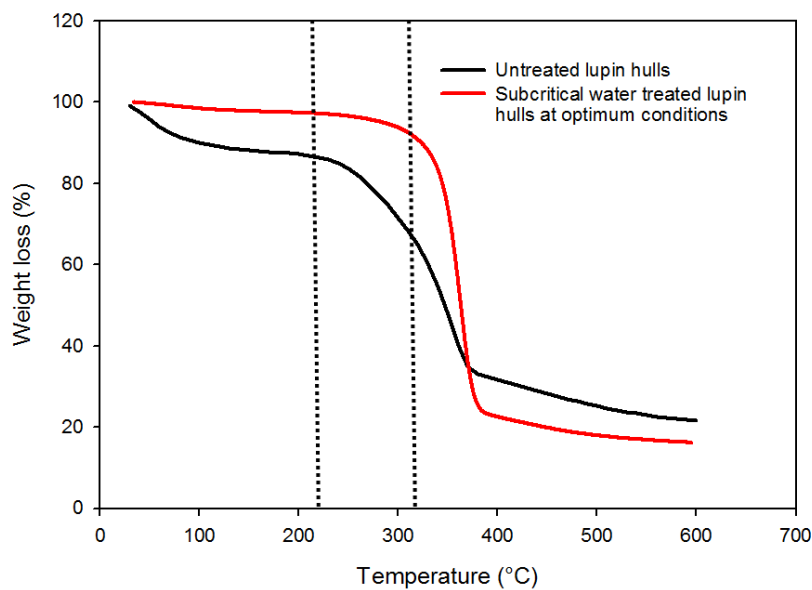


**Figure 3-5.** Thermo-gravimetric (TG) curves of untreated lupin hulls and subcritical water treated lupin hulls at optimum conditions of 180 °C, 50 bar, 5 mL/min, and pH of 6.2.

This is consistent with the increased CI of treated hulls as greater crystalline structure led to a higher resistance towards the thermal degradation. Ouajai and Shanks (2005) also reported that larger crystalline structure requires a higher decomposition temperature. The weight loss of untreated lupin hulls between 220 and 315 °C, which is attributed to the hemicelluloses decomposition, was around 23%. This weight loss is similar to the actual hemicellulose content of lupin hull, which is 25.4% (Table 3-1). The TG curves of lupin hulls displayed a substantial reduction in the weight loss after subcritical water treatment to ~6% in that temperature range, which is attributed to the extensive removal of hemicellulosic sugars with subcritical water treatment.

### 3.3.3.3. Scanning Electron Microscopy analysis

SEM images of solid residues were taken to obtain information about the surface morphology of lupin hull and to visualize changes occurred after subcritical water treatment. Figure 3-6 shows the SEM images of untreated and subcritical water treated lupin hulls at optimum conditions. The untreated hulls exhibited rigid and compact surface structures, and an intact morphology as shown in Figure 3-6a-c. Changes in the microscopic structures after treatment revealed in Figure 3-6d-f indicated that the subcritical water treatment could efficiently disintegrate lignocellulosic biomass cell wall, resulting on exposure of internal structure. Defibrillation of fiber bundles and separated microfibrils were visually observed (Fig. 3-6e and 3-6f) where structural breakdown and some cracks also appeared on the surface.

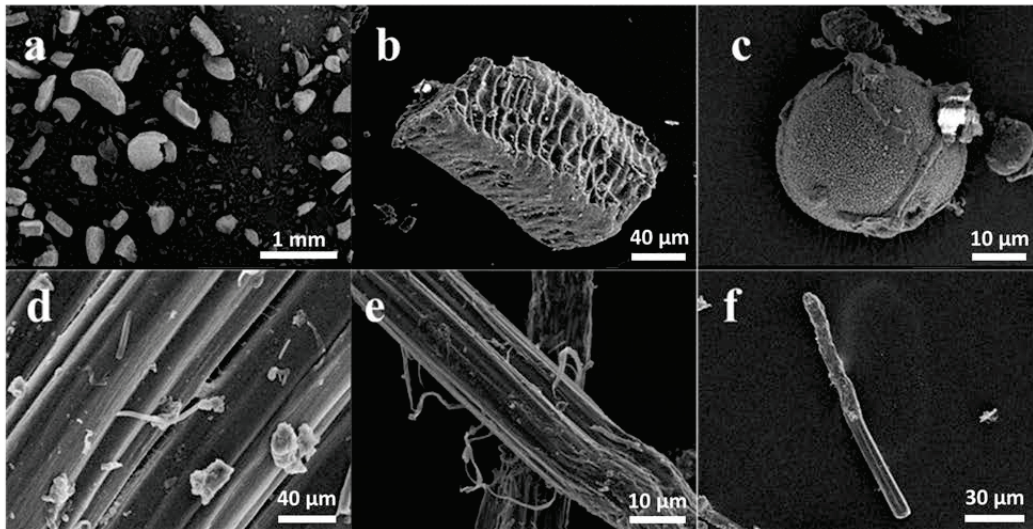


**Figure 3-6.** Scanning electron microscopy (SEM) images of lupin hulls: a), b), and c) untreated hulls, d), e), and f) subcritical water treated hulls at optimum conditions (180 °C, 50 bar, 5mL/min, pH 6.2).

The surface was uneven and covered with small debris and droplets. Previous studies have reported a range of discrete droplet morphologies appeared on the biomass surfaces, which were attributed to the molten lignin and subsequent condensation (Selig et al., 2007).

### **3.4. Conclusions**

Hydrolysis of sweet blue lupin hull was successfully performed using subcritical water technology to obtain hemicellulosic sugars. The yield was significantly affected by temperature, flow rate and pH, while the effect of pressure was not significant. Optimum process conditions for maximum hemicellulosic sugar yield in the extracts was found to be 180 °C, 50 bar, 5 mL/min, and pH 6.2 with a yield of 85.5%. At optimized conditions, increased crystallinity and thermal degradation stability of the solid residue confirmed the extensive removal of hemicellulose and/or lignin from lupin hulls leading a cellulose enriched residue (~80% cellulose). Defibrillation of fiber bundles with subcritical water treatment was observed with SEM.

## **Chapter 4. Cellulose fiber isolation and characterization from sweet blue lupin hull and canola straw\***

### **4.1. Introduction**

Agro-industrial residues represent an inexpensive, abundant, and readily available source of renewable lignocellulosic biomass. Obtaining high value-added compounds from this under-utilized biomass minimizes environmental concerns and adds high economic returns to the industry. Therefore, fractionation of agro-industrial residues to isolate cellulose fibers has created a great deal of research interest and an extraordinary attention as cellulose has a great number of uses within different industries. Various applications of cellulose, its derivatives, nanofibers and nanocrystals, include its use in paper making, building materials, pharmaceuticals, cosmetics, insulation, food, animal feed and liquid fuel production (Azizi Samir et al., 2005; Fukuzumi et al., 2009; Kadla and Gilbert, 2000; Kumar et al., 2002; Madani et al., 2011; Osong et al., 2015).

Isolation of cellulose can be performed by different procedures which have advantages and drawbacks related to the final composition and structural features. These methods include alkaline (Modenbach, 2013), acid (Silverstein et al., 2007), oxidation (Pedersen and Meyer, 2009), organosolv treatments (Pan et al., 2007), subcritical water treatment and/or their various combinations to remove the non-cellulosic components such as lignin and hemicellulose.

---

\*A version of this chapter has been submitted to Journal of Polymers and the Environment as Ciftci, D., Flores, R. and Saldaña, M.D.A. (2016). Cellulose fiber isolation and characterization from sweet blue lupin hull and canola straw.

Among them, alkaline treatment with sodium hydroxide (NaOH) is known to be very effective to achieve complete biomass hydrolysis. This treatment effectively solubilizes the lignin fraction as well as the hemicellulose fraction while exhibiting only minor cellulose solubilisation (Carvalho et al., 2008). This process destructs the cell wall of biomass by dissolving matrix materials like hemicelluloses and lignin, and cleaves the  $\alpha$ -ether linkages between lignin and hemicelluloses and the ester bonds between lignin and/or hemicelluloses (Kim et al., 2016). The NaOH treatments of lignocellulosic biomass have been reported to achieve 50% hemicellulose dissolution and 60-80% delignification at the conditions of 0.5–10% NaOH, 60-180 °C and 5-60 min treatment time (Kim and Lee, 2007; Tajkarimi et al., 2008; Wyman et al., 2005). However, NaOH treatment only is not sufficient to remove all of the non-cellulosic components.

Another well-known method especially for lignin elimination is the use of acidified sodium chlorite (ASC) treatment but this method can also affect hemicelluloses, depending on the processing conditions (Hubbell and Ragauskas, 2010). Under acidic conditions, sodium chlorite dissociates into highly reactive chlorine and chloride anion to destroy the cell wall matrix, resulting in a white colored residue upon lignin removal (Deshwal et al., 2004).

Efficiency of both treatments vary, depending considerably on experimental conditions such as temperature, concentration, and treatment time in addition to the type of feedstock and the amount of lignin content in the starting material. Thus, optimized combinations of NaOH and ASC offer a promising alternative to remove non-cellulosic components without impacting cellulose,

thereby resulting in high cellulose recovery. Successful isolation of cellulose fibers from energycane bagasse was reported by Yue et al. (2015) with the final composition of 84.1% cellulose, 2.4% hemicellulose and 6.5% lignin using NaOH treatment (20%/10 h/98 °C) followed by ASC (NaClO<sub>2</sub>/fibers: 0.75/1, v/w, and acetic acid/suspension: 1/50, v/v).

In the present study, lupin hull and canola straw were used as the feedstocks for the isolation of cellulose fibers using combined NaOH and ASC treatments. Lupin hull was chosen as a representative of a low lignin feedstock (<10%) and canola straw as a high lignin feedstock (20-25%) for comparison purposes of the treatment efficiency. In addition, their high cellulose contents (35-45%) make them ideal renewable biomass sources to obtain cellulose fibers. An extensive literature search indicated that no research in the context of cellulose isolation from these biomass sources using a combined NaOH treatment followed by ASC treatment has been reported to date. Therefore, the aim of this study was to optimize treatment conditions of NaOH followed by ASC treatment for maximum cellulose recovery from lupin hull and canola straw, and to investigate the effect of lignin content of the starting materials on the treatment efficiency. Effects of NaOH treatment parameters, such as concentration (5-20 wt.%), temperature (25-99 °C), time (2-10 h), and ASC treatment conditions (1.7 wt.%, 75 °C and 2-6 h time) on removal of non-cellulosic components (hemicellulose and lignin) were also evaluated. Chemical composition, crystallinity, thermal behavior, and morphological analysis of the raw and treated samples were

performed to investigate the effects of treatments on the structural features of fibers.

## **4.2. Materials and methods**

### **4.2.1. Materials**

Sweet blue lupin hull and canola straw were provided by Ceapro Inc. (Edmonton, AB, Canada) and Dr. Barry Irving (University of Alberta), respectively. Samples were ground to 1 mm particle size in a centrifugal mill (Retsch, Haan, Germany). ACS reagent grade chemicals, such as NaOH, sodium chlorite (NaClO<sub>2</sub>), acetic acid, sulfuric acid, and sugar standards (D(+)glucose, D(+)xylose, D(+)galactose, L(+)arabinose, and D(+)mannose with purity  $\geq$  96%) were obtained from Fisher Scientific (Pittsburgh, PA, USA) and used as received without further purification.

### **4.2.2. Cellulose isolation**

Before NaOH/ASC treatments, samples were extracted with toluene-ethanol (2:1, v/v) for 8 h at 80 °C in a Soxhlet apparatus to minimize the influence of extractives on the chemical composition analysis. For NaOH treatments, 5 g of lupin hull or canola straw were soaked at specific NaOH concentrations of 5-20%, with 20:1, v/w, liquid to solid ratio, for different times (2-10 h) under constant mixing. After treatments, the solid residue and liquid extract were separated by vacuum filtration. The obtained solid residues were washed repeatedly with distilled water until a neutral pH was reached, and then they were dried in an oven

at 40 °C for 48 h and the extracts were stored in the freezer at -18 °C for further analysis.

Dissolved lignin in the liquid extract at optimized NaOH treatments was removed by lowering the pH below 1.5 with the use of sulfuric acid. The precipitated lignin fraction was vacuum filtered, and washed with hot water many times until a neutral pH was reached and freeze-dried. The obtained lignin was then analyzed by thermogravimetric (TG) analysis and scanning electron microscopy (SEM).

NaOH treated samples at optimized conditions were then ASC treated for further removal of non-cellulosic components. Samples were treated at a constant concentration of 1.7% ASC (with 50:1, v/v, solution to acetic acid volume ratio) with 10:1, v/w, liquid to solid ratio and a temperature of 75 °C according to a modified method (Ruangudomsakul et al., 2015) for 2-6 h under constant mixing. Fresh ASC (~50 mL) was added every 2 h, after filtering the sample and removing the old ASC solution to maintain the pH below 4.0. The resultant samples were subsequently washed with abundant water and oven-dried at 40 °C for 48 h.

### **4.2.3. Characterization**

#### **4.2.3.1. Chemical composition**

Untreated and treated samples were analyzed for lignin, hemicellulose and cellulose contents following NREL standard analytical procedures (Sluiter et al., 2008) described in Chapter 3 (Section 3.2.4.3). The total lignin contents of the

samples were expressed as the sum of the acid insoluble lignin and acid soluble lignin. Total hemicellulosic sugars (xylose, galactose, arabinose, and mannose) and cellulose sugar (glucose) in the hydrolysates were determined using an Agilent 1290 high performance liquid chromatography (HPLC) system (Agilent Technologies, Santa Clara, CA, USA) with an evaporative light scattering detector (ELSD) and a Shodex sugar SP0810 column (300 mm×8 mm; Phenomenex, Torrance, CA, USA) operated at 80 °C. A 10% (v/v) acetonitrile solution was used as the mobile phase at a flow rate of 0.4 mL/min.

#### **4.2.3.2. X-ray diffraction analysis**

X-ray diffraction (XRD) analysis was performed using a PANalytical Empyrean X-ray diffractometer (XRD) (Empyrean, PANalytical B.V., Almelo, Netherlands) with a PIXcel 3D detector, over the  $2\theta$  range of 5-45 degrees. Cu K $\alpha$  source tube was used at the conditions of 40 kV and 40 mA. The scanning speed was 0.6 degrees  $2\theta$  per minute with a 0.01 step size. The crystallinity index (CI) of samples was determined using Eq. (3.1) ( $I_{002}$  at  $2\theta = 22.5^\circ$  and  $I_{am}$  at  $2\theta = 18.5^\circ$ ) described in Chapter 3, Section 3.2.5.1.

#### **4.2.3.3. Thermo-gravimetric analysis**

Thermo-gravimetric (TG) analysis was performed using a TG analyzer (TGA) 209 F1 Libra (TG 209 F1 Libra, NETZSCH, Selb, Germany) following the procedure described in Chapter 3, Section 3.2.5.2.

#### **4.2.3.4. Scanning Electron Microscopy analysis**

Scanning electron microscopy (SEM) images of the untreated and treated lupin hull and canola straw were analyzed using a field emission SEM (S4700 FE-SEM, Hitachi, Tokyo, Japan). The thin layer of sample was mounted on SEM specimen stubs with double-size conductive carbon tape and sputter-coated with chromium (Desk V HP TSC, Denton Vacuum LLC, NJ, USA) at 5 kV and 15 mA under low vacuum mode.

#### **4.2.4. Statistical analysis**

Data were presented as mean  $\pm$  standard deviation based on at least duplicate experiments and analyses. Statistical analysis was performed using the methodology described in Chapter 3, Section 3.2.6.

### **4.3. Results and discussion**

#### **4.3.1. Chemical composition**

Table 4-1 shows the chemical composition of raw and treated lupin hull and canola straw under different conditions. Untreated lupin hull consisted of  $45.2 \pm 2.1\%$  cellulose,  $25.4 \pm 1.4\%$  hemicellulose, and  $7.8 \pm 0.4\%$  lignin, while untreated canola straw consisted of  $38.5 \pm 1.5\%$  cellulose,  $24.3 \pm 1.6\%$  hemicellulose and  $21.4 \pm 0.9\%$  lignin. According to the compositional analysis of lupin hull, cellulose and hemicellulose contents are similar to those reported by Bailey et al. (1974), while their lignin content was lower ( $\sim 0.4\%$ ) compared to

this study, which can be related to the variety, harvesting conditions and/or the different analytical method applied for compositional analysis. On the other hand, cellulose, hemicellulose, and lignin contents of canola straw used in this study were similar to those reported by Pronky and Mazza (2012).

Treatments with NaOH were found to be efficient on affecting the chemical composition of lupin hull and canola straw samples as shown in Table 4-1. Increasing temperature and concentration of NaOH facilitated greater removal of hemicellulose and lignin components due to the destruction of inter- and intramolecular hydrogen bonds in the lignocellulose structure. After 2 h treatment time, the lignin content of the raw material decreased significantly from 7.8 to 5.7% in lupin hull, and from 21.4 to 16.4% in canola straw, while the hemicellulose content was reduced significantly from 25.4 to 8.6% in lupin hull, and from 24.3 to 12.7% in canola straw at 15% NaOH concentration and 75 °C.

**Table 4-1.** Chemical composition of lupin hull and canola straw before and after different treatments.

| Treatment conditions       | Lupin hull               |                         |                         |                         | Canola straw             |                          |                          |                          |
|----------------------------|--------------------------|-------------------------|-------------------------|-------------------------|--------------------------|--------------------------|--------------------------|--------------------------|
|                            | Total solid recovery (%) | Cellulose (%)           | Hemicellulose (%)       | Lignin (%)              | Total solid recovery (%) | Cellulose (%)            | Hemicellulose (%)        | Lignin (%)               |
| Untreated                  | 100 <sup>a*</sup>        | 45.2 ± 2.1 <sup>a</sup> | 25.4 ± 1.4 <sup>a</sup> | 7.8 ± 0.4 <sup>a</sup>  | 100 <sup>a</sup>         | 38.5 ± 1.5 <sup>a</sup>  | 24.3 ± 1.6 <sup>a</sup>  | 21.4 ± 0.9 <sup>a</sup>  |
| 5% NaOH, 25 °C, 2 h        | 76.5 ± 0.9 <sup>b</sup>  | 58.3 ± 0.3 <sup>b</sup> | 23.4 ± 0.3 <sup>b</sup> | 7.5 ± 0.1 <sup>a</sup>  | 76.2 ± 0.7 <sup>b</sup>  | 49.7 ± 0.4 <sup>b</sup>  | 22.1 ± 0.5 <sup>b</sup>  | 20.5 ± 0.4 <sup>b</sup>  |
| 5% NaOH, 50 °C, 2 h        | 75.9 ± 0.4 <sup>b</sup>  | 59.1 ± 0.2 <sup>b</sup> | 19.6 ± 0.2 <sup>c</sup> | 7.1 ± 0.2 <sup>b</sup>  | 73.5 ± 0.2 <sup>bc</sup> | 51.6 ± 0.3 <sup>c</sup>  | 20.3 ± 0.9 <sup>c</sup>  | 20.1 ± 0.3 <sup>bc</sup> |
| 5% NaOH, 75 °C, 2 h        | 71.3 ± 0.7 <sup>c</sup>  | 62.6 ± 0.9 <sup>c</sup> | 15.3 ± 1.4 <sup>d</sup> | 6.9 ± 0.1 <sup>bc</sup> | 69.1 ± 0.1 <sup>c</sup>  | 54.3 ± 0.3 <sup>d</sup>  | 18.2 ± 1.3 <sup>d</sup>  | 19.5 ± 0.3 <sup>c</sup>  |
| 10% NaOH, 25 °C, 2 h       | 70.3 ± 0.2 <sup>c</sup>  | 63.4 ± 0.6 <sup>c</sup> | 14.1 ± 0.5 <sup>c</sup> | 6.6 ± 0.1 <sup>c</sup>  | 66.2 ± 0.3 <sup>cd</sup> | 56.5 ± 0.6 <sup>e</sup>  | 17.4 ± 1.1 <sup>de</sup> | 19.1 ± 0.2 <sup>cd</sup> |
| 10% NaOH, 50 °C, 2 h       | 68.1 ± 0.2 <sup>cd</sup> | 65.2 ± 0.1 <sup>d</sup> | 13.2 ± 0.3 <sup>e</sup> | 6.3 ± 0.1 <sup>cd</sup> | 63.4 ± 0.5 <sup>d</sup>  | 58.2 ± 0.5 <sup>f</sup>  | 16.9 ± 0.4 <sup>e</sup>  | 19.0 ± 0.3 <sup>cd</sup> |
| 10% NaOH, 75 °C, 2 h       | 64.9 ± 0.4 <sup>d</sup>  | 68.5 ± 0.2 <sup>e</sup> | 11.4 ± 0.3 <sup>f</sup> | 6.1 ± 0.2 <sup>d</sup>  | 60.9 ± 0.2 <sup>d</sup>  | 61.2 ± 0.7 <sup>g</sup>  | 16.7 ± 0.2 <sup>e</sup>  | 18.4 ± 0.5 <sup>d</sup>  |
| 15% NaOH, 25 °C, 2 h       | 62.1 ± 0.5 <sup>de</sup> | 71.7 ± 0.1 <sup>f</sup> | 10.3 ± 0.3 <sup>g</sup> | 6.1 ± 0.2 <sup>d</sup>  | 56.4 ± 0.1 <sup>e</sup>  | 65.4 ± 0.6 <sup>h</sup>  | 14.9 ± 0.2 <sup>f</sup>  | 18.0 ± 0.2 <sup>d</sup>  |
| 15% NaOH, 50 °C, 2 h       | 60.6 ± 0.2 <sup>e</sup>  | 73.4 ± 0.1 <sup>g</sup> | 9.2 ± 0.2 <sup>h</sup>  | 5.8 ± 0.1 <sup>de</sup> | 55.9 ± 0.1 <sup>e</sup>  | 66.1 ± 0.3 <sup>hi</sup> | 14.6 ± 0.1 <sup>f</sup>  | 17.8 ± 0.1 <sup>d</sup>  |
| 15% NaOH, 75 °C, 2 h       | 57.4 ± 0.2 <sup>e</sup>  | 75.9 ± 0.1 <sup>h</sup> | 8.6 ± 0.1 <sup>h</sup>  | 5.7 ± 0.1 <sup>e</sup>  | 54.6 ± 0.1 <sup>e</sup>  | 67.2 ± 0.9 <sup>i</sup>  | 12.7 ± 0.3 <sup>g</sup>  | 16.4 ± 0.3 <sup>e</sup>  |
| 20% NaOH, 25 °C, 2 h       | 59.1 ± 0.2 <sup>e</sup>  | 71.2 ± 0.2 <sup>f</sup> | 11.1 ± 1.2 <sup>f</sup> | 6.3 ± 0.2 <sup>cd</sup> | 53.9 ± 0.3 <sup>e</sup>  | 65.7 ± 0.5 <sup>h</sup>  | 15.7 ± 0.3 <sup>e</sup>  | 17.9 ± 0.2 <sup>d</sup>  |
| 20% NaOH, 50 °C, 2 h       | 57.2 ± 0.3 <sup>ef</sup> | 73.3 ± 0.2 <sup>g</sup> | 9.8 ± 0.4 <sup>h</sup>  | 6.1 ± 0.3 <sup>d</sup>  | 52.3 ± 0.2 <sup>e</sup>  | 66.3 ± 0.4 <sup>hi</sup> | 14.5 ± 0.7 <sup>f</sup>  | 17.3 ± 0.4 <sup>d</sup>  |
| 20% NaOH, 75 °C, 2 h       | 53.7 ± 0.2 <sup>f</sup>  | 77.1 ± 0.1 <sup>h</sup> | 8.9 ± 0.2 <sup>h</sup>  | 5.9 ± 0.2 <sup>de</sup> | 50.1 ± 0.1 <sup>f</sup>  | 67.8 ± 0.5 <sup>i</sup>  | 13.9 ± 0.4 <sup>f</sup>  | 16.9 ± 0.4 <sup>e</sup>  |
| 15% NaOH, 75 °C, 6 h       | 54.5 ± 0.5 <sup>ef</sup> | 78.9 ± 0.2 <sup>i</sup> | 8.2 ± 0.3 <sup>h</sup>  | 5.5 ± 0.2 <sup>f</sup>  | 49.9 ± 0.1 <sup>f</sup>  | 72.0 ± 1.1 <sup>j</sup>  | 12.6 ± 0.2 <sup>g</sup>  | 13.8 ± 0.2 <sup>f</sup>  |
| 15% NaOH, 75 °C, 10 h      | 52.7 ± 0.7 <sup>fg</sup> | 81.3 ± 0.4 <sup>j</sup> | 8.6 ± 0.3 <sup>h</sup>  | 5.3 ± 0.1 <sup>f</sup>  | 48.8 ± 0.2 <sup>f</sup>  | 72.6 ± 1.4 <sup>j</sup>  | 12.4 ± 0.2 <sup>g</sup>  | 13.6 ± 0.4 <sup>f</sup>  |
| 15% NaOH, 99 °C, 6 h       | 49.9 ± 0.5 <sup>g</sup>  | 85.9 ± 1.6 <sup>k</sup> | 7.5 ± 0.2 <sup>i</sup>  | 4.7 ± 0.2 <sup>g</sup>  | 47.6 ± 0.1 <sup>fg</sup> | 75.0 ± 0.9 <sup>k</sup>  | 11.5 ± 0.3 <sup>h</sup>  | 12.3 ± 0.2 <sup>g</sup>  |
| 15% NaOH, 99 °C, 10 h      | 48.6 ± 0.7 <sup>g</sup>  | 87.1 ± 1.1 <sup>k</sup> | 7.2 ± 0.8 <sup>i</sup>  | 4.4 ± 0.2 <sup>g</sup>  | 47.0 ± 0.1 <sup>fg</sup> | 75.6 ± 0.7 <sup>k</sup>  | 11.8 ± 0.2 <sup>h</sup>  | 12.0 ± 0.3 <sup>g</sup>  |
| Opt**+1.7% ASC, 75 °C, 2 h | 47.1 ± 0.2 <sup>gh</sup> | 90.5 ± 0.1 <sup>l</sup> | 6.4 ± 0.2 <sup>j</sup>  | 2.9 ± 0.4 <sup>h</sup>  | 45.1 ± 0.6 <sup>g</sup>  | 77.7 ± 0.5 <sup>l</sup>  | 11.4 ± 0.3 <sup>hi</sup> | 10.8 ± 0.5 <sup>h</sup>  |
| Opt**+1.7% ASC, 75 °C, 4 h | 45.7 ± 0.1 <sup>h</sup>  | 93.2 ± 0.5 <sup>m</sup> | 4.6 ± 0.1 <sup>k</sup>  | 1.7 ± 0.1 <sup>i</sup>  | 44.1 ± 0.2 <sup>g</sup>  | 79.4 ± 0.4 <sup>m</sup>  | 11.0 ± 0.4 <sup>i</sup>  | 8.5 ± 0.7 <sup>i</sup>   |
| Opt**+1.7% ASC, 75 °C, 6 h | 44.3 ± 0.2 <sup>h</sup>  | 88.7 ± 0.6 <sup>n</sup> | Traces                  | 0.8 ± 0.1 <sup>j</sup>  | 43.3 ± 0.3 <sup>g</sup>  | 81.4 ± 0.5 <sup>n</sup>  | 10.3 ± 0.3 <sup>i</sup>  | 7.9 ± 0.3 <sup>i</sup>   |

Contents have been expressed on dry weight basis as mean ± standard deviation of at least duplicate determinations.

\* Means with different letters in the same column are different from each other at p<0.05.

\*\*Opt: Optimized condition (15% NaOH, 99 °C, 6 h).

On the contrary, the cellulose content increased significantly from 45.2 to 75.9% in lupin hull and from 38.5 to 67.2% in canola straw at the same treatment conditions. The chemical composition of 15% NaOH treated samples was not significantly different from those treated with 20% NaOH at all temperatures investigated for 2 h. This behavior may be attributed to the excessive swelling of the cellulose in the presence of 15-20% alkali concentration.

One of the functions of alkali is to serve as a swelling agent to cellulose, thereby allowing better extraction of hemicelluloses. Although mild alkali solutions could not be able to break the cellulose and hemicellulose complex efficiently, higher alkali concentrations might prevent the further separation of hemicelluloses from the fiber structure as it swells the microfiber too much (Rambabu et al., 2016). On the other hand, increasing 15% NaOH treatment time to 6 h and temperature to 99 °C resulted in improved removal of hemicellulose and lignin in both samples.

The hemicellulose and lignin contents after treatment with 15% NaOH, 99 °C for 6 h were further reduced to 7.5% and 4.7%, respectively, in lupin hull, and 11.5% and 12.3%, respectively, in canola straw. However, further increasing the treatment time to 10 h did not affect the chemical composition values significantly in both samples.

Fig. 4-1 shows the effect of NaOH treatment on hemicellulose and lignin removal amounts of lupin hull and canola straw. Although the amounts of removed lignin (50-60%) were similar for all NaOH treated samples of lupin hull and canola straw, the amounts of hemicellulose removal from lupin hull (up to

80%) were higher than those from canola straw (up to 70%). As known, lignin surrounds cellulose and hemicellulose, forming a complex structure that makes lignocellulosic biomass highly recalcitrant to enzymes, pathogens, and microorganisms (Lynd et al., 1991). Strong lignin interactions keep the hemicellulose unexposed and inaccessible. Depolymerization and removal of lignin provides improved susceptibility for the remaining hemicellulose and cellulose for further breakdown of their structures as lignin fails to act as a protective shield. Therefore, the efficient removal of hemicellulose depends on the low amount of lignin present in the starting material and/or efficient removal of lignin with the treatment applied. It is a challenge to completely delignify the biomass since lignin is located within the deep cell wall and tends to condensate. Lignin is physically stiff due to its strong polyring bonds of C–O–C, C–C and hydrophobic bonds (Sanchez et al., 2011).

To further remove the residual lignin and hemicellulose, the NaOH treated samples at optimized conditions (15% NaOH/99 °C/6 h) were then subjected to ASC treatment for 2 to 6 h at 75 °C with fresh ASC (~50 mL) added every 2 h. As anticipated, the hemicellulose and lignin contents of NaOH treated samples were further reduced and cellulose content was further increased as a function of treatment time. At the end of the 6 h ASC treatment, the lignin content of lupin hull decreased to 0.8%, while the lignin content of canola straw decreased to 7.9% as reported in Table 4-1.

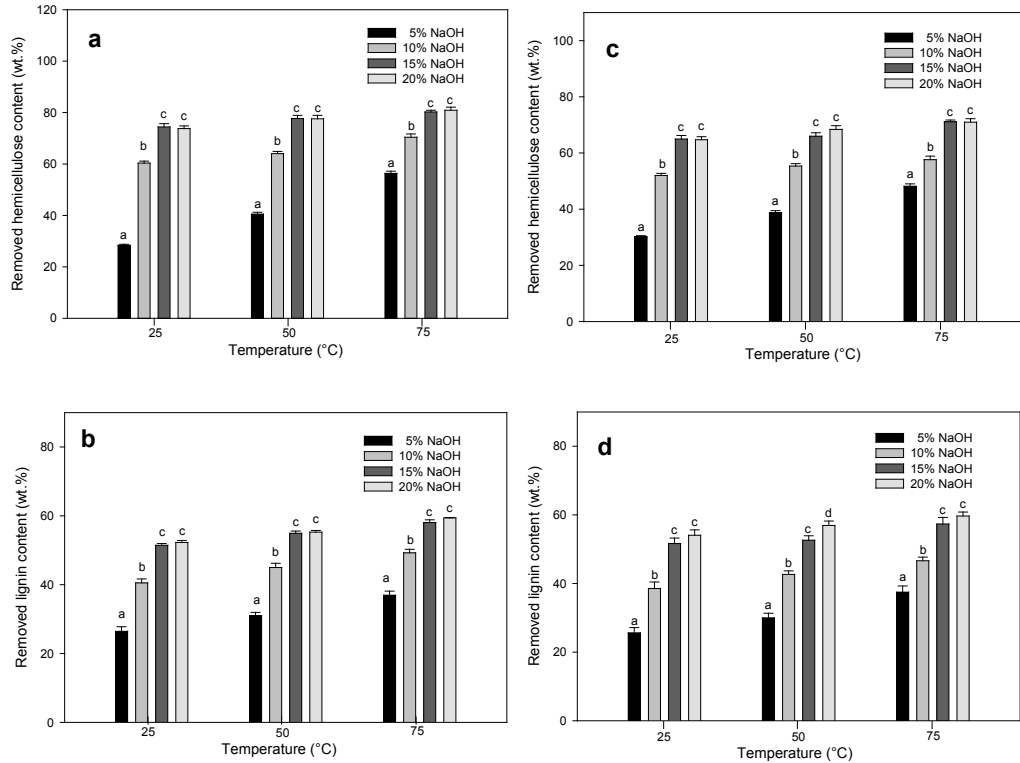


**Figure 4-1.** Effect of NaOH concentration and temperature on hemicellulose and lignin removal of (a, b) lupin hull, and (c, d) canola straw. Means with different letters within each temperature are different from each other at  $p < 0.05$ .

The cellulose content of canola straw increased continuously up to 81.4% after 6 h ASC treatment; however, the cellulose content of lupin hull first increased up to 93.2% after 4 h treatment, and then increasing the treatment time to 6 h resulted in a decrease of cellulose content to 88.7%, which was not the case for canola straw with a higher lignin content. It is hypothesized that the ASC treatment of biomass containing less than 1% lignin had a detrimental effect on degree of polymerization of cellulose due to hydrolysis and/or oxidative cleavage of the cellulose chain (Grierer, 1986). Therefore, degradation of cellulose in lupin hull at this condition could be related to its low lignin content of <1%. Hubbell

and Ragauskas (2010) treated two types of pure cellulose, Avicel PH-101 and Whatman filter paper, with ASC in the presence of varying amounts of incorporated lignin up to 30%. They also reported that ASC treatment caused significant damage to the cellulose component of the substrate, containing < 1% lignin.

Fig. 4-2 demonstrates the effects of ASC treatment time (2, 4 and 6 h) on cellulose, hemicellulose, and lignin recovery of lupin hull and canola straw treated at optimum NaOH conditions (15% NaOH/99 °C/6h). For both samples, more than 90% of the original cellulose fibers were recovered. However, a treatment time beyond 4 h seemed to have a negative impact on the cellulose recovery of lupin hull with about 7% decrease (Fig. 4-2a) probably due to cellulose degradation to glucose as the lignin amount was below 1% as discussed earlier, and very low hemicellulose content that was not detectable. The NaOH treatment followed by the ASC treatment of lupin hull and canola straw up to 6 h led to lignin recovery of 4.7% and 16.2%, indicating the removal of 95.2% and 83.7% of the original lignin, respectively.

Similarly, the hemicellulose fraction removal for lupin hull was much higher than that of canola straw, with amounts of 91.2% and 81.4% for lupin hull and canola straw, respectively. With the ASC treatment, noncellulosics were removed, and the solid residue turned into white color, suggesting successful isolation of cellulose-rich fraction.

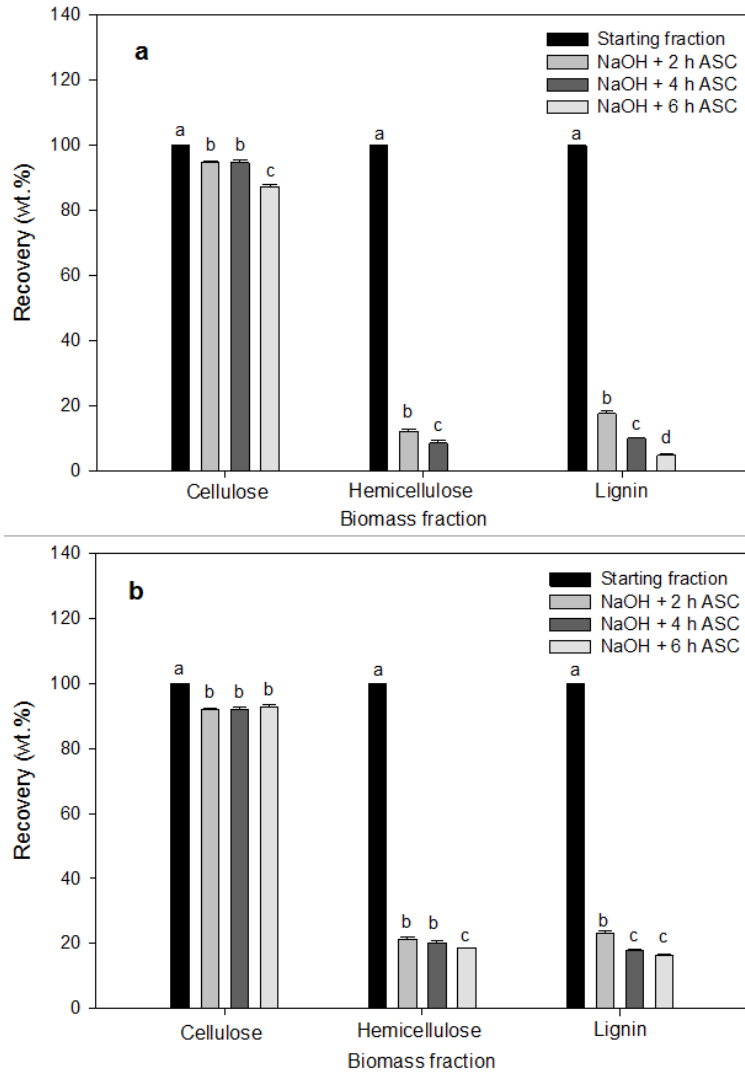


**Figure 4-2.** Effect of ASC treatment (1.7%/75 °C) time (2, 4 and 6 h) on cellulose, hemicellulose, and lignin recovery of (a) lupin hull and (b) canola straw treated at optimum NaOH conditions (15% NaOH/99 °C/6h). Means with different letters within each biomass fraction are different from each other at  $p < 0.05$ .

In the case of lupin hull, the solid residue appeared white after the first 2 h of treatment. However, the solid residue of canola straw still appeared yellow after the first 2 h of treatment, which was a visual evidence of certain amounts of hemicellulose and lignin present. Then, the white color of canola straw residue was obtained at the end of 4 h treatment time.

Overall, cellulose enriched fibers were obtained with more than 90% and 80% cellulose content from lupin hull and canola straw samples, respectively, as a result of combined NaOH and ASC treatments. However, higher amounts of non-cellulosic components removal (~95% of lignin and ~92% of hemicellulose) was observed for lupin hull compared to those of canola straw (~84% of lignin and ~81% of hemicellulose), which can be related with the much lower lignin content of lupin hull in the starting material.

#### **4.3.2. Crystallinity**

Fig. 4-3 shows the XRD patterns of untreated, NaOH and ASC treated lupin hull and canola straw and their corresponding CIs. The results clearly demonstrated the increase in the crystallinity of both samples after NaOH and ASC treatments. Moreover, the crystalline structure of cellulose in both samples was maintained after both treatments as all XRD diffractograms showed three peaks at around  $2\theta = 16.5^\circ$ ,  $22.5^\circ$  and  $34.5^\circ$ , which are associated with the typical crystalline structure of cellulose I (Nishiyama, 2009).

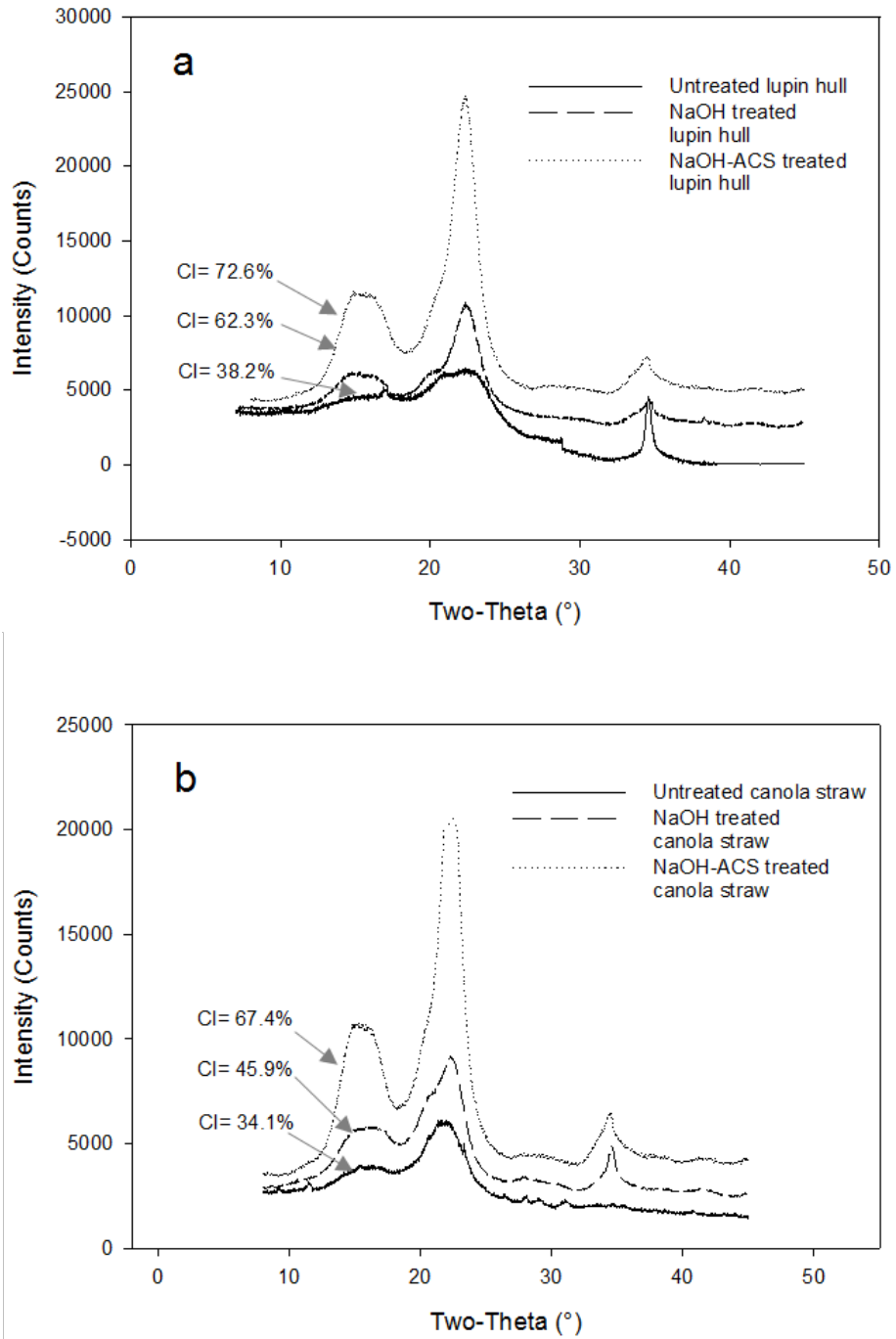


**Figure 4-3.** X-ray diffraction (XRD) patterns of untreated, NaOH (15%/99 °C/6h) and NaOH-ASC (ASC: 1.7%/75 °C/6h) treated (a) lupin hull, and (b) canola straw, and their crystallinity index (CI) values.

Separation of the molecular chains of cellulose in the presence of NaOH usually lead to destruction of cellulose I structure, which is then transformed into cellulose II (Revol et al., 1987). In this study, 15% NaOH concentration did not affect the cellulose structure.

Yue et al. (2015) reported that the cane bagasse conversion from cellulose I to cellulose II could not be obtained with NaOH concentrations of  $\leq 10$  wt.%. They evaluated treatments with 10 and 20% NaOH for 1.5-10 h at 98 °C and obtained a mixture of cellulose I and II structures in the 20% NaOH treated samples for 1.5 h, indicating the presence of peaks at  $2\theta = 15.16^\circ$  and  $16.60^\circ$ , and a small peak at  $2\theta = 12.22^\circ$ .

The CI value of untreated lupin hull (38.2%) was slightly higher than that of canola straw (34.1%). The CI values for the lupin hull treated by NaOH and NaOH-ASC were 62.3% and 72.6%, respectively. Similarly, the increased crystallinity was observed for canola straw samples, where the CI values for the NaOH treated and NaOH-ASC treated samples were found to be 45.9% and 67.4%, respectively.

Such an increase in crystallinity was attributed to the removal of amorphous lignin and hemicellulose as cellulose is crystalline in nature. The CI values of canola straw samples were less than those of lupin hull, which might be due to the fact that canola straw contains comparatively more amorphous components than that of untreated lupin hull and the treated lupin hull at the conditions tested. These results also implied that obtained cellulose fibers have

improved mechanical properties since higher crystallinity leads to higher tensile strength (Alemdar and Sain, 2007).

#### **4.3.3. Thermal behavior**

TG analysis was carried out to investigate the degradation characteristics and thermal stability of both samples at various stages of the isolation processes. Fig. 4-4 presents the effect of NaOH and ASC treatments on the thermal behavior of lupin hull and canola straw samples.

Thermal behavior of both samples changed significantly after treatments. NaOH and ASC treated samples showed improved thermal stability with increased onset temperature of degradation, which ascribed to the removal of amorphous hemicelluloses and lignin. Because these components can form free radicals, initiating the degradation at lower temperatures than the crystalline fractions. The onset of degradation of untreated lupin hull and canola straw started at temperatures of 238 °C and 232 °C, respectively. After NaOH treatment, the onset temperature increases to 301 °C for lupin hull, and 298 °C for canola straw due to the increased crystallinity of cellulose as discussed earlier. The onset of degradation further rises in the case of NaOH-ACS treated lupin hull (318 °C) and that of the canola straw (307 °C) since majority of the amorphous components were removed.

The thermal degradation curves of lignocellulosic biomass are composed of multi-stages due to the existence of lignin, hemicellulose, and other non-cellulosic constituents with different decomposition temperatures. The first stage

of the degradation begins at around 120 °C, which is regarded as the evaporation of loosely bound moisture on the surface and/or intermolecular hydrogen bonded water (Ray et al., 2002). As shown in Fig. 4-4, NaOH treated and NaOH-ASC treated samples have relatively lower moisture contents of 4-6% and 1-2% than untreated lupin hull and canola straw (10-12%). This is because untreated samples are composed of more hydrophilic components like hemicellulose, which can entrap greater amount of water (Mandal and Chakrabarty, 2011), and also depends on initial moisture content of the sample. The second stage of the degradation between 220 and 315 °C is attributed to the thermal decomposition of mainly hemicellulose and the breakdown of glycosidic linkages of cellulose (Manfredi et al., 2006). The weight loss of untreated samples between 220 and 315 °C (~20% for lupin hull and ~28% for canola straw) is higher than that of NaOH treated samples (~7% for lupin hull and ~15% for canola straw) since NaOH treated samples contain less hemicelluloses due to the effective removal during treatment. The third stage of degradation between 315 and 400 °C is associated with predominantly cellulose and lignin decomposition (Yang et al., 2006). Weight losses of the samples (~70% for lupin hull and ~45% for canola straw) in that region increased due to an increased cellulose content. The final stage of degradation above 400 °C is related to mainly lignin decomposition. However, lignin decomposition takes place in a broader temperature range than cellulose and hemicelluloses as observed in Fig. 4-4.

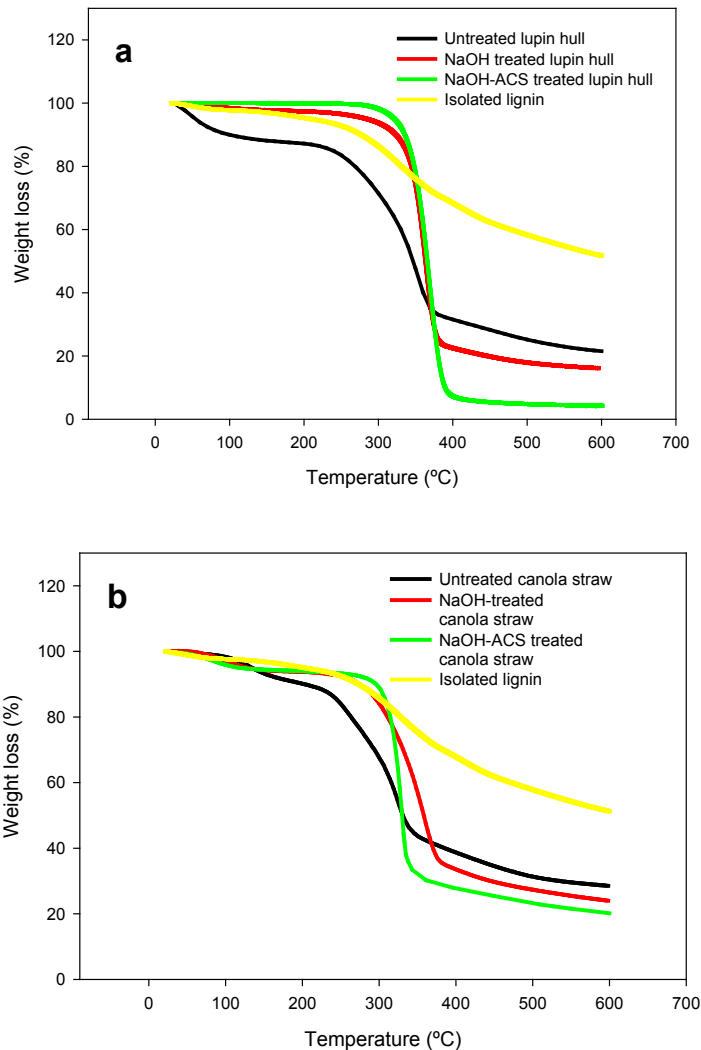


**Figure 4-4.** Thermo-gravimetric (TG) curves of untreated, NaOH (15%/99 °C/6h) and NaOH-ASC (ASC: 1.7%/75 °C/6h) treated (a) lupin hull, and (b) canola straw.

More than 50% of the isolated lignin from lupin hull and canola straw were maintained at a temperature of 600 °C as they require higher temperature to reach complete degradation (800-1000 °C) (Yang et al., 2007). The presence of various oxygen functional groups in lignin with different thermal stabilities leads to a broader decomposition temperature range (Brebú and Vasile, 2010).

#### 4.3.4. Morphology

The morphology of raw and NaOH/ASC treated samples were examined to elucidate the physical changes that occurred in lupin hull and canola straw samples after each treatment. Fig. 4-5 shows the SEM images of untreated, NaOH and ASC treated lupin hull and canola straw samples. Untreated samples were intact, displaying more compact and smooth surface structures with non-uniform shapes and low porosity (Fig. 4-5a-c). The significant change in fibers' morphologies was clear with disruption of the cell walls as a consequence of amounts of lignin and hemicellulose removal with 15% NaOH treatments at 99 °C for 6 h.

It was observed that NaOH treated fibers of lupin hull and canola straw had increased porosity (Fig. 4-5d-i). The holes observed in the NaOH treated samples made the fibers more accessible for subsequent ASC treatments for an effective removal of hemicellulose and lignin. Thus, more remarkable changes were observed due to the further deconstruction of the cell walls after ASC treatments of both samples at 75 °C for 6 h, which are visualized in Fig. 4-5j-l. The NaOH-ASC treated samples composed of 80-90% cellulose exhibits smoother, uniform and homogeneous fiber surface, creating a larger surface area and indicating the extensive removal of non-cellulosic components from lupin hull and canola straw.



**Figure 4-5.** Scanning electron microscopy (SEM) images of (a) untreated lupin hull, (b,c) untreated canola straw, (d-f) NaOH treated lupin hull, (g-i) NaOH treated canola straw, (j) NaOH-ASC treated lupin hull, (k,l) NaOH-ASC treated canola straw at the optimized conditions (NaOH: 15%/99 °C/6h, and ASC: 1.7%/75 °C/6h), (m-o) lignin from lupin hull, and (p-s) lignin from canola straw after NaOH treatment (15%/99 °C/6h).

Different morphological structures of precipitated lignins from the extracts were observed. Lupin hull lignin (Fig. 4-5m-o) exhibited more sponge-like image and appeared as agglomerated structures. On the other hand, lignin from canola straw (Fig. 4-5p-s) showed more rock-like structures. Cracks and holes were present on the surfaces and some smooth spherical forms were observed.

#### **4.4. Conclusions**

Cellulose fibers of lupin hull and canola straw were successfully produced using combined treatments with NaOH followed by ASC. The maximum cellulose content obtained was 93.2% for lupin hull after treatment with 15% NaOH at 99 °C for 6 h followed by 4 h ASC treatment. For canola straw, 81.4% cellulose content was obtained after treatment with 15% NaOH at 99 °C for 6 h followed by 6 h ASC treatment. The amount of non-cellulosic components removal was higher for lupin hull than that of canola straw. Lupin hull and canola straw lignin contents were reduced by about 90 and 82%, respectively. The maximum removed hemicellulose contents were 92 and 81% for lupin hull and canola straw, respectively. The treated samples had increased crystallinity up to 72.6% CI for lupin hull and 67.4% CI for canola straw and improved thermal stabilities, with onset degradation up to 318 °C for lupin hull and 307 °C for canola straw. The SEM images revealed that the isolated cellulose fibers from lupin hull and canola straw obtained after NaOH/ASC treatments had more homogeneity and uniformity with increased surface area.

## **Chapter 5. Cellulose nanofibers of lupin hull obtained by processing with subcritical water and ultrasonication\***

### **5.1. Introduction**

In the last few decades, research on cellulose nanofibers has intensified due to their unique characteristics, such as high surface area, high tensile strength, low coefficient of thermal expansion, good biocompatibility, non-toxicity and excellent mechanical properties (Eichhorn et al., 2010). They have shown great potential in many applications, including nanocomposites (Siro' and Plackett, 2010), optically transparent materials (Nogi and Yano 2008; Yano et al., 2005), aerogels (Pääkkö et al., 2008), films (Velásquez-Cock et al., 2016), templates (Kelly et al., 2014) and others.

Cellulose nanofibers have been isolated from various agricultural residues, such as wheat straw and soy hull (Alemdar and Sain, 2008), banana rachis (Zuluaga et al., 2009), rice straw (Hassan et al., 2012), corn stalks (Reddy and Yang, 2005), and soybean pods since they are readily available and inexpensive lignocellulosic feedstocks (Wang and Sain, 2007). Cellulose nanofibers are prepared from highly purified cellulose obtained after chemical/mechanical (Fujisawa et al., 2011; Saito et al., 2007) or enzymatic pretreatments (Pääkkö et al., 2007) by removal of the main matrix components, such as hemicellulose and lignin.

---

\*A version of this chapter has been submitted to Food and Bioprocess Technology as Ciftci, D., Flores, R. and Saldaña, M.D.A. (2016). Cellulose nanofibers of lupin hull obtained by processing with subcritical water and ultrasonication.

Subcritical water technology is an environmentally friendly approach for pretreatment of agricultural residues as it only utilizes pressurized hot water at elevated temperatures of 160-220 °C. Under these conditions, physicochemical properties of water changes, mainly dielectric constant decreases, and water behaves like certain organic solvents, such as methanol and ethanol. Therefore, it can dissolve substances of a wide range of polarity (Deng et al, 2005; Kim et al., 2009; Saldaña and Valdivieso-Ramirez, 2015).

After pretreatments, very high mechanical shearing is required to disintegrate the cell wall to liberate the cellulose nanofibers. These processes include grinding, milling or refining (Abe et al., 2007), cryocrushing (Chakraborty et al., 2005), microfluidization (Alila et al., 2013), and high pressure homogenization (Nakagaito and Yano, 2005; Turbak et al., 1983), as well as different combinations of these methods. In the last decade, ultrasonication method has been successfully applied for fibrillation of pretreated fibers into nanoscale (Chen et al., 2011, Cheng et al., 2007; Wang and Cheng, 2009; Wang et al, 2016). Ultrasonication of cellulose fibers in water involves the use of ultrasound waves (>20 kHz) to disrupt molecular interactions between cellulose microfibrils through a process known as cavitation. The ultrasound waves result in the vibration of fibers as they experience high-pressure and low-pressure cycles, which creates microscopic vacuum bubbles or voids in the liquid, causing collapse and individualizing microfibril bundles into the solution (Chen et al., 2011). The cavitation produces high shear forces at the ultrasonicator tip and

leads to cellulose in water dispersion to become intensely agitated to individualize into nanoscale.

In this study, sweet blue lupin hull, *Lupinus angustifolius*, was chosen to obtain cellulose nanofibers due to its low lignin content (2-8%) and high cellulose content (40-50%). Subcritical water treatment of lupin hull was conducted to obtain a cellulose-enriched residue (~80% cellulose) at 180 °C, 50 bar and 5 mL/min as discussed in Chapter 3. To date, there is no research available on the isolation of cellulose nanofibers from lupin hull or the use of subcritical water technology as a pretreatment method to obtain cellulose nanofibers. Therefore, the main objective of this study was to investigate the isolation and characterization of cellulose nanofibers using an environmentally friendly approach that reduces the use of toxic chemicals and waste. For this purpose, subcritical water treated lupin hull cellulose fibers were further purified using a bleaching treatment with acidified sodium chlorite for 4 h. Then, fibrillation of highly purified cellulose into nanoscale was performed via high intensity ultrasonic treatment. Effects of ultrasonication parameters, such as applied amplitude (20-80%) and time (15-35 min) on the fibrillation process of cellulose fibers were investigated. Besides, water retention values of fibers were determined to evaluate the degree of fibrillation. The structural and physicochemical properties of the obtained nanofibers were characterized by scanning electron microscopy (SEM), transmission electron microscopy (TEM), Fourier transform infrared (FTIR) spectroscopy, X-ray diffraction (XRD) and thermogravimetric (TG) analysis.

## **5.2. Materials and methods**

### **5.2.1. Materials**

Lupin hulls supplied by Ceapro Inc. (Edmonton, AB, Canada) were ground in a centrifugal mill using a 1 mm sizeve (Retsch, Haan, Germany). All chemicals used, such as sodium chlorite ( $\text{NaClO}_2$ ) and acetic acid, were of laboratory grade and obtained from Fisher Scientific (Pittsburgh, PA, USA).

### **5.2.2. Preparation of cellulose fibers**

Cellulose rich residues used in this study were extracted at optimized conditions from lupin hull using subcritical water technology as described in Chapter 3 (Section 3.2.3). Then, samples were bleached using 1.7% acidified sodium chlorite according to a modified method (Ruangudomsakul et al., 2015) that was described in Chapter 4 (Section 4.2.2) for 4 h to achieve sufficient delignification.

### **5.2.3. Preparation of cellulose nanofibers**

Purified cellulose fibers were soaked in 100 mL of distilled water at a fiber content of 0.1% (w/v). The aqueous dispersions were then treated with a high intensity ultrasonicator (Model 705, 700 W, 50/60 Hz, Fischer Scientific, Pittsburgh, PA, USA) equipped with a cylindrical titanium alloy probe tip of 1.27 cm in diameter. The ultrasonication of the samples was carried out at defined amplitude (20-80%) for varying time (15-35 min). Ultrasonic treatments were performed in an ice/water bath to prevent heat generation. The obtained aqueous

dispersions were frozen at -18 °C and then freeze-dried (Free Zone 1.0 L Benchtop Freeze Dry System, Labconco, Kansas City, MO, USA) at -45 °C for 48 h. Cellulose nanofibers obtained were then analyzed for morphology, functional groups, crystallinity, and thermal stability. Oven-dried cellulose nanofibers were obtained by pouring 5 mL of sample into an aluminum mould with 5 cm diameter and drying in an oven at 40 °C for 48 h to be then analyzed for morphology.

#### **5.2.4. Determination of lignin content**

Lignin content analysis after cellulose fiber treatment with acidified sodium chlorite was carried out following the NREL standard analytical procedure (Sluiter et al., 2008) that was described in Chapter 3 (Section 3.2.4.3).

#### **5.2.5. Water retention value**

The water retention values (WRV) of resultant cellulose nanofiber dispersions were measured using a centrifugation technique (Cheng et., 2010). Briefly, cellulose nanofiber dispersions were subjected to centrifugation at 900g for 30 min at 20 °C. The wet sediment obtained after centrifugation was dried overnight at 105 °C. The WRV was determined using the equation below:

$$WRV (\%) = \frac{W_w - W_d}{W_w} * 100 \quad (5.1)$$

where,  $W_w$  is the weight of the sample after centrifugation and  $W_d$  is the weight of the sample after drying.

### **5.2.6. Microscopic analysis**

The SEM images of the purified cellulose, air-dried and freeze-dried cellulose nanofiber dispersions were taken using field emission SEM (S4700 FE-SEM, Hitachi, Tokyo, Japan) as described in Chapter 4 (Section 4.2.3.4).

The TEM analyses of cellulose nanofiber dispersions were performed with a TEM microscope (H7500 TEM, Hitachi, Tokyo, Japan) operated at 80 kV. One drop of aqueous nanofiber suspension was placed onto carbon-coated TEM grids and the sample was then negatively stained with 1% uranyl acetate and allowed to dry under ambient conditions. Diameters of cellulose nanofibers were calculated using the ImageJ processing software IJ1.46 by loading the TEM images into the software and measuring the fiber diameters. Scale bars on each TEM image were used for calibration of the software. Approximately, 100 measurements were done using 10 TEM images. The average diameters and size distributions were determined from particle sizes obtained by drawing straight lines from the selected fibers in the corresponding TEM images.

### **5.2.7. Fourier Transform Infrared Spectroscopy analysis**

Infrared spectra of cellulose nanofibers were characterized by an FTIR using attenuated total reflectance (ATR) (Nicolet 380, Thermo Scientific, Waltham, MA, USA). Raw and freeze dried cellulose nanofiber samples were directly pressed onto the diamond internal reflection element of the ATR accessory. The experiments were conducted in the range of 4000 to 400  $\text{cm}^{-1}$  with

a resolution of  $4 \text{ cm}^{-1}$  and a total of 128 scans per sample. Data collection was done using the Nicolet Omnic 8.3 software.

### **5.2.8. X-ray Diffraction analysis**

XRD patterns of purified cellulose, cellulose nanofibers were measured using a PANalytical Empyrean XRD (Empyrean, PANalytical B.V., Almelo, Netherlands) as described in Chapter 4 (Section 4.2.3.2). The crystallinity index (CI) of the samples was determined using Eq. (3.1) ( $I_{002}$  at  $2\theta = 22.5^\circ$  and  $I_{am}$  at  $2\theta = 18.5^\circ$ ) described in Chapter 3 (Section 3.2.5.1).

### **5.2.9. Statistical analysis**

Data were presented as mean  $\pm$  standard deviation based on at least duplicate experiments and analyses. Statistical analysis was performed using the methodology described in Chapter 3 (Section 3.2.6).

## **5.3. Results and discussion**

Chemical composition of untreated lupin hull was determined to be  $45.2 \pm 2.1\%$  cellulose,  $25.4 \pm 1.4\%$  hemicellulose, and  $7.8 \pm 0.4\%$  lignin in the previous study reported in Chapter 3. In this study, subcritical water treatment of lupin hull was carried out at the optimized conditions of  $180 \text{ }^\circ\text{C}$ , 50 bar and 5 mL/min using a semi-continuous flow type subcritical water system, resulting in most of the hemicellulose removal ( $>85.5\%$ ). However, subcritical water treatment does not ensure the complete removal of lignin due to lignin recondensation (Pu et al.,

2015). After subcritical water treatment, the final lignin content was 15% due to the removal of most of the hemicellulose and other minor components. The presence of residual lignin might reduce the efficiency of cellulose fibrillation as lignin is believed to be a major impediment to cellulose accessibility. Therefore, a bleaching treatment was required for residual lignin removal. Then, subcritical water treated lupin hull was subjected to a delignification process with acidified sodium chlorite to obtain highly purified cellulose fibers (~97%), which led to the reduction of the lignin content to  $1.27 \pm 0.05\%$ .

### **5.3.1. Water retention value**

To investigate the effects of ultrasonic treatment parameters, amplitude and time, on the degree of fibrillation of cellulose, the WRV of ultrasonicated lupin hull cellulose nanofibers were determined. The WRV is a measure of the fiber's swelling capacity, which is expressed as the percentage of water contained in a sample after centrifugation (Cheng et al., 2007).

The WRV of the untreated lupin hull cellulose was found to be approximately 157% as shown in Figure 5-1. Ultrasonication of the samples at 20% amplitude for 15-35 min did not affect the WRV significantly (161-166%). However, treatments at higher amplitudes (50% and 80%) resulted in higher WRV (194-305%). Higher WRV relates to the higher degree of fibrillation (Cheng et al., 2010). The higher WRV values indicate more nanofibers are isolated or more voids are formed among the fibers. Therefore, an increased swelling capacity arise from a more exposed fiber surface area to absorb water

due to deconstructed fiber bundles obtained at an increased amplitude. A rapid WRV increase was observed after 15 min treatment time for both ultrasonicated samples at 50% and 80% amplitude, with the maximum values being approximately 263% at 50% amplitude and 305% at 80% amplitude for 35 min treatment time, indicating that more water accessible surface area was created through extensive degree of fibrillation at these conditions. The increase of the WRV with increased deconstruction of the fibers has also been reported elsewhere (Heidarian et al., 2016; Wang and Cheng, 2009). Based on the WRV evaluations, four samples with the higher WRV values were chosen for morphology and size analysis as they are expected to show better fibrillations.

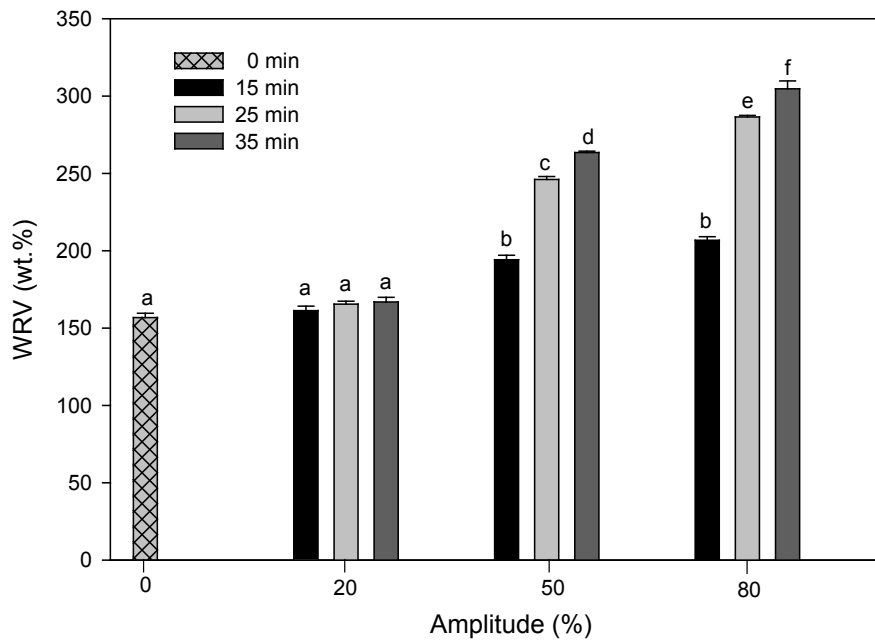


**Figure 5-1.** Water retention value (WRV) of untreated and ultrasonicated lupin hull cellulose at different amplitudes (20, 50 and 80%) for varying times (15, 25 and 35 min). Means with different letters within all amplitudes are different from each other at  $p < 0.05$ .

### 5.3.2. Morphology and size

Morphologies and fiber size distributions of the lupin hull cellulose ultrasonicated at different amplitudes (50 and 80%) for varying time (15-35 min) were presented in Figure 5-2, revealing successful fibrillations at nano-scale.

It is clear that the morphology and size of the isolated cellulose nanofibers were affected by the two process parameters evaluated. All TEM images displayed a classical web-like network structure, consisting of long entangled nanoscale cellulosic filaments, with the lengths estimated to be several microns as seen in Figure 5-2a-d. Measuring the exact lengths of cellulose nanofibers were not possible as the start and end points of the fibers cannot be distinguished due to entangled structures. The overall diameter size distribution narrowed down as the ultrasonication amplitude and time increased. It is clear from Figure 5-2a that 25 min of ultrasonication at 50% amplitude was not strong enough to separate large cellulose nanofiber bundles. Diameter size analysis showed that the ultrasonicated fibers at 50% amplitude for 25 min had a diameter range of 20-80 nm, and more than 75% of the fibers had diameters between 40 and 60 nm with an average diameter of 46 nm. Increasing ultrasonication time to 35 min at 50% amplitude resulted in improved fibrillation, with an average diameter of 32 nm (Fig. 5-2b), where approximately 60% of the fibers were found to be in the range of 20-40 nm.

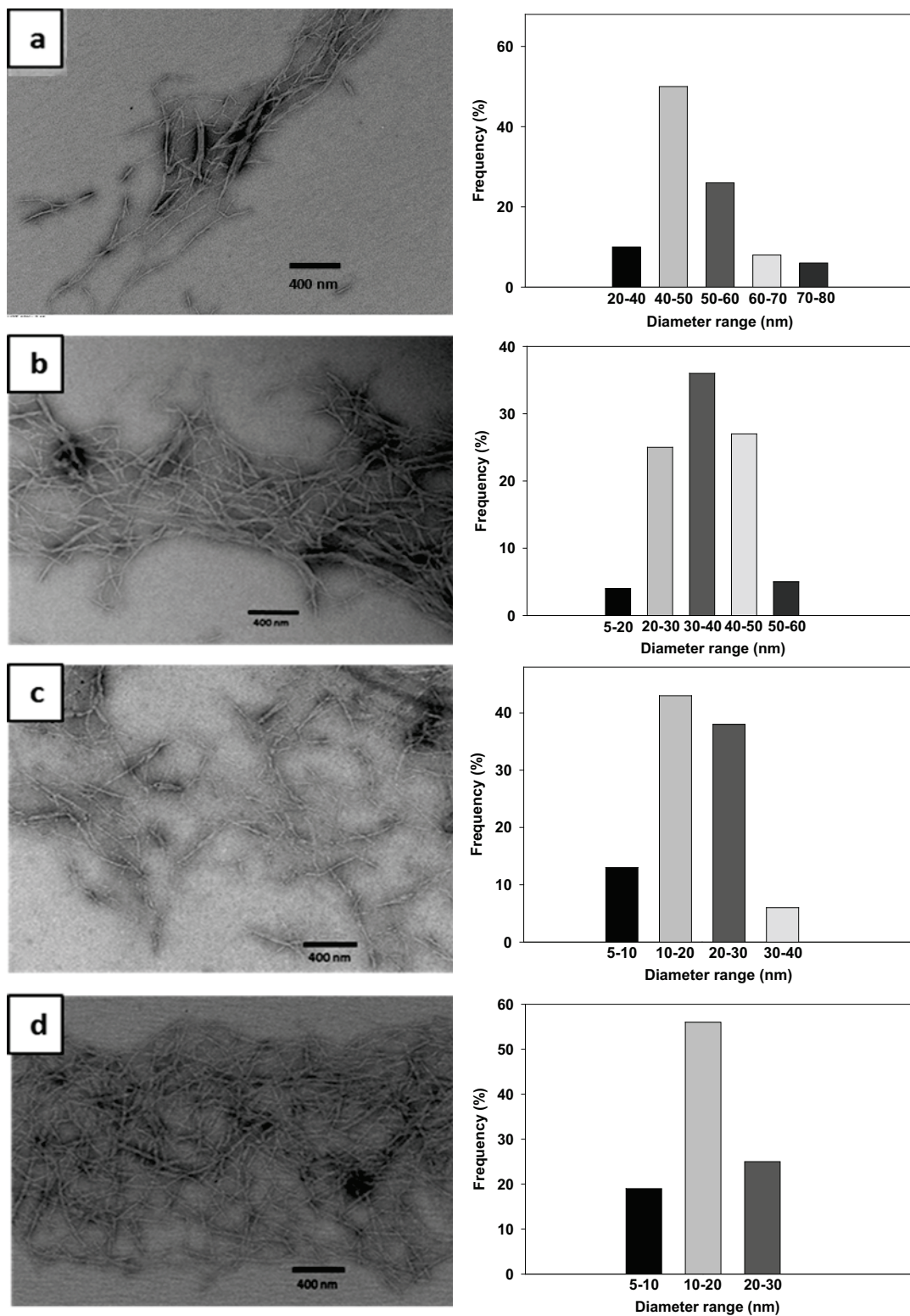


**Figure 5-2.** Transmission electron microscopy (TEM) images and size distribution of lupin hull cellulose ultrasonicated at different conditions: (a) 50% amplitude for 25 min, (b) 50% amplitude for 35 min, (c) 80% amplitude for 25 min, and (d) 80% amplitude for 35 min.

Increasing ultrasonication amplitude to 80% was very effective on fibrillation. It was observed that ultrasonication of fibers at 80% amplitude for 25 min produced a dispersion of high aspect ratio nanofibers with a decreased average diameter of 19 nm (Fig. 5-2c).

A 10 min increase in the ultrasonication time with a total time of 35 min further improved the extent of fibrillation to obtain nanofibers with an average diameter of 15 nm, resulting in more entangled fiber network due to strong hydrogen bonds as a large number of hydroxyl groups were exposed with the decreased fiber size. Almost 75% of the nanofibers displayed diameters between 5 and 20 nm, and the missing 25% fibers were in the range of 20-30 nm.

The effect of amplitude on fibrillation is related with the intensity as intensity of sonication is directly proportional to the amplitude of vibration (Mason, 2000). Therefore, an increase in the amplitude of vibration led to an increase in the intensity of vibration, favoring cellulose fibrillation to nano-size. Longer treatment times at higher amplitudes resulted in better fibrillation, which positively correlated with the WRV values (Figure 5-3) as swelling capacity increased with the decreased size.

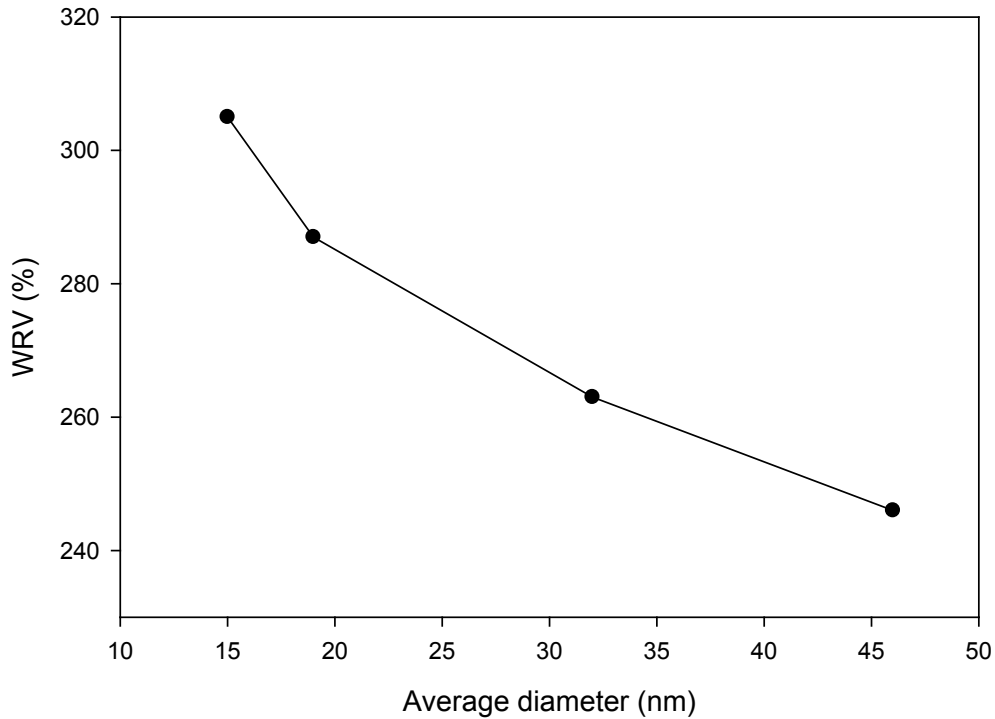


**Figure 5-3.** Effect of WRV values on the average diameter size at 50-80% amplitude for 25-35 min.

Even though improved fibrillations with smaller size were found at higher amplitudes, further increase of amplitude and time could produce more agglomerated and entangled nanofibers. Moreover, longer processing times at high amplitudes may increase the chance of cellulose degradation and disrupt the structural integrity of the fibers (Li et al., 2012). Optimization of minimum amplitude required is important to achieve the cavitation threshold to obtain the desired fibrillation. Amiralian et al. (2015) reported that the ultrasonication of chemically pretreated (alkali treated and bleached) *Triodia pungens* fibers at low amplitude (20%) for either 5 or 20 min, resulted in a high aspect ratio cellulose nanofiber with an average diameter of 4.1 and 6.8 nm, respectively. The

morphologies and size distributions of the cellulose nanofibers obtained were in good agreement with the results of the WRV measurements as the sample with the well nanofibrillated network and the lowest average diameter size had the highest WRV.

Figure 5-4 compares the SEM images of purified lupin hull cellulose fibers and isolated cellulose nanofibers at 80% amplitude for 35 min after oven drying at 40 °C for 48 h and freeze drying at -45 °C for 48 h. During oven drying of the aqueous dispersions of cellulose nanofibers, the adjacent individual nanofibers first collapsed due to the capillary force (Nyström et al., 2010). Then, the attraction of nanofibers to one another occurred, forming agglomerates, which exhibited a rough surface structure (Fig. 5-4b). Agglomeration among the fibers are promoted by hydrogen bonds interactions due to the abundance of hydroxyl groups on the cellulose nanofiber surface (Peng et al., 2012), which may attract particular interest for producing cellulose nanofiber films. On the other hand, freeze drying of the aqueous dispersions minimized the aggregation of the cellulose nanofibers, forming porous structure as seen in Figure 5-4c. However, the morphology of freeze dried nanofibers are influenced by the diameter size and the concentration of the cellulose in dispersion affecting the self-organizing behavior of the fibers (Han et al., 2013).

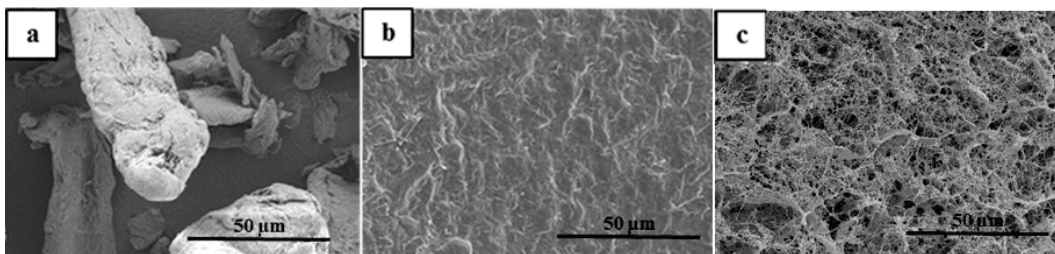


**Figure 5-4.** Scanning electron microscopy (SEM) images of (a) purified lupin hull cellulose microfibrils, (b) isolated cellulose nanofibers (80% amplitude for 35 min); oven dried at 40 °C for 48 h, and (c) freeze dried at -45 °C for 48 h.

### 5.3.3. Attenuated Total Reflectance-Fourier Transform Infrared Spectroscopy

Major components of agricultural residues, such as cellulose, hemicellulose and lignin are composed of alkanes, aromatics, esters, ketones, and alcohols with different oxygen containing functional groups. Thus, Attenuated Total Reflectance FTIR (ATR-FTIR) spectral analysis of the untreated lupin hull, purified cellulose fibers, and cellulose nanofibers were conducted to evaluate the functional group changes in the fibers after ultrasonication (Fig. 5-5). The peak observed at 3000-3600  $\text{cm}^{-1}$  band in the spectra of all samples was associated to the OH stretching vibrations of hydrogen bonded hydroxyl group, which was related to specific intermolecular hydrogen bonds of cellulose (Yang et al., 2007). The peaks in the range of 1734  $\text{cm}^{-1}$  and 1600  $\text{cm}^{-1}$  (C=O stretching) in untreated lupin hull were attributed to the acetyl and uronic ester groups of hemicelluloses or the ester linkage of the carboxylic groups of the ferulic and *p*-coumaric acids of lignin (Sun et al., 2005). No equivalent peaks were observed in the ATR-FTIR spectra of the purified cellulose and cellulose nanofibers, ensuring the removal of

most hemicelluloses and lignin. The existence of these peaks was reported earlier (Alemdar and Sain, 2008; Ruangudomsakul et al., 2015). The peak appearance at around  $896\text{ cm}^{-1}$  indicated the  $\beta$ -glycosidic linkages of glucose ring of cellulose (Xiao et al., 2001), which existed in the spectra of all samples. This peak was more intense in purified cellulose and cellulose nanofibers, revealing the removal of hemicellulose and lignin. The other characteristic peaks of cellulose at around  $3297$ ,  $1131$  and  $1046\text{ cm}^{-1}$  were significantly pronounced upon removal of noncellulosics from lupin hull.

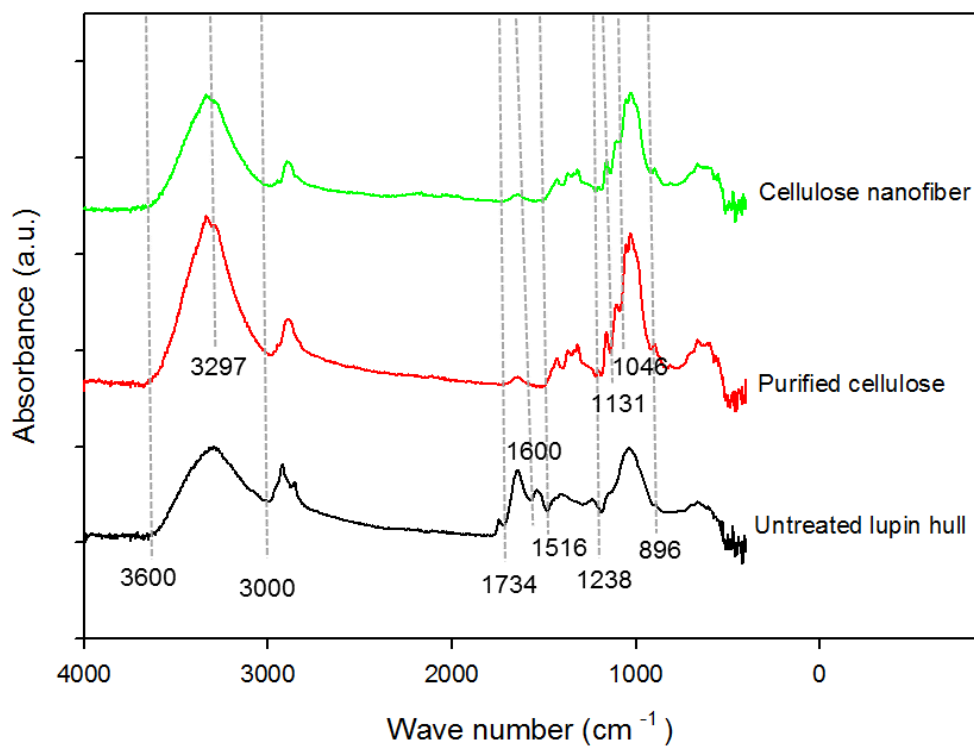


**Figure 5-5.** Attenuated Total Reflectance Fourier Transform Infrared Spectroscopy (ATR-FTIR) spectra of untreated lupin hull, purified lupin hull cellulose and isolated cellulose nanofibers (80% amplitude for 35 min).

The spectrum of untreated hull was significantly different from those of purified cellulose and cellulose nanofibers. The peak absorptions arising from noncellulosics were mostly removed in the purified cellulose after subcritical water and ASC treatments. No significant differences were observed between the spectrum of purified cellulose and cellulose nanofibers, which indicated that no new functional groups were generated. However, the peak absorption intensities slightly changed, which could be attributed to the effect of ultrasonication process on the molecular or supramolecular structure of cellulose.

#### **5.3.4. Crystallinity**

Figure 5-6 compares the XRD patterns of the resultant cellulose nanofibers with the subcritical water treated-bleached cellulose fibers. All diffractograms presented typical cellulose I structure with three well-defined crystalline peaks at around  $2\theta = 16.5^\circ$ ,  $22.5^\circ$  and  $34.5^\circ$  (Nishiyama et al., 2002), indicating that the molecular arrangement of cellulose was not affected by the mild pre- or post-treatments applied in this study. The crystallinity index (CI, percentage of crystalline cellulose in the total cellulose) values of the samples were calculated using Eq. (3.1) based on the peak heights of crystalline ( $I_{002}$ ) and amorphous ( $I_{am}$ ) regions of cellulose. The CI value of purified cellulose was calculated as 75.4%. No significant change was observed in the CI values of the ultrasonicated samples at 50% amplitude for 25 and 35 min and 80% amplitude for 25 min compared to the purified cellulose fibers (~ 75% CI). However, a slight decrease in CI value to 73.1% was observed as ultrasonication time

increased from 25 min to 35 min at constant 80% amplitude. This might indicate that the crystalline region of the nanofibers was damaged upon ultrasonication at the high amplitude (80%) and long time use (35 min). Such a decrease in crystallinity with increasing ultrasonication time was previously reported (Amiralian et al., 2015; Chen et al., 2015; Wang and Cheng, 2009), which was attributed to the non-selectivity (act on both amorphous and crystalline regions) of ultrasonication process (Li et al., 2012). Therefore, ultrasonic cavitation does not only affect the amorphous regions, but also the crystalline regions of the cellulose, depending on the intensive of the vibrational energy and processing time.

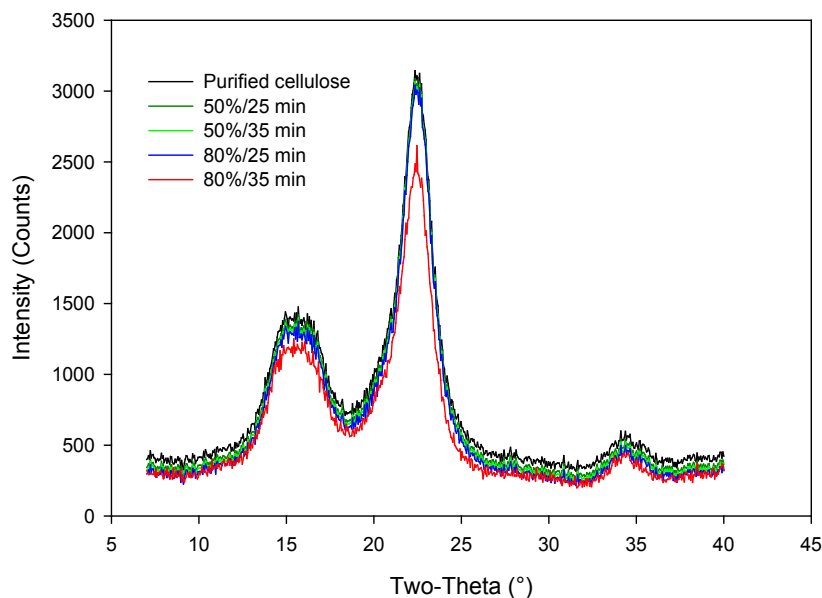


**Figure 5-6.** X-ray diffraction (XRD) patterns of ultrasonicated lupin hull cellulose at different conditions: 50% amplitude for 25 min, 50% amplitude for 35 min, 80% amplitude for 25 min, and 80% amplitude for 35 min.

Despite the decrease in crystallinity at high intensity ultrasonication conditions, the cellulose nanofibers obtained had high crystallinity (>70%), which is associated with the high rigidity and stiffness (Bhatnagar and Sain, 2005), offering promising applications where high tensile strength is demanded.

#### **5.4. Conclusions**

Cellulose nanofibers were isolated from lupin hull using an environmentally friendly subcritical water-assisted technology followed by high intensity ultrasonication. The results revealed successful nanofibrillation as the ultrasonication amplitude and time were increased to 80% and 35 min. The improvement in the degree of nanofibrillation of the cellulose fibers was also confirmed with the increased WRV values from 161% to 305%. The smallest average diameter obtained after subcritical water treatment followed by ultrasonication at 80% amplitude and 35 min was 15 nm. The ATR FTIR spectra showed the effective removal of hemicellulose and lignin achieved after subcritical water and bleaching treatments. Obtained nanofibers had high crystallinity (above 70% CI), suggesting potential applications in nanopaper production, biomedical materials, and food packaging.

## **Chapter 6. Characterization of aqueous suspensions of cellulose nanofibers from lupin hull\***

### **6.1. Introduction**

Owing to its inexhaustibility and renewability, cellulose is considered to be the most suitable resource for the production of environmentally friendly materials, replacing oil-derived ones. In recent years, there is a growing interest in the isolation of cellulose nanofibers from lignocellulosic biomass due to their desirable characteristics, such as high aspect ratio, low thermal expansion, good mechanical and optical properties, low weight, low density, and biodegradability. As mentioned previously, cellulose nanofibers may find applications in various products such as nanocomposites, reinforcing agents, coating additives, food packaging, filtration media, functional films, thickening agents, rheology modifiers, templates, and adsorbents (Abdul Khalil et al., 2012; Ayadi et al., 2016; Belbekhouche et al., 2011; Brinchi et al., 2013; Dong et al., 2013; Korhonen et al., 2011; Nakagaito et al., 2010).

Cellulose nanofibers can be produced from plant fiber cellulose using different mechanical approaches, such as high pressure homogenization or microfluidizers (Dufresne et al., 2000; Turback et al., 1983; Zhang et al., 2012), super grinding/refiner-type treatments (Iwamoto et al., 2007; Taniguchi and Okamura, 1998), cryogenic crushing (Alemdar and Sain, 2008), and high intensity ultrasonication (Cheng et al., 2009; Wang, et al., 2016) in various combinations.

---

\*A version of this chapter has been submitted to *Fibers and Polymers* as Ciftci, D., Flores, R. and Saldaña, M.D.A. (2016). Characterization of aqueous suspensions of cellulose nanofibers from lupin hull.

Some researchers have employed chemical pre-treatments, such as enzymatic treatment (Pääkkö et al., 2007) or surface modifications of cellulose fibers to add ionic groups on the surface by oxidation and carboxymethylation to achieve better fibrillation during mechanical treatments (Besbes et al., 2011; Hubbe et al., 2008; Wågberg et al., 2008). Cellulose nanofibers are generally produced in the form of aqueous suspensions as water helps the swelling of the cellulose fiber and thus facilitates the breaking of hydrogen bonds between the cellulose cell walls during the fibrillation process. Such aqueous suspensions of cellulose nanofibers are able to form hydrogel structures, i.e., cross-linked three-dimensional hydrophilic polymeric networks capable of absorbing large amounts of water and swelling due to the highly hydrophilic nature of native cellulose (Lasseguette et al., 2008; Pääkkö et al., 2007).

Self-standing cellulose nanofiber hydrogels were reported by some researchers with the treatment of cellulose nanofiber suspensions with acid (Saito et al., 2011) and alkaline media (Abe and Yano, 2011), or using cross-linking agents like metal cations (e.g. silver nanoparticles) (Dong et al., 2013). Such cellulose nanofiber suspensions or hydrogels have great potential for applications in fields such as tissue engineering, including scaffolds to store human cells, drug delivery, sorbents, sensors, contact lenses and water purification (Hubbe et al., 2008). They can be further converted to other cellulose nanofiber forms like aerogels via suitable drying methods, freeze drying and supercritical drying. Characteristics of the suspensions or gels might vary depending on the raw material, cellulose fiber composition, production methods (fibrillation and/or

chemical pre-treatment) and surface functionalization (oxidation or carboxymethylation) of cellulose nanofibers. The rheological behavior is one of the key characteristics of cellulose nanofiber suspensions, which can influence various manufacturing steps, such as pumping, mixing or coating, as well as its final industrial applications. Few reports are available on the rheological properties of cellulose nanofiber suspensions, which mostly include surface functionalized nanofibers like 2,2,6,6-tetramethylpiperidine-1-oxyl radical (TEMPO)-mediated oxidation (Herrick et al., 1983; Lasseuguette et al., 2008; Lotti et al., 2011; Lie et al., 2015; Pääkkö et al., 2007; Rezayati Charani et al., 2013, Tatsumi et al., 2002).

In this study, varying concentrations (0.1-1.9 wt.%) of cellulose nanofiber in water suspensions were prepared by ultrasonication of lupin hull cellulose obtained via combination of subcritical water and bleaching treatments. To the best of the author's knowledge, there is no study on the use of lupin hull for hydrogel formation or the use of subcritical water-assisted treatment in the nanofibrillation process. The objective of this study was to examine the effects of concentration on the morphology, crystallinity, thermal stability and rheological properties of the obtained cellulose nanofiber suspensions or hydrogels.

## **6.2. Materials and methods**

### **6.2.1. Materials**

Lupin hulls (Ceapro Inc., Edmonton, AB, Canada) were used as the starting material to prepare cellulose nanofiber hydrogels. Sodium chlorite

(NaClO<sub>2</sub>) (≥99.5% purity) and acetic acid (>99.7 % purity) were obtained from Fisher Scientific (Pittsburgh, PA, USA). Distilled water was used in the preparation of all suspensions/hydrogels.

### **6.2.2. Preparation of cellulose nanofiber suspensions**

Lupin hull cellulose fibers were obtained after subcritical water and bleaching treatments. Subcritical water treatments of the hulls at process conditions of 180 °C, 50 bar and 5 mL/min, as described in Chapter 3 (Section 3.2.3), resulted in cellulose enriched fibers (~80% cellulose). Then, a bleaching treatment described in Chapter 4 (Section 4.2.2) was conducted for 4 h to obtain the purified cellulose fibers (Ruangudomsakul et al., 2015). Preparation of cellulose nanofiber suspensions in various concentrations (0.1-1.9 wt.%) were carried out by the ultrasonication of purified cellulose fibers in water for 40 min at 80% amplitude using an ultrasonicator (Model 705, 700 W, 50/60 Hz-Fischer Scientific, Pittsburgh, PA, USA) following the procedure described in Chapter 5 (Section 5.2.3). For the X-ray diffraction (XRD) and thermo-gravimetric (TG) analyses, the suspensions were first frozen at -18 °C and then freeze-dried at -45 °C and 15 Pa for 2 days using a freeze-dryer (Free Zone 1.0 L Benchtop Freeze Dry System, Labconco, Kansas City, MO, USA).

### **6.2.3. Microscopic analysis**

The morphologies of the cellulose nanofibers were investigated with transmission electron microscopy (TEM) (H7500 TEM, Hitachi, Tokyo, Japan) following the procedure described in Chapter 5 (Section 5.2.6).

### **6.2.4. X-ray diffraction analysis**

X-ray diffraction (XRD) analysis was performed using a PANalytical Empyrean Diffractometer (Empyrean, PANalytical B.V., Almelo, Netherlands) as described in Chapter 4 (Section 4.2.3.2). The crystallinity index (CI) of the samples was determined using Eq. (3.1) ( $I_{002}$  at  $2\theta = 22.5^\circ$  and  $I_{am}$  at  $2\theta = 18.5^\circ$ ) described in Chapter 3, Section 3.2.5.1.

### **6.2.5. Thermo-gravimetric analysis**

Thermo-gravimetric (TG) analyses were performed using a TGA 209 F1 Libra TG Analyzer (TG 209 F1 Libra, NETZSCH, Selb, Germany) following the procedure described in Chapter 3 (Section 3.2.5.2).

### **6.2.6. Rheological behavior**

Rheological measurements of cellulose nanofiber suspensions were carried out using a rotational rheometer (Physica MCR 301, Anton Paar, Ashland, VA, USA) equipped with a cone and plate geometry (cone angle,  $1.0092^\circ$ ; diameter, 24.972 mm; truncation, 49  $\mu\text{m}$ ) at 25  $^\circ\text{C}$ . Steady-state viscosity measurements were carried out in a shear rate range from 0.01 to 1000  $\text{s}^{-1}$ . Strain

sweep test was performed to determine the linear viscoelastic region within a strain range from 0.01% to 100% at a frequency of 1 Hz prior to frequency sweep tests. Then, frequency sweep measurements were conducted in angular frequency range of 0.1-100 rad/s at 1% strain. Data were analyzed using the RheoPlus software.

### **6.2.7. Statistical analysis**

Data were presented as mean  $\pm$  standard deviation based on at least duplicate experiments and analyses. Statistical analyses were performed using the methodology described in Chapter 3, Section 3.2.6.

## **6.3. Results and discussion**

### **6.3.1. Morphology and structure**

Ultrasonication of purified cellulose fibers in water resulted in the formation of long and entangled nanofiber networks. Figure 6-1a-d shows the TEM images of the obtained cellulose nanofiber suspensions at 0.1-1.9 wt.% concentrations. Cellulose nanofibers with lower concentrations of 0.1 and 0.7 wt.% presented a classical web-like network structures with long entangled nanofiber filaments with diameters of 5-30 nm, and 5-60 nm, respectively, and lengths of several microns (Fig. 6-1a and 6-1b). However, nanofibers were strongly aggregated as the concentration increased to 1.6 and 1.9 wt.%, appearing as bundles or clusters with widths in the range of 5-100 nm (Fig. 6-1c and 6-1d), which was attributed to the higher availability of interacting hydroxyl groups on

the surface of cellulose nanofibers, leading to agglomeration (Zimmermann et al., 2004).

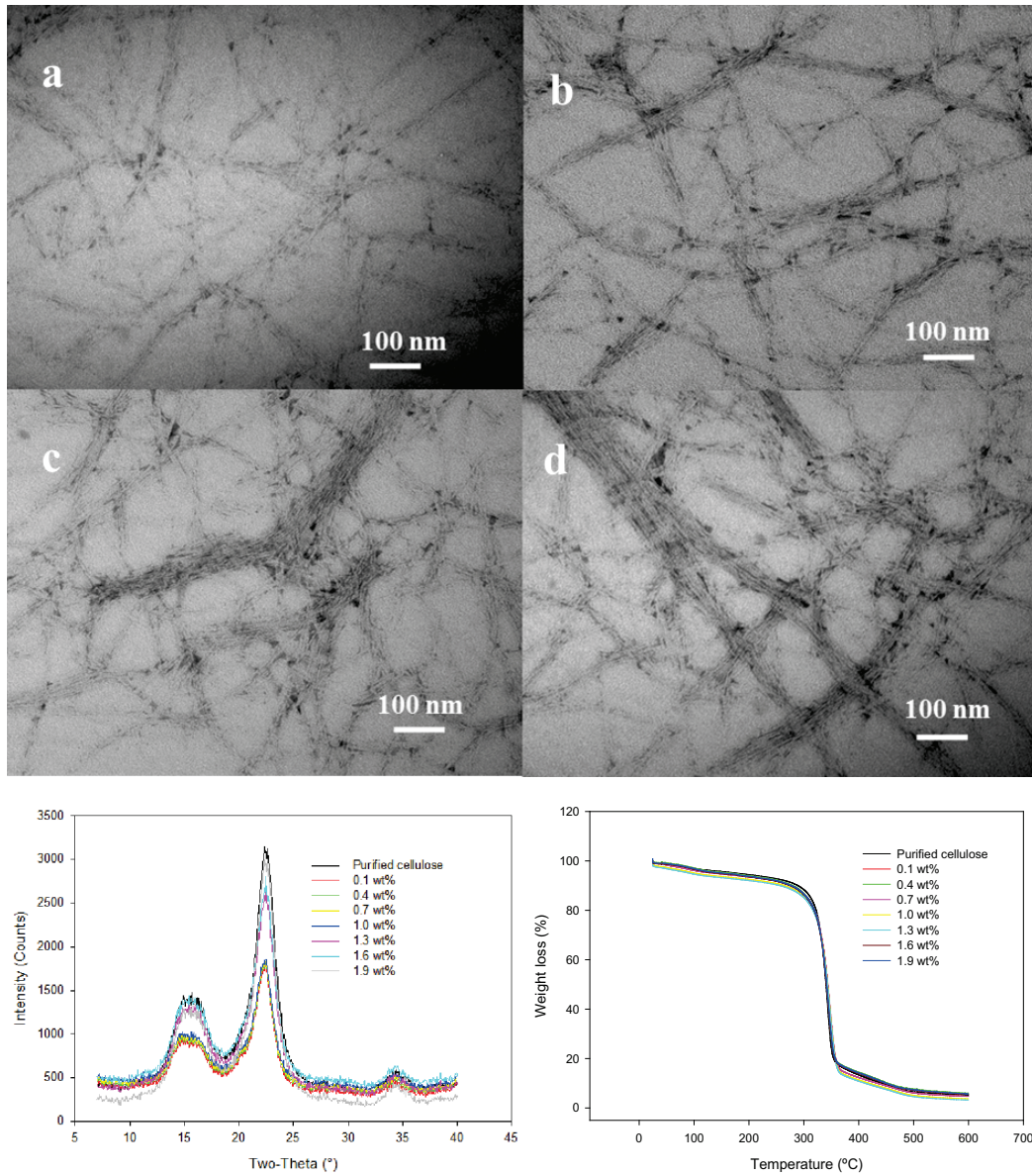


**Figure 6-1.** Morphology and structural characteristics of cellulose nanofibers at different concentrations: TEM images of (a) 0.1 wt.%, (b) 0.7 wt.%, (c) 1.6 wt.%, and (d) 1.9 wt.%, (e) XRD patterns, (f) TG curves.

Figure 6-1e shows that all samples had the major diffraction peaks at  $2\theta=16.5^\circ$ ,  $22.5^\circ$  and  $34.5^\circ$ , indicating the typical crystal patterns of cellulose I type (Nishiyama et al., 2002) since native structure was maintained after the nanofibrillation process, which included treatments with subcritical water, bleaching, and ultrasonication. The CI values calculated using Eq. (3.1) indicated that the CI values significantly ( $p<0.05$ ) decreased from 75% to 71% as the concentration decreased from 1.9 wt.% to 0.1 wt.%.

The reason that lower concentrations of cellulose nanofiber suspensions had lower CI could be related with agitation time. Even though all suspensions were processed for 40 min with an ultrasonicator, suspensions with higher concentrations could not be agitated and stirred equally due to their increased viscosity. Thus, they had a lower chance of passing the ultrasonicator probe tip and were subjected to less ultrasonication energy. The longer ultrasonication time might have led to a slight destruction of crystalline surfaces causing such a decrease in crystallinity.

The degree of crystallinity of the fibers has a close relationship with their thermal degradation behavior (Isogai, 2013). Damaging the crystalline structure could lead to a decrease in its thermal stability. Figure 6-1f shows the comparison of the TG curves of subcritical water treated and bleached lupin hull cellulose with the cellulose nanofiber suspensions at different concentrations. All suspensions exhibited a degradation behavior that is highly similar to that of the purified cellulose fibers with the onset of degradation temperature occurring at approximately  $310^\circ\text{C}$ . Results obtained indicate that the decrease of crystallinity

was not significant enough to affect its thermal stability as there was no significant decrease in the onset degradation temperature.

### **6.3.2. Rheological properties**

Figure 6-2a-h. presents the rheological properties of the cellulose nanofiber suspensions. Steady-state viscosities of the suspensions (0.1-1.9 wt.%) as a function of the shear rate were shown in Figure 6-2a. Increasing concentrations resulted in increased viscosity, indicating that a more rigid and entangled network was created as the concentration increased, leading also to higher resistance to flow. Regardless of the concentration, all samples displayed a typical shear-thinning behavior as the viscosity declined with increasing shear rate. This behavior can be attributed to the breakdown of the entangled nanofiber network caused by high shearing, which led to a sharp drop in the viscosity.

Shear-thinning behavior of cellulose nanofiber suspensions was also reported in different studies (Lasseguette et al. 2008; Lotti et al., 2011; Lie et al., 2015; Pääkkö et al., 2007; Rezayati Charani et al., 2013). However, different trends of shear-thinning behaviors were reported, depending on the raw material, the treatment and/or fibrillation methods. Lie et al. (2015) observed the four-region shear-thinning behavior for cellulose nanofiber (Celish KY 100-S grade) suspensions obtained using super high pressure homogenizer (2070 bar/10 passes) in the concentration range of 0.25-1.5 wt.%.

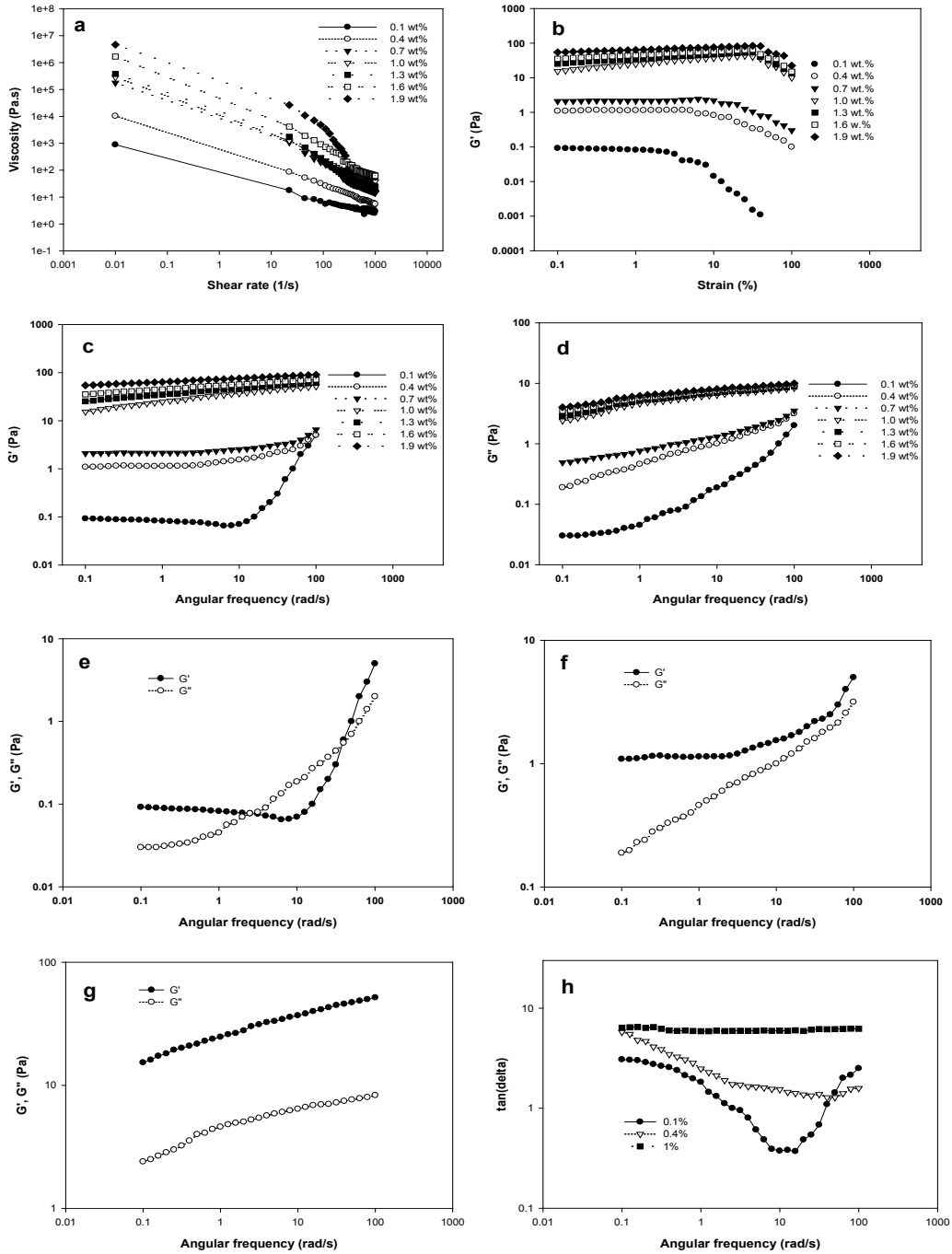


**Figure 6-2.** Rheological properties of cellulose nanofiber suspensions at different concentrations: (a) Steady-state viscosity, (b) strain sweep test, (c)  $G'$  (0.1-1.9 wt.%), (d)  $G''$  (0.1-1.9 wt.%), (e)  $G'$  and  $G''$  (0.1 wt.%), (f)  $G'$  and  $G''$  (0.4 wt.%), (g)  $G'$  and  $G''$  (1.0 wt.%), (h) loss tangent (0.1, 0.4 and 1.0 wt.%).

But, Lotti et al. (2011) reported the three-region shear-thinning behavior of nanofiber suspensions derived from Piceaabies pulp using a homogenizer (600 bar/10 passes). Rezayati Charani et al. (2013) observed the linear shear-thinning behavior of the nanofiber suspensions derived from kraft pulp using a PFI mill.

Oscillatory shear measurements were conducted to study the linear viscoelastic properties of the cellulose nanofiber hydrogel structures. In the first step, a strain sweep test was performed to determine the linear viscoelastic regions. Figure 6-2b shows that the nonlinear behavior of the dynamic moduli (storage ( $G'$ ) modulus) was observed after exceeding a critical strain of approximately 5% for the concentrations of 0.1, 0.4 and 0.7 wt.%, and 50% for the concentrations above 0.7 wt.%, which is related to the destruction of the elastic hydrogel network after that point.

Figure 6-2c-g presents the frequency sweep measurements performed in the linear viscoelastic region at 1% strain. The influence of concentration on dynamic moduli was evident. Increasing concentration of the suspension resulted in an increase of both  $G'$  and  $G''$  values (Fig. 6-2c and 6-2d). The highest value of  $G'$  was obtained as  $\sim 10^2$  Pa at the highest concentration of 1.9 wt.%, whereas the lowest value was found as  $10^{-1}$  Pa at  $\sim 0.1$  wt.% suspension. The  $G'$ , which relates to the elastic character, describes the measure of the stiffness of the nanofiber network of the suspension. Thus, the larger value of  $G'$  is an indication of the stronger network structure formation (Carreau et al., 2002). For all the suspensions except 0.1 wt.% concentration, the  $G'$  values were always higher than

$G''$  values (approximately 10-fold) in the angular frequency range of 0.1-100 rad/s, exhibiting gel-like behavior.

For suspensions with concentrations of 0.4 and 0.7%, the  $G'$  presented frequency independent behavior at low angular frequency region (0.1-5 rad/s), and then increased in the higher angular frequency region, whereas  $G''$  steadily increased with frequency in all regions maintaining  $G' > G''$  trend (gel-like behavior) at all times. For 0.1 wt.% concentration,  $G'$  displayed relatively frequency independent behavior until reaching around 10 rad/s, and then dramatically increased with angular frequency, while  $G''$  was increasing continuously throughout the entire angular frequency region. However, change and reorganization of the network structure took place with the observation of two cross-over points of  $G'$  and  $G''$  ( $G' = G''$ ). At higher concentrations in the range of 1-1.9 wt.%, the dynamic moduli of suspensions increased steadily with angular frequency. Increasing the concentration from 1 to 1.9 wt.% led to relatively more frequency independent tendency of moduli, indicating formation of a stronger gel network.

Figure 6-2h shows the loss tangent values ( $G'/G''$ ) as a function of angular frequency. A more stable gel structure was obtained with 1 wt.% concentration and above. Below 1 wt.%, loss tangent values were not stable due to weak network structure/gels with less cross-linking. The stronger network structure created at a high concentration was stable enough to resist the frequency as the rate for destroying and rebuilding the network structure could be balanced.

Formation of cellulose nanofiber gel structure (hydrogel) is attributed to the physical cross-linking due to the formation of an entangled network structure, arising from the high aspect ratio and the high specific surface area of the nanofibers (Lasseuguette et al., 2008; Pääkkö et al., 2007). Increasing concentration led to increased degree of physical cross-linking due to the availability of more inter- and intra-molecular hydrogen bonds and highly entangled network, forming viscous hydrogels.

#### **6.4. Conclusions**

Cellulose nanofiber suspensions/hydrogels were prepared by ultrasonication of lupin hull cellulose obtained via combination of subcritical water and bleaching treatments. The TEM images showed that long entangled nanofiber network structures were formed. Fibers were aggregated as the concentration increased from 0.1 to 1.9 wt.%. Resultant suspensions had high crystallinity (~70%) and high thermal degradation temperature (~310 °C). All samples displayed a typical shear-thinning behavior. Increasing concentration of the suspension led to an increase of the dynamic moduli. All suspensions, except at 0.1 wt.% concentration showed gel-like structures over the entire range of angular frequency. Increasing concentration resulted in the formation of more stable and stronger hydrogels. The obtained cellulose nanofiber hydrogels (above 0.7 wt.%) with high crystallinity and thermal stability might be used as ideal building blocks for the formation of highly porous and lightweight aerogels to be used in thermal insulation, filtration, catalysis, medical and pharmaceutical fields.

## **Chapter 7. Lupin cellulose nanofiber aerogel preparation by supercritical CO<sub>2</sub> drying and freeze drying\***

### **7.1. Introduction**

Aerogels are ultra lightweight and highly porous solid materials that have stimulated interest in a variety of applications, such as thermal/acoustic insulation, filtration, catalysis, and cushioning (Akimov, 2003). They are known for their extremely low densities (0.0011 to  $\sim 0.5$  g/cm<sup>3</sup>), high porosity (> 80%), high specific surface area (up to 1000 m<sup>2</sup>/g), low thermal conductivity ( $\sim 15$  mW/m K), low dielectric permittivity, and shock absorption (Hüsing and Schubert, 1998; Tan et al., 2001; Tingaut et al., 2012). Such materials obtained from cellulose nanofibers have received great attention due to renewability, biodegradability, and biocompatibility of cellulose, which is the most abundant biopolymer on Earth (Syverud and Stenius, 2009; Yano and Nakahara, 2004). This class of materials offer new applications in medical and pharmaceutical fields, where biocompatibility and biodegradability are needed (Aulin et al., 2010), as well as in environmentally friendly packaging, high performance and biodegradable nanocomposites (Pääkkö et al., 2008). Moreover, chemical functionality of resultant cellulose nanofiber aerogels creates more application areas, such as development of super hydrophobic materials via post-treatment with titanium dioxide nanoparticles (Korhonen et al., 2011) and silanes (Cervin et al., 2012) to be used as oil adsorbents or separation medium for oil/water mixtures.

---

\*A version of this chapter has been submitted to The Journal of Supercritical Fluids as Ciftci, D., Ubeyitogullari, A., Razera Huerta, R., Ciftci, O.N., Flores, R. and Saldaña, M.D.A. (2016). Lupin cellulose nanofiber aerogel preparation by supercritical CO<sub>2</sub> drying and freeze drying.

They exhibit increased ductility and flexibility arising from high aspect ratio and crystalline structure of nanofibers compared to traditional organic and inorganic aerogels from derivatives of cellulose microfibers and metal oxides, which are usually brittle (Liebner et al., 2008; Olsson et al., 2010; Pääkkö et al., 2008). Moreover, addition of chemical crosslinkers are not required in the gelation process. The aqueous gel is formed owing to the intramolecular hydrogen bonding and the long and entangled nanofiber network. “Sponge-like” aerogels are developed by replacing the liquid in the gel of cellulose nanofibers by air via a suitable drying method that minimizes the collapse of the network structure.

The first study on aerogels based on cellulose nanofibers was reported by Pääkkö et al. (2008) using two different freeze drying methods, cryogenic and vacuum, with 2 wt.% aqueous cellulose nanofiber suspension, which was obtained from enzymatic treatment and fibrillation of softwood pulp. Using both methods, aerogels with a low density of around  $0.02 \text{ g/cm}^3$  and high porosity of up to 98% were obtained. Regarding the surface area, the cryogenic freeze drying yielded a value of  $66 \text{ m}^2/\text{g}$ , while the vacuum freeze drying yielded a lower value of  $20 \text{ m}^2/\text{g}$ . Similar freeze drying methods have been employed to obtain cellulose nanofiber aerogels from biomass such as wood pulp and poplar wood by other researchers (Aulin et al., 2010; Chen et al., 2011; Sehaqui et al., 2010). To reduce the extent of nanofiber aggregation in freeze drying during sublimation of water, Sehaqui et al. (2011) conducted solvent exchange from water to *tert*-butanol prior to freeze drying to obtain aerogel based on wood pulp 2,2,6,6-tetramethyl-1-piperidinyloxy (TEMPO)-oxidated cellulose nanofibers (1 wt.% solid content in

aqueous suspension). The resultant specific surface areas were as high as 153-284 m<sup>2</sup>/g due to replacing water with *tert*-butanol. Freeze drying after *tert*-butanol solvent exchange to obtain cellulose nanofiber aerogels was successfully employed in other studies (Fumagalli et al., 2013; Saito et al., 2011; Wan et al., 2015). Recently, some researchers have focused on the preparation of cellulose nanofiber aerogels using supercritical drying (Korhonen et al. 2011; Sehaqui et al., 2011), which is a superior method for the preparation of aerogels as it avoids the formation of surface tension and liquid-vapor interfaces in the pores of the material during drying (Pierre and Pajonk, 2002). Supercritical carbon dioxide (SCCO<sub>2</sub>) has been the most appropriate fluid due to its mild critical pressure and temperature conditions (74 bar and 31 °C). Korhonen et al. (2011) obtained cellulose nanofiber aerogels from undried hardwood kraft pulp with 1.7 wt.% aqueous suspension either by freeze drying in liquid nitrogen or liquid propane or by supercritical drying to prepare aerogel templates with the purpose of producing inorganic hollow nanotube aerogels by atomic layer deposition onto such templates. They reported that, in contrast to freeze drying, supercritical drying resulted in aerogels without major interfibrillar aggregation.

Drying the gel/hydrogel plays an important role on the final aerogel properties, including density, porosity, specific surface area and morphology, in addition to the influence of raw material and concentration of the starting gel. In the case of cellulose nanofiber aerogel preparation, pretreatment/fibrillation methods and surface charge of cellulose nanofibers might be critical for most of the resultant aerogel properties. Thus, the aim of the present study was to

investigate the effects of two different variables involved in the formation of the aerogels, such as the drying method and the concentration of the starting hydrogel. Lupin hull cellulose fibers obtained by combined subcritical water and mild bleaching treatment were used as the starting material. Hydrogels with varying concentrations of cellulose fibers in the range of 1-2 wt.% were prepared via ultrasonication. Two different drying processes, freeze drying and SCCO<sub>2</sub> drying, were examined to form aerogels from the cellulose nanofiber hydrogels. Aerogel properties, such as density, porosity, specific surface area, pore size, and morphology, were evaluated. Crystalline structure and thermal stability of the aerogels were also investigated.

## **7.2. Materials and methods**

### **7.2.1. Materials**

Lupin hulls were kindly provided by Ceapro Inc. (Edmonton, AB, Canada). Lupin hulls were ground to particle size < 1 mm with a centrifugal mill (Retsch, Haan, Germany). The CO<sub>2</sub> (99.99% purity) was purchased from Matheson Tri-Gas, Inc. (Montgomeryville, PA, USA). All chemicals used, such as sodium chlorite and ethanol, were of laboratory grade and obtained from Fisher Scientific (Pittsburgh, PA, USA).

### **7.2.2. Preparation of cellulose nanofiber hydrogels**

Lupin hull cellulose fibers were used as the starting material to prepare cellulose nanofiber hydrogels. First, cellulose-rich residue was obtained using

subcritical water technology at the optimized process conditions of 180 °C, 50 bar and 5 mL/min, as described in Chapter 3 (Section 3.2.3). Then, the samples were bleached for 4 h according to a modified method (Ruangudomsakul et al., 2015) described in Chapter 4 (Section 4.2.2) to obtain purified cellulose. Formation of hydrogels at various concentrations was induced by ultrasonication of lupin hull cellulose fibers in water for 40 min at 80% amplitude using an ultrasonicator (Model 705, 700 W, 50/60 Hz-Fischer Scientific, Pittsburgh, PA, USA) following the procedure described in Chapter 5 (Section 5.2.3).

### **7.2.3. Preparation of cellulose nanofiber aerogels by freeze drying**

Cellulose nanofiber hydrogels (7 mL) were placed in cylindrical tubes (6.0 cm height and 1.5 cm diameter) and frozen either by a rapid freezing with liquid nitrogen at -196 °C for 10 s or in a regular freezer at -18 °C for 24 h before the freeze-drying process. Then, the water in the frozen hydrogel was sublimated at -45 °C and 15 Pa for 2 days using a freeze dryer (FreeZone, Labconco Corp., Kansas, MO, USA) where water in the solid state was converted into gas phase and removed.

### **7.2.4. Preparation of cellulose nanofiber aerogels by supercritical carbon dioxide drying**

Cellulose nanofiber aerogels were prepared from cellulose nanofiber hydrogels by first replacing the water in the hydrogels with ethanol via a multistage solvent exchange process, and then removing the ethanol from the

alcogels using SCCO<sub>2</sub> drying. During the solvent exchange process, the hydrogels (7 mL) were soaked in 30, 50, 70, and 100% (v/v) excess ethanol (200 mL) for 1 h residence time, and 100% ethanol for 4 days, where ethanol was decanted and replaced with fresh ethanol every day to obtain the alcogel. The alcogels were then placed in cylindrical polypropylene molds to prepare alcogel monoliths. Monolith shape was preferred because hydrogels were placed in test tubes of cylindrical shape. Moreover, monolith shape allowed to make measurements to determine the density of the aerogels. Finally, the ethanol in the alcogel monoliths were removed by SCCO<sub>2</sub> drying to obtain cellulose nanofiber aerogels.

SCCO<sub>2</sub> drying was carried out in a laboratory scale SCCO<sub>2</sub> extraction system (SFT-110, Supercritical Fluids, Inc., DE, USA) similarly to the method used by Comin et al. (2012) and Ubeyitogullari and Ciftci (2016). Briefly, first the alcogels were placed into a perforated (0.002 mm hole diameter) polypropylene basket (6.0 cm height and 1.5 cm diameter) that had a stainless steel frit on top of the perforated bottom. The basket was then placed into the high pressure vessel, containing the alcogel that was placed on the frit. Then, an excess amount of ethanol (20 mL) was poured into the basket to account for the loss of ethanol from the alcogel through evaporation before the set pressure and temperature were reached. Temperature of the vessel was set to 40 °C using the temperature controller. After the set temperature was reached, the system was pressurized to 100 bar and kept at the set pressure for 10 min using the double head syringe pump (model 260D, Teledyne ISCO, Lincoln, NE, USA). Then, the shut off valve was opened and the CO<sub>2</sub> flow rate was set to 0.5 L/min (measured at ambient

conditions) and maintained constant using the micrometering valve. The CO<sub>2</sub> flow rate was measured by a gas flow meter. SCCO<sub>2</sub> drying was performed at the set pressure, temperature, and CO<sub>2</sub> flow rate for 4 h. After that time, the system was depressurized at the same CO<sub>2</sub> flow rate and temperature, and the samples were collected from the vessel and stored at room temperature (21 °C) until characterized.

## **7.2.5. Characterization of the aerogels**

### **7.2.5.1. Bulk density and porosity**

Volume of the aerogel monolith was determined from its final dried dimensions that were measured using a caliper with a precision of 0.05 mm, and the weight of aerogel monolith was determined using a sensitive electronic balance with a precision of 0.1 mg. Then, the bulk density ( $d_a$ ) values were obtained by calculating the ratio of the mass to the volume.

The porosity (P) of the aerogels was calculated using the  $d_a$  values in Eq. (7.1), where the density of the crystalline cellulose nanofibers ( $d_n$ ) is equal to 1.6 g/cm<sup>3</sup> (Chen et al., 2011).

$$P (\%) = \left(1 - \frac{d_a}{d_n}\right) * 100 \quad (7.1)$$

### **7.2.5.2. Specific surface area and pore size**

Brunauer–Emmett–Teller (BET) surface area and Barrett-Joyner-Halenda (BJH) pore size of the cellulose nanofiber aerogels were determined by low-

temperature nitrogen adsorption-desorption method (ASAP 2020, Micromeritics Instrument Corporation, Norcross, GA, USA). Small pieces of aerogel samples (0.1-0.3 g) were placed in the sample tube, and then degassed under vacuum at 115 °C for 10 h prior to analysis. Nitrogen sorption experiments were performed at -196 °C. Specific surface area was determined at a relative pressure ( $p/p_0$ , equilibrium pressure of nitrogen at the sample surface/saturation pressure of nitrogen) between 0.05 and 0.3 by multipoint BET adsorption characteristics. Pore size distribution was at  $p/p_0 > 0.35$ .

### **7.2.5.3. Microscopic analysis**

Cross-sections of 1 mm thickness were cut from the aerogel monoliths, and their morphology was analyzed by a field emission scanning electron microscope (FE-SEM) (S4700 FE-SEM, Hitachi, Tokyo, Japan) as described in Chapter 4 (Section 4.2.3.4).

The morphology of the cellulose nanofibers in the hydrogels were studied with transmission electron microscopy (TEM) (H7500 TEM, Hitachi, Tokyo, Japan) following the procedure described in Chapter 5 (Section 5.2.6). Diameters of cellulose nanofibers were calculated using the ImageJ processing software (IJ1.46) by loading the TEM images into the software and measuring the fiber diameters. Scale bars on each TEM image were used for calibration of the software. Approximately 100 measurements were done using 10 TEM images. The average diameters and size distributions were determined by drawing straight lines from the selected fibers in the corresponding TEM images.

#### **7.2.5.4. X-ray diffraction analysis**

Crystallinity of the aerogel samples was determined using a PANalytical Empyrean Diffractometer (Empyrean, PANalytical B.V., Almelo, Netherlands) as described in Chapter 4 (Section 4.2.3.2). The crystallinity index (CI) of the samples was determined using Eq. (3.1) ( $I_{002}$  at  $2\theta = 22.5^\circ$  and  $I_{am}$  at  $2\theta = 18.5^\circ$ ) described in Chapter 3, Section 3.2.5.1.

#### **7.2.5.5. Thermo-gravimetric analysis**

Thermo-gravimetric (TG) analyses of the aerogel samples (5-10 mg) were done using a TG 209 F1 Libra TG analyzer (TG 209 F1 Libra, NETZSCH, Selb, Germany) following the procedure described in Chapter 3 (Section 3.2.5.2).

#### **7.2.6. Statistical analysis**

Data were presented as mean  $\pm$  standard deviation based on at least duplicate experiments and analyses. Statistical analyses were performed using the SPSS (version 17.0) software package at 95% confidence interval.

### **7.3. Results and discussion**

#### **7.3.1. Aerogel properties**

Lightweight and white sponge-like aerogels were obtained without significant collapse upon complete removal of water through freeze drying and ethanol removal through SCCO<sub>2</sub> drying. Table 7-1 shows the properties of the cellulose nanofiber aerogels prepared by those drying techniques from cellulose nanofiber hydrogels at different concentrations ranging from 1 to 2 wt.% (initial

solid cellulose nanofiber content in the hydrogel). The resultant aerogel properties were greatly affected by the initial hydrogel concentration and the drying method employed as shown in Table 7-1. The SCCO<sub>2</sub> drying resulted in ‘better’ aerogel properties, such as lower density, higher porosity and higher specific surface area compared to those of freeze-dried aerogels at each concentration level investigated. Decreasing hydrogel concentration regardless of the drying method employed resulted in a decrease in density, and increase in porosity and specific surface area of the aerogels obtained.

The lowest density of 0.009 g/cm<sup>3</sup> was achieved at 1 wt.% hydrogel concentration with SCCO<sub>2</sub> drying, whereas the freeze-dried aerogel had a density of 0.023 g/cm<sup>3</sup> at the same concentration due to collapsing of the pores during water sublimation, which resulted in more cellulose nanofiber per unit volume.

The density of the aerogel is negatively correlated with the porosity as shown in Eq. (7.1). As a result of such relationship, the highest porosity was calculated as 99.4% for the SCCO<sub>2</sub>-dried aerogel, having the lowest density of 0.009 g/cm<sup>3</sup>.

The lowest porosity was calculated as 96.6% for the freeze-dried aerogel which had the highest density of 0.054 g/cm<sup>3</sup> at 2 wt.% concentration. Eventhough, concentration and drying method had significant effect on average pore size and pore volume of the aerogels, with the values in the range of 7.1-11.7 nm, and 0.08-0.36 cm<sup>3</sup>/g, respectively, there was no pattern.

**Table 7-1.** Comparison of cellulose nanofiber aerogel properties obtained via different drying methods.

| Property  | SCCO <sub>2</sub> drying         |                               |                               | Freeze drying                 |                               |                               |
|---|----------------------------------|-------------------------------|-------------------------------|-------------------------------|-------------------------------|-------------------------------|
|   | 1 wt. %                          | 1.5 wt. %                     | 2 wt. %                       | 1 wt. %                       | 1.5 wt. %                     | 2 wt. %                       |
| Density (g/cm <sup>3</sup> )                    | 0.009 <sup>a*</sup><br>(0.000)** | 0.019 <sup>b</sup><br>(0.001) | 0.050 <sup>c</sup><br>(0.001) | 0.023 <sup>a</sup><br>(0.001) | 0.030 <sup>b</sup><br>(0.001) | 0.054 <sup>c</sup><br>(0.001) |
| Porosity (%)                                    | 99.4 <sup>a</sup><br>(0.3)       | 98.8 <sup>b</sup><br>(0.5)    | 96.9 <sup>c</sup><br>(0.5)    | 98.6 <sup>a</sup><br>(0.3)    | 98.1 <sup>a</sup><br>(0.5)    | 96.6 <sup>b</sup><br>(0.3)    |
| BET surface area (m <sup>2</sup> /g)            | 115 <sup>a</sup><br>(4)          | 93 <sup>b</sup><br>(7)        | 72 <sup>c</sup><br>(5)        | 20 <sup>a</sup><br>(1)        | 18 <sup>b</sup><br>(1)        | 16 <sup>c</sup><br>(2)        |
| BJH desorption pore size (nm)                   | 8 <sup>a</sup><br>(2.2)          | 11.7 <sup>b</sup><br>(1.7)    | 7.1 <sup>c</sup><br>(2.1)     | 10.8 <sup>a</sup><br>(1.8)    | 10.9 <sup>a</sup><br>(1.4)    | 9.4 <sup>b</sup><br>(1.9)     |
| BJH desorption pore volume (cm <sup>3</sup> /g) | 0.32 <sup>a</sup><br>(0.03)      | 0.36 <sup>a</sup><br>(0.02)   | 0.17 <sup>b</sup><br>(0.05)   | 0.08 <sup>a</sup><br>(0.01)   | 0.09 <sup>a</sup><br>(0.02)   | 0.09 <sup>a</sup><br>(0.02)   |

\* Means in the same row within each drying method (SCCO<sub>2</sub> drying and freeze drying) with different letters are significantly different at p<0.05.

\*\*Data values in parentheses are standard errors.

BET: Brunauer–Emmett–Teller; BJH: Barrett-Joyner-Halenda.

The BET surface area (specific surface area determined using the BET method) of freeze-dried aerogels significantly increased from 16 to 20 m<sup>2</sup>/g with decreasing concentration from 2 to 1 wt.%, while the concentration increase had a more pronounced effect on the BET surface area of SCCO<sub>2</sub>-dried aerogels with values increasing from 72 to 115 m<sup>2</sup>/g as the concentration decreased from 2 to 1 wt.%.

A similar phenomenon where increasing hydrogel concentration and density led to a lower BET surface area of the resultant aerogel was also observed for aerogel formation based on cellulose nanofibers (Aulin et al., 2010; Pääkkö et al., 2008), or cellulose (Jin et al., 2004). Increasing hydrogel concentration per unit volume results in an increased density with less porous structure and therefore resulted in less surface area. Aulin et al. (2010) prepared cellulose nanofiber aerogels at 0.0031-3.13 wt.% of carboxymethylated nanofibers of dissolved pulp. They reported that aerogels obtained from 2 wt.% hydrogel resulted in a density of 0.02 g/cm<sup>3</sup> and BET area of 15 m<sup>2</sup>/g, whereas increasing the concentration to 3.13 wt.% yielded a higher density of 0.030 g cm<sup>-3</sup> with a lower BET area of 11 m<sup>2</sup>/g due to the presence of more nanofiber per unit volume, which results in a denser structure. Comparison of the present aerogel BET surface area values with the previous aerogel studies based on cellulose nanofibers in the similar concentration range tested in this study showed that the BET surface area was affected by many parameters in addition to concentration, such as freezing type/speed and additional solvent exchange time and the solvent used. The values for BET areas of cellulose nanofiber freeze-dried aerogels (2

wt.%) obtained in this study were similar to those of vacuum freeze-dried aerogels reported by Pääkkö et al. (2008), who obtained the area of 20 m<sup>2</sup>/g using 2 wt.% cellulose nanofiber gel of softwood pulp. On the other hand, BET surface area values of this study were lower than those obtained by Sehaqui et al. (2011), who conducted an additional solvent exchange step with *tert*-butanol prior to freeze drying, achieving 153-284 m<sup>2</sup>/g with 1 wt.% concentration of wood pulp cellulose nanofiber hydrogel. However, the use of *tert*-butanol in the solvent exchange step for the preparation of aerogels from coconut shell cellulose nanofiber gel (0.5 wt.%) resulted in much lower BET surface area (9.1 m<sup>2</sup>/g) (Wan et al., 2015), which could be related to the influence of the other variables involved in the formation of aerogels, such as the source, treatment/mechanical fibrillation method used or surface charge of the starting cellulose nanofibers. Surface modification pretreatments of cellulose fibers to add ionic groups on the surface by oxidation and carboxymethylation before mechanical treatments can affect the final aerogel properties, resulting in high specific surface areas.

### **7.3.2. Morphology**

#### **7.3.2.1. Cellulose nanofiber hydrogels**

Aerogel properties might vary depending on the initial hydrogel characteristics of the cellulose nanofibers. In this study, ultrasonication of cellulose fibers in water resulted in formation of the hydrogel structures via formation of a nanofiber network. As native cellulose has a highly hydrophilic nature, cellulose nanofibers are able to retain a large amount of water (Hoffman,

2002). Thus, aqueous suspensions of cellulose nanofibers show gel-like properties because of the formation of an entangled network structure attributed to the high aspect ratio and the high specific surface area of the nanofibers (Lasseguette et al., 2008; Pääkkö et al., 2007). Besides, chemical cross-linker addition was not required to induce gelation of the present hydrogels, which were formed by the physical cross-linking of the cellulose nanofibers.

The TEM images of hydrogels displayed a classical web-like network structure, revealing long entangled nanofiber filaments with diameters of 5-100 nm, and lengths in several microns which is challenging to measure (Fig. 7-1). As a result of the physical cross-linking due to extensive inter- and intra-molecular hydrogen bonding and entanglements, formation of white, sponge-like aerogels with well-defined shapes without significant shrinkage were observed.

Flow ability of the hydrogels varied with changing concentration from 1 to 2 wt.%. A partial gelatinous structure was observed in the 1 wt.% hydrogel; however, increasing the concentration above 1 wt.% resulted in viscous hydrogels with increased aggregation of nanofibers and no flow ability (inset pictures, Figure 7-1). It was reported by Chen et al. (2011) that increasing cellulose nanofiber content from 0.1 to 1.5 wt.% resulted in increased strength of the formed aerogels due to the increased degree of physical cross-linking caused by more extensive inter- and intra-molecular hydrogen bonds and entanglements in the viscous hydrogels. They evaluated the effect of hydrogel concentration obtained from wood cellulose nanofibers on water uptake capability of the resultant aerogels and reported that water uptake capability (ratio of water to

aerogel) of aerogels decreased from 155 to 54 with increasing concentration from 0.1 to 1.5 wt.% due to an increase of such physical cross-linking.

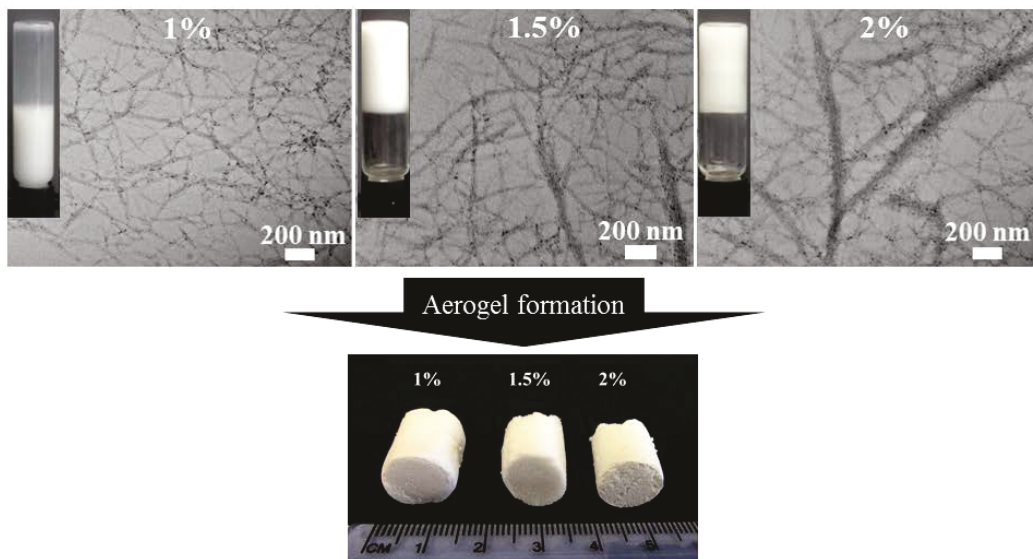


**Figure 7-1.** Transmission electron microscopy (TEM) images of the cellulose nanofiber hydrogels (1, 1.5, and 2 wt.%) and the appearance of the resultant aerogels at macroscopic level.

### 7.3.2.2. Supercritical carbon dioxide-dried aerogels

The morphologies of  $\text{SCCO}_2$ -dried aerogels as a function of the initial hydrogel concentration are presented in Figure 7-2. Using  $\text{SCCO}_2$  drying (100 bar, 40 °C, 0.5 L/min  $\text{CO}_2$  flow rate, measured at ambient conditions) to prepare aerogels was effective to form highly porous structures. These  $\text{SCCO}_2$  drying conditions were selected based on previous reports on the formation of aerogels (Comin et al., 2012; Ubeyitogullari and Ciftci, 2016), and preliminary tests performed in this study for lowest pressure and temperature for efficient ethanol removal from the alcogel.

The morphologies with three-dimensional open nanoporous network structure of entangled nanofibers are shown in the SEM images in Figure 7-2. At 1 wt.% concentration, more homogenous and porous aerogel network structure was seen, which was built up with individual cellulose nanofibers without any visible or occasional aggregation of fibers (Fig. 7-2a-c). However, random formation of bigger fiber bundles and aggregates were observed (Fig. 7-2d-i) as the concentration was increased from 1 to 2 wt.%, which was the result of increased attraction among nanofibers due to more extensive hydrogen bonding.

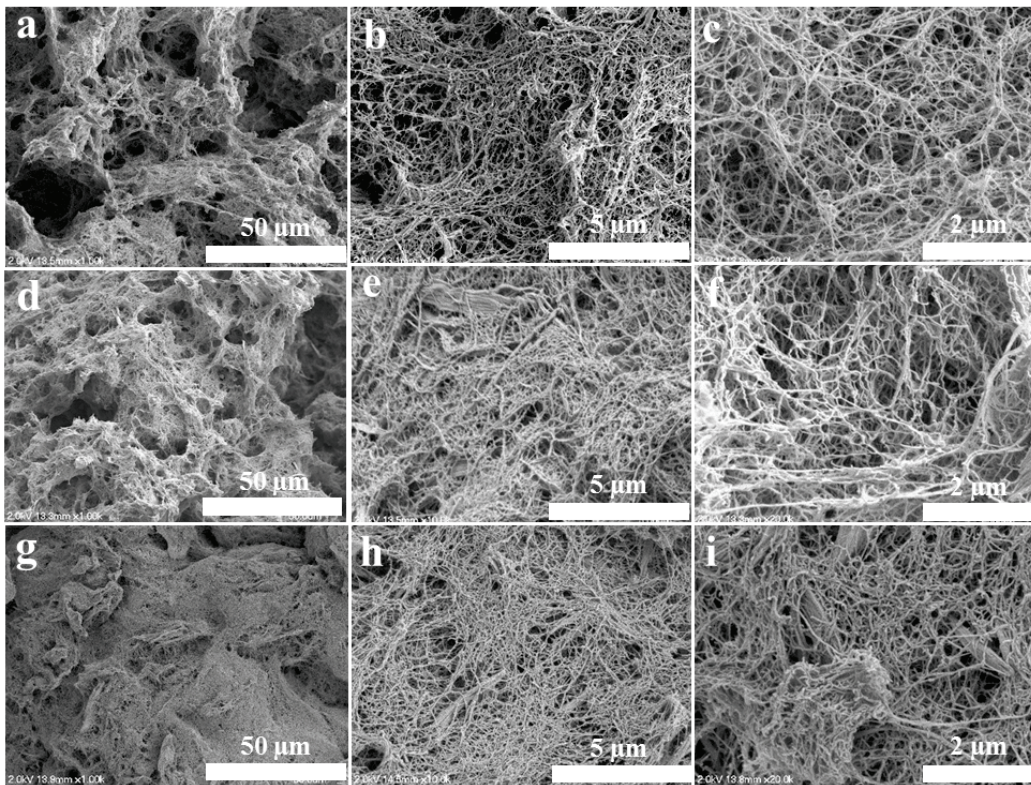


**Figure 7-2.** The morphologies of supercritical carbon dioxide (SCCO<sub>2</sub>)-dried aerogels as a function of the initial hydrogel concentration ((a-c) 1 wt.%, (d-f) 1.5 wt.%, and (g-i) 2 wt.%).

### 7.3.2.3. Freeze-dried aerogels

Morphologies of the freeze-dried aerogels (Fig. 7-3), initially frozen with liquid nitrogen, were different than those of SCCO<sub>2</sub>-dried ones. As expected, the SCCO<sub>2</sub> drying method was more effective in forming aerogels, exhibiting more homogenous porous structures that were composed of thinner and not aggregated individualized fibers, which is attributed to the lack of any liquid-vapor interface and surface tensions in the gel pores (Pierre and Pajonk, 2002).

Figure 7-3a-b showed that the cellulose nanofibers in the 1 wt.% hydrogel self-assembled into long fibers in the longitudinal direction during the freeze-drying process. When the hydrogel concentration exceeded 1 wt.%, the number of pores decreased accompanied with the formation of more sheet-like structures. Even though the average pore sizes were found to be in the range of 9.4-10.9 nm as reported in Table 7-1, formation of micrometer-sized pores were also identified on the sheet like surfaces (Fig. 7-3d and 7-3f).

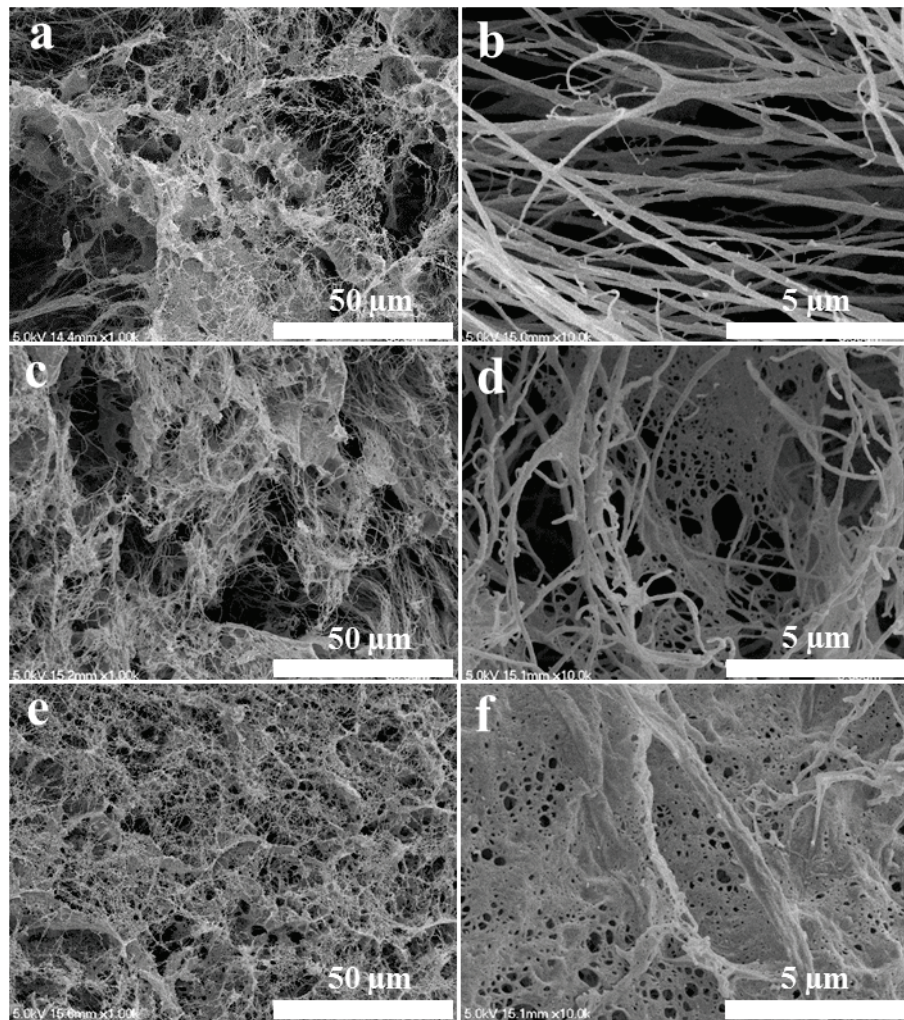


**Figure 7-3.** The morphologies of freeze-dried aerogels as a function of the initial hydrogel concentration ((a and b) 1 wt.%, (c and d) 1.5 wt.%, and (e and f) 2 wt.%).

### ***Effect of the initial freezing stage***

Freeze drying of cellulose nanofiber hydrogels involves two major stages. The initial stage is freezing of the water in the hydrogels into ice crystals with nanofibers trapped among them, leading to the formation of an ordered structure, and the final stage is the sublimation of the water molecules, resulting in the formation of a porous network structure (Voronova et al., 2012). Freezing speed at the initial stage of freeze drying plays an important role, affecting the microstructure properties of the formed aerogels, which can be related with the size and distribution of the ice crystals formed during freezing (Quievy et al., 2010). Figure 7-4 compares the morphologies of the aerogels obtained with the two different freezing methods of the initial stage of freeze drying, where 1 wt.% hydrogels were frozen with liquid nitrogen (rapid freezing) at a temperature of -196 °C, and with regular freezing in the freezer (slow freezing) at a temperature of -18 °C. The use of rapid and slow freezing methods prior to sublimation resulted in aerogels with different structures. Using rapid freezing with liquid nitrogen was more effective in preserving the porous network structure (Fig. 7-4a-b). More compact two-dimensional sheet-like structures were formed, displaying wave-like roughness after the relatively slow freezing process at -18 °C (Fig. 7-4c-d).

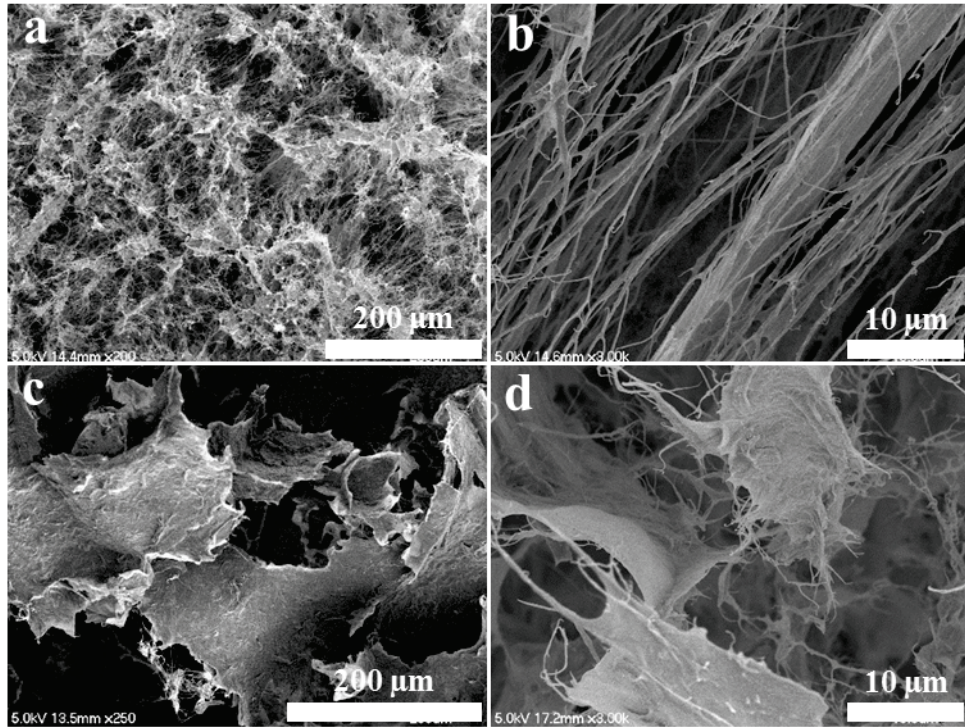


**Figure 7-4.** The morphologies of freeze-dried aerogels with (a and b) rapid freezing using liquid nitrogen and with (c and d) slow freezing using regular freezer at a hydrogel concentration of 1 wt.%.

### 7.3.3. Crystallinity

Figure 7-5 shows the comparison of the X-ray diffraction patterns of the purified cellulose and  $\text{SCCO}_2$ -dried aerogels as a function of the initial hydrogel concentration. Crystalline structure arrangement of the native cellulose was maintained in all aerogels after the applied treatments (subcritical water treatment, bleaching, ultrasonication and drying) as all the patterns displayed a typical cellulose I structure with three well-defined crystalline peaks around  $2\theta = 16.5^\circ$ ,  $22.5^\circ$  and  $34.5^\circ$  (Nishiyama et al., 2002).

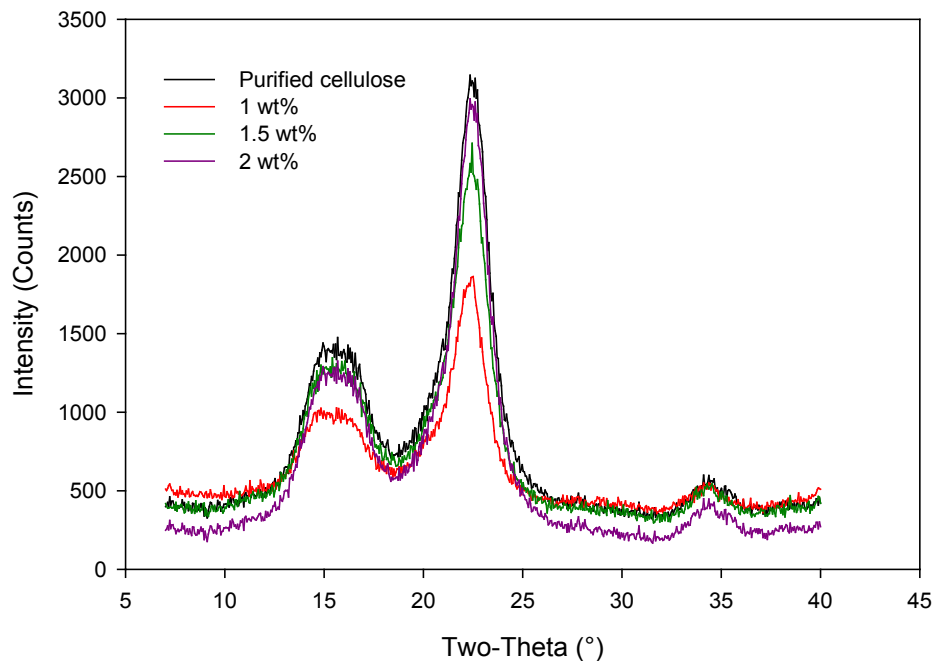


**Figure 7-5.** X-ray diffraction (XRD) patterns of the aerogels prepared at different concentrations.

The CI of the purified cellulose was 75.4%. The CI value of the 1 wt.% (72.4%) aerogel was slightly lower than that of the 1.5 wt.% aerogel (73.7%) and the 2 wt.% aerogel (75.1%), but it was not statistically significantly different ( $p > 0.05$ ). Such a decrease in crystallinity might be attributed to the damaging effect of the ultrasonication process at increased intensity (increased time and/or amplitude).

Li et al. (2012) reported a significant decrease in the crystallinity of microcrystalline cellulose from 82% to 73% after ultrasonication at 1500 W for 15 min to obtain cellulose nanocrystals. Even though all the aqueous cellulose fibers were processed for 40 min in this study, the hydrogels with concentrations

of 1.5 and 2 wt.% might not be adequately agitated as the one with 1 wt.% due to increased viscosity and, thus decreased flow ability during ultrasonication. Furthermore, the resultant cellulose nanofiber aerogels still had high crystallinity index with a value above 70%, which is crucial in terms of their potential industrial applications like insulation as high crystallinity is closely related with high thermal stability and good mechanical properties.

#### **7.3.4. Thermal stability**

Investigation of thermal stability is important in determining the capability of cellulose nanofiber aerogels for high-temperature applications like thermal insulation. Figure 7-6 presents the TG curves of subcritical water treated and bleached lupin hull cellulose and the SCCO<sub>2</sub>-dried cellulose nanofiber aerogels at different concentrations of 1-2 wt.%. All SCCO<sub>2</sub>-dried aerogels displayed a decomposition behavior that is highly similar to that of the purified cellulose fibers with the onset of degradation temperature occurring at approximately 310 °C. A decrease in the onset degradation temperature would be expected in case of damaged crystalline region, which could lead to a decrease in the thermal stability (Isogai, 2013). There was not such a decrease in the thermal stability, indicating that the above-mentioned crystallinity decrease for the 1 wt.% aerogel was not significant enough to affect its thermal stability.

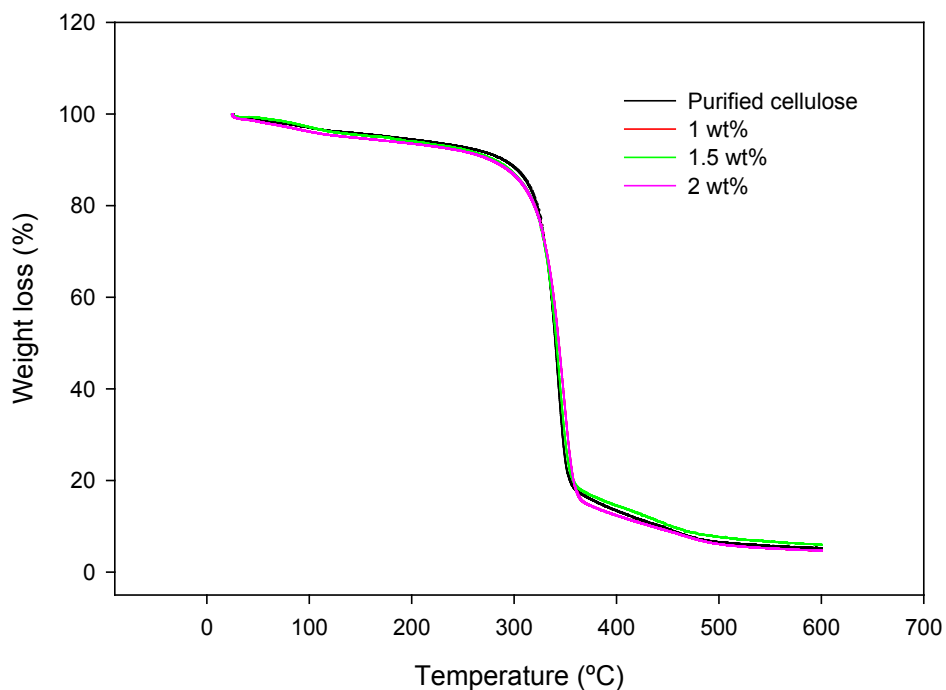


**Figure 7-6.** Thermo-gravimetric (TG) curves of aerogels with different concentrations.

#### 7.4. Conclusions

Highly porous and lightweight aerogels based on cellulose nanofibers were successfully prepared using SCCO<sub>2</sub> drying and freeze drying methods. The resulting aerogels had the highest specific surface area of 115 m<sup>2</sup>/g, the highest porosity of 99% and the lowest density of 0.009 g/cm<sup>3</sup> via SCCO<sub>2</sub> drying of 1 wt.% hydrogel with a three-dimensional open nanoporous network structure. Increasing the concentration from 1 to 2% led to more aggregated structures and large fiber bundles after SCCO<sub>2</sub> drying and liquid nitrogen freeze drying, while formation of two-dimensional sheet-like structures was observed during regular freeze drying. All resultant aerogels had high crystallinity (>72%) and thermal

stability (thermal degradation temperature of 310 °C). This new class of aerogel is based on renewable and biodegradable cellulose nanofibers, and offers various application areas, including environmentally friendly food packaging and tissue engineering scaffolds.

## **Chapter 8. Summary, conclusions, and recommendations**

### **8.1. Summary and conclusions**

Among the vast available lignocellulosic biomass sources, agro-industrial by-products such as potato peel, lupin hull, and canola straw are particularly suitable to obtain high value-added products since they do not compete with the food sector. These lignocellulosic biomass sources mainly contain hemicellulose, cellulose and lignin, where removal of hemicellulose and lignin leads to high value cellulose. Production of cellulose nanofibers and its further processing to obtain cellulose nanofiber hydrogels and aerogels are efficient ways to utilize such underutilized and low-value by-products to obtain high profit in addition to minimizing environmental concerns. Cellulose nanofibers have a number of desirable characteristics, such as high aspect ratio, low thermal expansion, good mechanical and optical properties, low weight, low density and biodegradability (Abdul Khalil et al., 2012; Agarwal et al., 2006). Attractive applications of cellulose nanofibers and hydrogels/aerogels based on cellulose nanofibers include environmentally friendly food packaging, tissue engineering scaffolds, thickening agents, rheology modifiers, adsorbents, carriers for catalysts, drug release and thermal/acoustic insulation (Aulin et al., 2010; Belbekhouche et al., 2011; Brinchi et al., 2013; Chen et al., 2011; Fukuzimi et al., 2009; Nakagaito et al., 2010; Sehaqui et al., 2011).

Traditional cellulose nanofiber production methods from biomass use hazardous chemicals and solvents, and generate waste streams raising environmental concerns. Thus, there is a critical need for alternative methods that

eliminates or reduces the use of hazardous chemicals and solvents and waste generation.

Subcritical water treatment using pressure to maintain the water in the liquid state at elevated temperatures of 100-374 °C is attracting considerable attention as an environmentally friendly technology for lignocellulosic biomass processing as it avoids the use of hazardous chemicals and neutralization of sludges (Brunner, 2009; Saldaña and Valdivieso-Ramirez, 2015). Subcritical water has unique properties of dielectric constant, ionic product, density, viscosity, diffusivity, electric conductance, and solvent ability that can be tuned by changing temperature (Kruse and Dinjus, 2007). Therefore, it offers an alternative way for the removal of noncellulosics like hemicellulose and/or lignin of biomass to obtain cellulose enriched residues that are mainly composed of cellulose nanofibers. Hydrogels and aerogels can be further obtained after cellulose nanofiber fibrillation and the use of suitable drying processes, such as freeze drying and/or supercritical carbon dioxide drying.

In this thesis, sweet blue lupin (*lupinus angustifolius*) hull was selected as a raw material for cellulose nanofiber production. Lupin is a legume crop with 450 species mainly cultivated in Australia (Bailey et al., 1974). Recently, the use of lupin seeds as a food source is increasing due to its many health benefits. Lupin protein has shown cholesterol lowering activity (Sirtori et al., 2004), and its  $\gamma$ -conglutin, an unusual basic 7S protein, has shown hypoglycemic effects (Vargas-Guerrero et al., 2014). Currently, some bread manufacturers use lupin hull flour for high fiber bread making; however, huge amounts of lupin hulls are still left as

waste. One unique aspect of lupin hull is its low lignin content, which facilitates access to the hemicellulose fraction to deconstruct lignocellulose complex. To the best of the author's knowledge, there is no study on the use of lupin hull for the production of cellulose and cellulose nanofibers. In addition to lupin hull, canola straw was studied as a high-lignin biomass. Canola straw, one of the major by-products of the agricultural industry in Canada, is a potential source of cellulose. Canola straw was used to compare the processes efficiency with a low-lignin (lupin hull) and a high-lignin biomass (canola straw) for cellulose isolation. However, further studies to form hydrogels and aerogels were conducted using only lupin hull due to its low lignin content.

In Chapter 3, hydrolysis of lupin hulls was performed with subcritical water technology using a biomass refinery approach, targeting the removal of the maximum level of hemicellulose sugars to obtain a cellulose-rich residue. The effects of process parameters, such as pressure (50-200 bar), temperature (160-220 °C), flow rate (2-10 mL/min), and pH (2-12) were investigated and proper optimization was carried out for the removal of maximum hemicellulose sugars from lupin hull. Optimum subcritical water treatment conditions were found to be 180 °C, 50 bar, 5 mL/min, and pH 6.2, which removed 85.5% of the hemicellulose sugars (xylose, arabinose, glucose, galactose and mannose) in the extracts in 40 min. The analysis of the solid residue showed that the cellulose content increased from 61.4% (160 °C/50 bar) to 86.8% (220 °C/50 bar) when compared with the initial percentage of 45.2%, and the lignin content varied from 25.6% (160 °C/50 bar) to 5.7% (220 °C/50 bar). The increased crystallinity from

38.2 to 58.6% and thermal stability of the solid residue confirmed the removal of most of the hemicellulose and lignin from lupin hulls. In addition, defibrillation of fiber bundles after subcritical water treatment was observed with scanning electron microscopy.

In Chapter 4, cellulose fibers were isolated from lupin hull and canola straw using a combination of sodium hydroxide (NaOH) and acidified sodium chlorite (ASC) treatments. The aim of this study was to optimize the treatment conditions of NaOH (5-20%, 25-75 °C and 2-10 h) and ASC (1.7%, 75 °C for 2-6 h) to remove the maximum amount of lignin and hemicellulose, leading to a high recovery of cellulose, as well as to investigate the effect of lignin content of the starting materials on the treatment efficiency. The maximum cellulose content obtained was 93.2% for lupin hull after 4 h ASC treatment of NaOH-treated (15% NaOH, 99 °C, 6 h) samples, and 81.4% for canola straw after 6 h ASC treatment of NaOH treated (15% NaOH, 99 °C, 6 h) samples. The amount of non-cellulosic components removal was higher for lupin hull than that of canola straw due to the lower lignin content of lupin hull. The lignin contents of lupin hull and canola straw were reduced by about 90 and 82%, respectively. The maximum removed hemicellulose contents were 92 and 81% for lupin hull and canola straw, respectively. Improved crystallinities with up to 72.6% for lupin hull and 67.4% for canola straw were observed, indicating that amorphous noncellulosics removal was higher in lupin hull. Thermal stabilities with onset degradation temperature of up to 318 °C for lupin hull and 307 °C for canola straw were observed, indicating that lupin hull had a higher cellulose content as cellulose is crystalline in nature

and thermally more stable. The scanning electron microscopy images revealed that the isolated cellulose fibers had more homogeneity and uniformity with increased surface area.

The findings in Chapters 3 and 4 emphasized that the subcritical water treatment (180 °C, 50 bar, 5 mL/min, pH 6.2 and 40 min) was as efficient as NaOH treatment (15% NaOH, 99 °C, and 6 h) to obtain cellulose-enriched fibers from lupin hull. Therefore, the use of subcritical water treatment could be an environmentally friendly alternative. Further purification of subcritical water treated lupin hulls was successfully conducted using ASC treatment as performed in Chapter 4, where 93.2% final cellulose content was achieved. Due to the higher level of cellulose recovery, only lupin hulls were used for the following Chapters 5-7.

In Chapter 5, production of cellulose nanofibers from lupin hull was performed using the subcritical water treated residue (180 °C, 50 bar and 5 mL/min) obtained in Chapter 3, which was further purified by a bleaching treatment with ASC as described in Chapter 4. Then, fibrillations into nano-scale were conducted with ultrasonic treatments at different amplitudes (20-80%) and times (15-35 min). The results revealed successful nanofibrillation as the ultrasonication amplitude and time were increased to 80% and 35 min, respectively. The smallest average diameter obtained was 15 nm at 80% amplitude for 35 min. Resultant cellulose nanofibers had high crystallinity, with above 70% crystallinity index.

In Chapter 6, rheological characterization of the aqueous suspensions of cellulose nanofibers from lupin hull was carried out. The suspensions of nanofibers were prepared using the same approach described in Chapter 5, with varying concentrations of 0.1-1.9 wt.%. The effects of concentration on the morphology, crystallinity, thermal stability and rheological properties of the obtained cellulose nanofiber suspensions were investigated. Transmission electron microscopy images revealed the long entangled nanofiber network structures. Strongly aggregated fibers were observed as the concentration increased from 0.1 to 1.9 wt.%. Resultant suspensions had high crystallinity (~70%) and high thermal degradation temperature (~310 °C). Samples displayed a typical shear-thinning behavior at all concentrations investigated. All suspensions except 0.1 wt.% concentration showed gel-like structures over the entire range of angular frequency. Increasing concentration led to an increase in the dynamic moduli, favoring the formation of hydrogels with stronger network.

Based on the findings described in Chapters 6, cellulose nanofiber suspension/hydrogel concentration range of as 1-1.9 wt.%, where stronger gel network structures were observed, was adapted for the formation of cellulose nanofiber aerogels in the next study.

In Chapter 7, highly porous and lightweight aerogels were prepared based on cellulose nanofibers obtained using the same approach described in Chapter 5. Two drying processes, SCCO<sub>2</sub> drying and freeze drying, were evaluated for the formation of aerogels at initial hydrogel concentrations of 1, 1.5 and 2 wt.%. The effects of concentration and drying method on the resultant aerogel properties,

crystallinity, thermal behavior, and morphology were investigated. The properties evaluated were density, porosity, specific surface area, pore size and pore volume. The resulting aerogels obtained by SCCO<sub>2</sub> drying of 1 wt.% hydrogel had three-dimensional open nanoporous (~8 nm) network structures, with the highest specific surface area of 115 m<sup>2</sup>/g, the highest porosity of 99.4% and the lowest density of 0.009 g/cm<sup>3</sup>, whereas freeze drying at the same hydrogel concentration resulted in aerogels with specific surface area of 20 m<sup>2</sup>/g, porosity of 98.6% and density of 0.023 g/cm<sup>3</sup>. High crystallinity (72%) and thermal stability (thermal degradation temperature of 310 °C) was maintained in the SCCO<sub>2</sub>-dried aerogels.

Overall, throughout the research presented in this PhD thesis, cellulose nanofibers and highly porous cellulose nanofiber aerogels were successfully produced using a more environmentally approach that reduce the use of hazardous chemicals. The findings are promising for the utilization of underutilized low-value feedstocks, mainly lupin hull, to obtain high value-added products, cellulose nanofibers, hydrogels and aerogels. The renewability and biodegradability of cellulose nanofiber and its hydrogels and aerogels make it a promising potential alternative material in the current petroleum oil crisis as a response to the current environmental concerns and waste management issues.

## **8.2. Recommendations**

Cellulose was enriched from low-lignin lupin hulls using subcritical water treatment. Another approach for Chapter 3, especially for the high-lignin biomass, could be using high pressure carbonated water that can be generated by

pressurizing water and CO<sub>2</sub> mixture, resulting in the formation of carbonic acid. Such an approach could allow the recovery of hemicellulose and lignin fractions using a chemical-free pressurized water- and CO<sub>2</sub>-based method.

Further research on the recovery and use of co-products obtained from hemicellulose and lignin fractionation throughout the cellulose nanofiber production process, including subcritical water treatment (Chapter 3), chemical treatments with NaOH/ASC (Chapter 4), and subcritical water-assisted ASC (Chapter 5) treatment is needed for their exploitation according to a lignocellulose biorefinery concept. Such approach can generate various high-value products and fractions. Each process can be optimized for a targeted product or fraction in terms of yield and quality.

Cellulose nanofibers can be obtained in different forms, namely, hydrogel, aerogel, film, and powder. Industrial applications of the cellulose nanofibers depend on their physical form. Powder form of the cellulose nanofiber is desired for convenient storage and transportation, as well as to develop different formulations for targeted industrial applications such as nanocomposite reinforcement and hydrogel formation. However, aggregation is a major issue in cellulose nanofiber drying. Therefore, more research is needed to develop new drying methods or improved spray drying with a new design that can preserve nanoscale structure and ensure its redispersibility in water (Chapter 5).

Shelf life and stability of the cellulose nanofiber hydrogel could be studied over months at both refrigeration and room temperature conditions for efficient utilization in the industry (Chapter 6).

Future studies for Chapter 7 should evaluate mechanical properties (e.g., tensile test, compressibility) and chemical functionality (e.g., chemical interaction with the loaded compound, hydrophobicity, hydrophilicity) of the cellulose nanofiber aerogels for various industrial applications (e.g., insulation, electronics, energy). Finally, specific food and industrial applications of the cellulose nanofiber aerogels could be explored, such as bioactive carriers and energy storage for batteries.

## References

- Abdul Khalil, H.P.S., Bhat, A.H. and Ireana Yusra, A.F. (2012). Green composites from sustainable cellulose nanofibrils: A review. *Carbohydrate Polymer*, 87:963-979.
- Abe, K. and Yano, H. (2011). Formation of hydrogels from cellulose nanofibers. *Carbohydrate Polymers*, 85:733-737.
- Abe, K., Iwamoto, S. and Yano, H. (2007). Obtaining cellulose nanofibers with a uniform width of 15 nm from wood. *Biomacromolecules*, 8:3276-3278.
- Agarwal, M., Lvov, Y. and Varahramyan, K. (2006). Conductive wood microfibrils for smart paper through layer-by-layer nano-coating. *Nanotechnology*, 17:5319-5325.
- Akimov, Y.K. (2003). Fields of application of aerogels (review). *Instruments and Experimental Techniques*, 46:287-299.
- Akiya, N. and Savage, P.E. (2002). Roles of water for chemical reactions in high-temperature water. *Chemical Reviews*, 102:2725-2750.
- Alemdar, A. and Sain, M. (2008). Biocomposites from wheat straw nanofibers: morphology, thermal and mechanical properties. *Composites Science and Technology*, 68:557-565.
- Alila, S., Besbes, I., Vilar, M. R., Mutje, P. and Boufi, S. (2013). Non woody plants as raw materials for production of microfibrillated cellulose (MFC): a comparative study. *Industrial Crops and Products*, 41:250-259.
- Allen, S.G., Schulman, D., Lichwa, J., Antal, M.J., Laser, M., Lynd, L.R. (2001). A comparison between hot liquid water and steam fractionation of corn fiber. *Industrial and Engineering Chemistry Research*, 40:2934-2941.
- Almazán, O., González, L. and Gálvez, L. (2001). The sugarcane, its by- products and co-products. *Sugar Cane International*, 7:3-8.
- Alvarez, V.H., Cahyadi, J., Xu, D. and Saldaña, M.D.A. (2014). Optimization of phytochemicals production from potato peel using subcritical water: Experimental and dynamic modeling. *Journal of Supercritical Fluids*, 90:8-17.
- Amiralian, N., Annamalai, P. K., Memmott, P. and Martin, D. J. (2015). Isolation of cellulose nanofibrils from *Triodia pungens* via different mechanical methods. *Cellulose*, 22:2483-2498.
- Ando, H., Sakaki, T., Kokusho, T., Shibata, M., Uemura, Y. and Hatate, Y. (2000). Decomposition behavior of plant biomass in hot-compressed water. *Industrial and Engineering Chemistry Research*, 39:3688-3693.

- Angellier, H., Putaux, J.L., Molina-Boisseau, S., Dupeyre, D. and Dufresne, A. (2005). Starch nanocrystal fillers in an acrylic polymer matrix. *Macromolecular Symposium*, 221:95-104.
- Ankerfors, M. and Lindstrom, T. (2007). On the manufacture and use of nanocellulose. 9<sup>th</sup> International Conference on Wood and Biofibre Plastic Composites, May 21-23, Madison, Wisconsin, USA.
- Araki, J., Wada, M., Kuga, S. and Okano, T. (1998). Flow properties of microcrystalline cellulose suspension prepared by acid treatment of native cellulose. *Colloids and Surfaces A*, 142:75-82.
- Aulin, C., Netrval, J., Wågberg, L. and Lindström, T. (2010). Aerogels from nanofibrillated cellulose with tunable oleophobicity. *Soft Matter*, 6:3298-3305.
- Avgerinos, G.C. and Wang D.I.C. (1983). Selective delignification for fermentation of enhancement. *Biotechnology and Bioengineering*, 25:67-83.
- Ayadi, F., Martín-García, B., Colombo, M., Polovitsyn, A., Scarpellini, A., Ceseracciu, L., Moreels, I. and Athanassiou, A. (2016). Mechanically flexible and optically transparent three-dimensional nanofibrous amorphous aerocellulose. *Carbohydrate Polymers*, 149:217-223.
- Azeredo, H.M.C. (2009). Nanocomposites for food packaging applications. *Food Research International*, 42:1240-1253.
- Aziz, S. and Sarkanen, K. (1989). Organosolv pulping-a review. *Tappi Journal*, 72:169-175.
- Azizi Samir, M.A.S., Alloin, F. and Dufresne, A. (2005). Review of recent research into cellulosic whiskers, their properties and their application in nanocomposite field. *Biomacromolecules*, 6:612-626.
- Azizi Samir, M.A.S., Alloin, F., Paillet, M. and Dufresne, A. (2004). Tangling effect in fibrillated cellulose reinforced nanocomposites. *Macromolecules*, 37:4313-4316.
- Bailey, R.W., Mills, S.E. and Hove, E.L. (1974). Composition of sweet and bitter lupin seed hulls with observations on the apparent digestibility of sweet lupin seed hulls by young rats. *Journal of the Science of Food and Agriculture*, 25:955-961.
- Banerjee, S., Sen, R. and Pandey R.A. (2009). Evaluation of wet air oxidation as a pretreatment strategy for bioethanol production from rice husk and process optimization. *Biomass and Bioenergy*, 33:1680-1686.
- Belbekhouche, S., Bras, J., Siqueira, G., Chappey, C., Lebrun, L., Khelifi, B., Marais, S. and Dufresne, A. (2011). Water sorption behavior and gas barrier properties of cellulose whiskers and microfibrils films. *Carbohydrate Polymer*, 83:1740-1748.

- Ben-Ghedalia, D. and Miron, J. (1981). The effect of combined chemical and enzyme treatment on the saccharification and in vitro digestion rate of wheat straw. *Biotechnology and Bioengineering*, 23:823-831.
- Ben-Ghedalia, D. and Shefet, G. (1983). Chemical treatments for increasing the digestibility of cotton straw. *Journal of Agricultural Science*, 100:393-400.
- Besbes, I., Vilar, M.R. and Boufi, S. (2011). Nanofibrillated cellulose from alfa, eucalyptus and pine fibres: preparation, characteristics and reinforcing potential. *Carbohydrate Polymers*, 86:1198-1206.
- Bhatnagar, A. and Sain, M. (2005). Processing of cellulose nanofiber-reinforced composites. *Journal of Reinforced Plastics and Composites*, 24:1259-1268.
- Bjerre, A.B., Olesen, A.B., Fernqvist, T., Ploger, A. and Schmidt, A.S. (1996). Pretreatment of wheat straw using combined wet oxidation and alkaline hydrolysis resulting in convertible cellulose and hemicellulose. *Biotechnology and Bioengineering*, 49:568-577.
- Bledzki, A.K. and Gassan, J. (1999). Composites reinforced with cellulose based fibres. *Progress in Polymer Science*, 24:221-274.
- Bobleter, O. (1994). Hydrothermal degradation of polymer derived from plants. *Progress in Polymer Science*, 19:797-841.
- Brebu, M. and Vasile, C. (2010). Thermal degradation of lignin-A review. *Cellulose Chemistry and Technology*, 44:353-363.
- Brinchi, L., Cotana, F., Fortunati, E. and Kenny, J.M. (2013). Production of nanocrystalline cellulose from lignocellulosic biomass: Technology and applications. *Carbohydrate Polymer*, 94:154-169.
- Brodeur, G., Yau, E., Badal, K., Collier, J., Ramachandran, K.B. and Ramakrishnan, S. (2011). Chemical and physicochemical pretreatment of lignocellulosic biomass: A review. *Enzyme Research*, 10:40-61.
- Brown, Z.K., Fryer, P.J., Norton, I.T. and Bridson, R.H. (2010). Drying of agar gels using supercritical carbon dioxide. *Journal of Supercritical Fluids*, 54:89-95.
- Brunner, G. (2009). Near critical and supercritical water. Part I. Hydrolytic and hydrothermal processes. *Journal of Supercritical Fluids*, 47:373-381.
- Buranov, A.U. and Mazza, G. (2007). Fractionation of flax Shives by water and aqueous ammonia treatment in a pressurized low-polarity water extractor. *Journal of Agricultural and Food Chemistry*, 55:8548-8555.
- Buranov, A.U. and Mazza, G. (2008). Lignin in straw of herbaceous crops. *Industrial Crops and Products*, 28:237-259.

- Cantarella, M., Cantarella, L. and Gallifuoco, A. (2004). Effect of inhibitors released during steam-explosion treatment of poplar wood on subsequent enzymatic hydrolysis and SSF. *Biotechnology Progress*, 20:200-206.
- Carreau, P.J., Cotton, F., Citerne, G.P., Moan, M. (2002). Rheological properties of concentrated suspensions: application to foodstuffs. In: Welti-Chanes, J., Barbosa-Canovas, G.V., Aguilera, J.M. (Eds.), *Engineering and Food for the 21st Century*. CRC Press, FL, USA, pp. 327-346.
- Carvalho, F., Duarte, L.C. and Gírio, F.M. (2008). Hemicellulose biorefineries: A review on biomass pretreatments. *Journal of Scientific and Industrial Research*, 67:849-864.
- Cervin, N.T., Aulin, C., Larsson, P.T. and Wågberg, L. (2012). Ultra porous nanocellulose aerogels as separation medium for mixtures of oil/water liquids. *Cellulose*, 19:401-410.
- Chakraborty, A., Sain, M. and Kortschot, M. (2005). Cellulose microfibrils: A novel method of preparation using high shear refining and cryocrushing. *Holz-Forschung*, 59:102-107.
- Chen, W., Yu, H., Li, Q., Liu, Y. and Li, J. (2011). Ultralight and highly flexible aerogels with long cellulose I nanofibers. *Soft Matter*, 7:10360-10368.
- Chen, W., Yu, H., Liu, Y., Chen, P., Zhang, M. and Hai, Y. (2011). Individualization of cellulose nanofibers from wood using high-intensity ultrasonication combined with chemical pretreatments. *Carbohydrate Polymers*, 83:1804-1811.
- Chen, W., Yu, H., Liu, Y., Hai, Y., Zhang, M. and Chen, P. (2011). Isolation and characterization of cellulose nanofibers from four plant cellulose fibers using a chemical-ultrasonic process. *Cellulose*, 18:433-442.
- Chen, Y., Wu, Q., Huang, B., Huang, M. and Ai, X. (2015). Isolation and characteristics of cellulose and nanocellulose from lotus leaf stalk agro-wastes. *BioResources*, 10:684-696.
- Cheng, Q., Wang, J., McNeel, J. and Jacobson, P. (2010). Water retention value measurements of cellulosic materials using a centrifuge technique. *BioResources*, 5:1945-1954.
- Cheng, Q., Wang, S., Rials, T. and Lee, S. (2007). Physical and mechanical properties of polyvinyl alcohol and polypropylene composite materials reinforced with fibril aggregates isolated from regenerated cellulose fibers. *Cellulose*, 14:593-602.
- Chum, H.L., Johnson, D.K. and Black, S. (1988). Organosolv pretreatment for enzymatic hydrolysis of poplars: 1. Enzyme hydrolysis of cellulosic residues. *Biotechnology and Bioengineering*, 31:643-649.

- Ciftci, D. and Saldaña, M. D. A. (2015). Hydrolysis of sweet blue lupin hull using subcritical water technology. *Bioresource Technology*, 194:75-82.
- Comin, L.M., Temelli, F., and Saldaña, M.D.A. (2012). Barley beta-glucan aerogels via supercritical CO<sub>2</sub> drying. *Food Research International*, 48:442-448.
- Curren, M.S.S. and King, J.W. (2001). Solubility of triazine pesticides in pure and modified subcritical water. *Analytical Chemistry*, 73:740-745.
- Delgado-Zamarreno, M.M., Bustamante-Rangel, M., Sierra-Manzano, S., Vergugo-Jara, M. and Carabias-Martinez, R. (2009). Simultaneous extraction of tocotrienols and tocopherols from cereals using pressurized liquid extraction prior to LC determination. *Journal of Separation Science*, 32:1430-1436.
- Deng, C. H., Ji, J., Wang, X. C. and Zhang, X. M. (2005). Development of pressurized hot water extraction followed by headspace solid-phase microextraction and gas chromatography-mass spectrometry for determination of ligustilides in *Ligusticum chuanxiong* and *Angelica sinensis*. *Journal of Separation Science*, 28:1237-1243.
- Deshwal, B.R., Jo, H. D. and Lee, H.K. (2004). Reaction kinetics of decomposition of acidic sodium chlorite. *Canadian Journal of Chemical Engineering*, 82:619-623.
- Diamond, L.W. and Akinfiev, N.N. (2003). Solubility of CO<sub>2</sub> in water from -1.5 to 100 °C and from 0.1 to 100 MPa: Evaluation of literature data and thermodynamic modelling. *Fluid Phase Equilibria*, 208:265-290.
- Digman, M.F., Shinnars, K.J., Casler, M.D., Dien, B.S., Hatfield, R.D., Jung, H.J.G. (2010). Optimizing on-farm pretreatment of perennial grasses for fuel ethanol production. *Bioresource Technology*, 101:5305-5314.
- Dogan, N. and McHugh, T.H. (2007). Effects of Microcrystalline Cellulose on Functional Properties of Hydroxy Propyl Methyl Cellulose Microcomposite Films. *Journal of Food Science*, 72:16-22.
- Dong, H., Snyder, J.F., Tran, D.T. and Leadore, J.L. (2013). Hydrogel, aerogel and film of cellulose nanofibrils functionalized with silver nanoparticles. *Carbohydrate Polymers*, 95:760-767.
- Dong, S.P. and Roman, M. (2007). Fluorescently labeled cellulose nanocrystals for bioimaging applications. *Journal of the American Chemical Society*, 129:13810-13811.
- Dong, X.M, Kimura, T. Revol, J.F and Gray, D.G. (1996). Effects of ionic strength on the isotropic-chiral nematic phase transition of suspensions of cellulose crystallites. *Langmuir*, 12:2076-2082.

- Dong, X.M., Revol, J.F. and Gray, D. (1998). Effect of microcrystallite preparation conditions on the formation of colloid crystals of cellulose. *Cellulose*, 5:19-32.
- Duchemin, B.J.C., Staiger, M.P., Tucker, N. and Newman, R.H. (2009). Aerocellulose based on all-cellulose composites. *Journal of Applied Polymer Science*, 115:216-221.
- Dufresne, A. (2010). Polymer nanocomposites from Biological Sources. In: Nalwa, H.S. (Ed.), *Encyclopedia of Nanoscience and Nanotechnology*. American Scientific Publisher, Valencia.
- Dufresne, A., Dupeyre, D. and Vignon, M.R., (2000). Cellulose microfibrils from potato tuber cells: processing and characterization of starch-cellulose microfibril composites. *Journal of Applied Polymer Science*, 76:2080-2092.
- Ebringerova, A. (2005). Structural diversity and application potential of hemicelluloses. *Macromolecular Symposium*, 232:1-12.
- Ebringerova, A., Hromadkova, Z. and Heinze, T. (2005). Hemicellulose. Polysaccharides 1: structure, characterization and use. *Advances in Polymer Sciences*, 186:1-67.
- Eichhorn, S., Dufresne, A., Aranguren, M., Marcovich, N., Capadona, J., Rowan, S., Weder, C., Thielemans, W., Roman, M., Renneckar, S., Gindl, W., Veigel, S., Keckes, J., Yano, H., Abe, K., Nogi, M., Nakagaito, A., Mangalam, A., Simonsen, J., Benight, A., Bismarck, A., Berglund, L. and Peijs, T. (2010). Review: current international research into cellulose nanofibres and nanocomposites. *Journal of Materials Science*, 45:1-33.
- Elazzouzi-Hafraoui, S., Nishiyama, Y., Putaux, J.-L., Heux, L., Dubreuil, F. and Rochas, C. (2008). Preparation and enzymatic hydrolysis of nanoparticles made from single xyloglucan polysaccharide chain. *Biomacromolecules*, 9:57-65.
- Excoffier, G., Toussaint, B., Vignon, M.R. (1991). Saccharification of steam-exploded poplar wood. *Biotechnology and Bioengineering*, 38:1308-1317.
- Faulon, J., Carlson, G.A. and Hatcher, P.G. (1994). A three-dimensional model for lignocellulose from gymnospermous wood. *Organic Geochemistry*, 21:1169-1179.
- Fengel, D. and Wegener, G. (1984). *Wood: Chemistry, ultrastructure, reactions*. De Gruyter, Berlin, 613.
- Frone, A.N., Panaitescu, D.M. and Donescu, D. (2011). Some aspects concerning the iso-lation of cellulose micro- and nano-fibers. *U.P.B. Science Bulletin, Series B*, 73:133-152.

- Fujisawa, S., Okita, Y., Fukuzumi, H., Saito, T. and Isogai, A. (2011). Preparation and characterization of TEMPO-oxidized cellulose nanofibril films with free carboxyl groups. *Carbohydrate Polymers*, 84:579-583.
- Fukuzumi, H., Saito, T., Iwata, T., Kumamoto, Y. and Isogai, A. (2009). Transparent and high gas barrier films of cellulose nanofibers prepared by TEMPO-mediated oxidation. *Biomacromolecules*, 10:162-165.
- Fukuzumi, H., Saito, T., Iwata, T., Kumamoto, Y. and Isogai, A. (2009). Transparent and high gas barrier films of cellulose nanofibers prepared by TEMPO-mediated oxidation. *Biomacromolecules*, 10:162-165.
- Fumagalli, M., Ouhab, D., Boisseau, S.M. and Heux, L. (2013). Versatile gas-phase reactions for surface to bulk esterification of cellulose microfibrils aerogels. *Biomacromolecules*, 14:3246-3255.
- Garcia-Aparicio, M.P., Ballesteros, I., Gonzalez, A. (2006). Effect of inhibitors released during steam-explosion pretreatment of barley straw on enzymatic hydrolysis. *Applied Biochemistry and Biotechnology*, 129:278-288.
- Gavillon, R. and Budtova, T. (2008). Aerocellulose: new highly porous cellulose prepared from cellulose-NaOH aqueous solutions. *Biomacromolecules*, 9:269-277.
- Goh, C.S., Tan, K.T., Lee, K.T. and Bhatia, S. (2010). Bio-ethanol from lignocellulose: status, perspectives and challenges in Malaysia. *Bioresource Technology*, 101:4834-4841.
- Grierer, J. (1986). Chemistry of delignification. *Wood Science and Technology*, 20:1-33.
- Gross, J. and Fricke, J. (1992). Ultrasonic velocity measurements in silica, carbon and organic aero gels. *Journal of Non-Crystalline Solids*, 145:217-222.
- Grunert, M., and Winter, W.T. (2002). Nanocomposites of cellulose acetate butyrate reinforced with cellulose nanocrystals. *Journal of Polymers and the Environment*, 10:27-30.
- Guo, G.L., Hsu, D.C., Chen, W.H., Chen, W.H. and Hwang, W.S. (2009). Characterization of enzymatic saccharification for acid-pretreated lignocellulosic materials with different lignin composition. *Enzyme and Microbial Technology*, 45:80-87.
- Han, J., Zhou, C., Wu, Y., Liu, F. and Wu, Q. (2013). Self-Assembling behavior of cellulose nanoparticles during freeze-drying: effect of suspension concentration, particle size, crystal structure, and surface charge. *Biomacromolecules*, 14:1529-1540.
- Hanim, S.S., Norsyabilah, R., Nor Suhaila, M.H., Noraishah, A. and Siti Kartina, A.K. (2012). Effects of temperature, time and pressure on the hemicelluloses

yield extracted using subcritical water extraction. *Procedia Engineering*, 42:562-565.

Harkin, J.M. (1973). Lignin. In: Butler, G.W. and Bailey, R.W. (Eds.), *Chemistry and biochemistry of herbage*. Academic press, New York, pp. 3232-3373.

Hassan, M. L., Mathew, A. P., Hassan, E. A., El-Wakil, N. A. and Oksman, K. (2012). Nanofibers from bagasse and rice straw: process optimization and properties. *Wood Science and Technology*, 46:193-205.

Hassan, M.L., Hassan, E.A. and Oksman, K.N. (2011). Effect of pretreatment of bagasse fibers on the properties of chitosan/microfibrillated cellulose nanocomposites. *Journal of Materials Science*, 46:1732-1740.

Heidarian, P., Behzad, T. and Karimi, K. (2016). Isolation and characterization of bagasse cellulose nanofibrils by optimized sulfur-free chemical delignification. *Wood Science and Technology*, 50:1071.

Henriksson, M., Berglund, L.A., Isaksson, P., Lindstrom, T. and Nishino, T. (2008). Cellulose nanopaper structures of high toughness. *Biomacromolecules*, 9:1579-1585.

Henriksson, M., Henriksson, G., Berglund, L.A. and Lindstrom, T. (2007). An environmentally friendly method for enzyme-assisted preparation of microfibrillated cellulose (MFC) nanofibers. *European Polymer Journal*, 43:3434-3441.

Herrick, F.W., Casebier, R.L., Hamilton, J.K. and Sandberg, K.R. (1983). Microfibrillated cellulose: Morphology and accessibility. *Journal of Applied Polymer Science: Applied Polymer Symposium*, 37:797-813.

Himmel, M.E., Adney, W.S., Baker, J.O., Elander, R., McMillan, J.D. and Nieves, R.A. (1997). Advanced bioethanol production technologies: A perspective. *Fossil Fuels and Biomass*, 666:2-45.

Hoffman, A.S. (2002). Hydrogels for biomedical applications. *Advanced Drug Delivery Reviews*, 54:3-12.

Holtzapple, M.T, Jun, J.H., Ashok, G., Patibandla, S.L. and Dale, B.E. (1991). The Ammonia Freeze Explosion (AFEX) Process - A practical lignocellulose pretreatment. *Applied Biochemistry and Biotechnology*, 28:59-74.

Hongdan, Z., Shaohua, X. and Shubin, W. (2013). Enhancement of enzymatic saccharification of sugarcane bagasse by liquid hot water pretreatment. *Bioresource Technology*, 143:391-396.

Howard, R.L., Abotsi, E., Rensburg, E.L. and Howard, S. (2003). Lignocellulose biotechnology: issues of bioconversion and enzyme production. *African Journal of Biotechnology*, 2:602-619.

Hu, G., Heimann, J. and Rojas, O. (2008). Feedstock pretreatment strategies for producing ethanol from wood, bark, and forestresidues. *BioResources*, 3:270-294.

Hubbe, M.A., Rojas, O.J., Lucia, L.A. and Sain, M. (2008). Cellulosic nanocomposites: Review. *BioResources*, 3:929-980.

Hubbell, C.A. and Ragauskas, A.J. (2010). Effect of acid-chlorite delignification on cellulose degree of polymerization. *Bioresource Technology*, 101:7410-7415.

Hüsing, N. and Schubert, U. (1998). Aerogels airy materials: Chemistry, structure, and properties. *Angewandte Chemie*, 37:23-45.

Isogai, A. (2013) Wood nanocelluloses: fundamentals and applications as new biobased nanomaterials. *Journal of Wood Science*, 59:449-459.

Ivanov, C., Popa, M., Ivanov, M. and Popa, A.A. (2007). Synthesis of poly(vinyl alcohol) - methyl cellulose hydrogel as possible scaffolds in tissue engineering. *Journal of Optoelectronics and Advanced Materials*, 9:3440-3444.

Iwamoto, S., Nakagaito, A.N. and Yano, H. (2007). Nano-fibrillation of pulp fibers for the processing of transparent nanocomposites. *Applied Physics A: Materials Science and Processing*, 89:461-466.

Iyer, P.V., Wu, Z.W., Kim, S.B. and Lee, Y.Y. (1996). Ammonia recycled percolation process for pretreatment of herbaceous biomass. *Applied Biochemistry and Biotechnology*, 57-58:121-132.

Jin, H., Nishiyama, Y., Wada, M. and Kuga, S. (2004). Nanofibrillar cellulose aerogels. *Colloids and Surfaces A: Physicochemical and Engineering Aspects*, 240:63-67.

John, J.J. and Thomas, S. (2008). Biofibres and biocomposites. *Carbohydrate Polymers*, 71:343-364.

Jorgensen, H., Kristensen, J.B. and Felby, C. (2007). Enzymatic conversion of lignocellulose into fermentable sugars: Challenges and opportunities. *Biofuels, Bioproducts and Biorefining*, 1:119-134.

Kadla, J.F. and Gilbert, R.D. (2000). Cellulose structure: A review. *Cellulose Chemistry and Technology*, 34:197-216.

Karagöz, S., Bhaskar, T., Muto, A. and Sakata, Y. (2005). Comparative studies of oil compositions produced from sawdust, rice husk, lignin and cellulose by hydrothermal treatment. *Fuel*, 84:875-884.

Kelly, J. A., Giese, M., Shopsowitz, K. E., Hamad, W. Y. and MacLachlan, M. J. (2014). The development of chiral nematic mesoporous materials. *Accounts of Chemical Research*, 47:1088-1096.

- Kenar, J.A., Eller, F. J., Felker, F.C., Jackson, M.A. and Fanta, G.F. (2014). Starch aerogel beads obtained from inclusion complexes prepared from high amylose starch and sodium palmitate. *Green Chemistry*, 16:1921-1930.
- Kim, J.S., Lee, Y.Y. and Kim, T.H. (2016). A review on alkaline pretreatment technology for bioconversion of lignocellulosic biomass. *Bioresource Technology*, 199:42-48.
- Kim, S. and Holtzapfle, M.T. (2005). Lime pretreatment and enzymatic hydrolysis of corn stover. *Bioresource Technology*, 96:1994-2006.
- Kim, T.H. and Lee, Y.Y. (2005). Pretreatment and fractionation of corn stover by ammonia recycle percolation process. *Bioresource Technology*, 96:2007-2013.
- Kim, T.H. and Lee, Y.Y. (2006). Fractionation of corn stover by hot-water and aqueous ammonia treatment. *Bioresource Technology*, 97:224-232.
- Kim, T.H. and Lee, Y.Y. (2007). Pretreatment of corn stover by soaking in aqueous ammonia at moderate temperatures. *Applied Biochemistry and Biotechnology*, 137:81-92.
- Kim, W. J., Kim, J., Veriansyah, B., Kim, J. D., Lee, Y. W., Oh, S. G. and Tjandrawinata, R. R. (2009). Extraction of bioactive components from *Centella asiatica* using subcritical water. *Journal of Supercritical Fluids*, 48:211-216.
- Kim, Y., Mosier, N.S. and Ladisch, M.R. (2009). Enzymatic digestion of liquid hot water pretreated hybrid poplar. *Biotechnology Progress*, 25:340-348.
- Kin, Z. (1990). The acetolysis of beech wood. *Tappi Journal*, 73:237-238.
- Kistler, S.S. Coherent expanded aerogels and jellies. (1931). *Nature*, 127: 741.
- Klemm, D., Heublein, B. and Fink, H.P. (2005). Cellulose: Fascinating biopolymer and sustainable raw material. *Angewandte Chemie International*, 44:3358-3393.
- Klouda, L. and Mikos, A.G. (2008). Thermoresponsive hydrogels in biomedical applications. *European Journal of Pharmaceutics and Biopharmaceutics*, 68:34-45.
- Kobayashi, H. and Fukuoka, A. (2013). Synthesis and utilisation of sugar compounds derived from lignocellulosic biomass. *Green Chemistry*, 15:1740-176.
- Korhonen, J.T., Hiekkataipale, P, Malm, J., Karppinen, M., Ikkala, O. and Robin H.A. (2011). Inorganic hollow nanotube aerogels by atomic layer deposition onto native nanocellulose templates. *ACS Nano*, 5:1967-1974.
- Korhonen, J.T., Kettunen, M., Ras, R.H.A. and Ikkala, O. (2011). Hydrophobic nanocellulose aerogels as floating, sustainable, reusable, and recyclable oil absorbents. *ACS Applied Materials & Interfaces*, 3:1813-1816.

- Krishna, S.H. and Chowdary, G.V. (2000). Optimization of simultaneous saccharification and fermentation for the production of ethanol from lignocellulosic biomass. *Journal of Agricultural and Food Chemistry*, 48:1971-1976.
- Kruse, A. and Dinjus, E. (2007). Hot compressed water as reaction medium and reactant: properties and synthesis reactions. *Journal of Supercritical Fluids*, 39:362-380.
- Kruse, A. and Gawlik, A. (2003). Biomass conversion in water at 330-410 °C and 30-50 MPa. Identification of key compounds for indicating different chemical reaction pathways. *Industrial and Engineering Chemistry Research*, 42:267-279.
- Kuhad, R. C., Singh, A. and Eriksson, K. E. (1997). Microorganisms and enzymes involved in degradation of plant fiber cell walls. *Advances in Biochemical Engineering / Biotechnology*, 57:45-125.
- Kumar, P., Barrett, D.M., Delwiche, M.J. and Stroeve, P. (2009). Methods for pretreatment of lignocellulosic biomass for efficient hydrolysis and biofuel production. *Industrial and Engineering Chemistry Research*, 48:3713-3729.
- Kumar, V., Reus-Medina, M.D.L. and Yang, D. (2002). Preparation, characterization, and tableting properties of a new cellulose-based pharmaceutical aid. *International Journal of Pharmaceutics*, 235:129-140.
- Kurabi, A., Berlin, A., Gilkes, N., Kilburn, D., Bura, R. and Robinson, J. (2005). Enzymatic hydrolysis of steam-exploded and ethanol organosolv-pretreated Douglas-Firby novel and commercial fungal cellulases. *Applied Biochemistry and Biotechnology*, 121:219-230.
- Kurlovich, B.S. (Ed.) (2002). Lupins (Geography, Classification, Genetic Resources and Breeding), Intan, St. Petersburg.
- Kvien, I. Tanem, B.S. and Oksman, K. (2005). Characterization of cellulose whiskers and their nanocomposites by atomic force and electron microscopy. *Biomacromolecules*, 6:3160-3165.
- Lasseguette, E., Roux, D. and Nishiyama, Y. (2008). Rheological properties of microfibrillar suspension of TEMPO-oxidized pulp. *Cellulose*, 15:425-433.
- Lawther, J.M., Sun, R. and Banks, W.B. (1996). Effect of steam treatment on the chemical composition of wheat straw. *Holzforschung*, 50:365-371.
- Lee, H.V., Hamid, S.B.A. and Zain, S. K. (2014). Conversion of lignocellulosic biomass to nanocellulose: structure and chemical process. *The Scientific World Journal*, 2014:631013.
- Lee, K.Y. and Mooney, D.J. (2001). Hydrogels for tissue engineering. *Chemical Reviews*, 101:1869-1880.

Li, W., Yue, J. and Liu, S. (2012). Preparation of nanocrystalline cellulose via ultrasound and its reinforcement capability for poly (vinyl alcohol) composites. *Ultrasonics Sonochemistry*, 19:479-485.

Liebner, F., Potthast, A., Rosenau, T., Haimer, E. and Wendland, M. (2008). Cellulose aerogel: Highly porous ultra-lightweight materials. *Holzforschung*, 62:129-135.

Liimatainen, H., Suopajarvi, T., Sirviö, J., Hormi, O. and Niinimäki, J. (2014). Fabrication of cationic cellulosic nanofibrils through aqueous quaternization pretreatment and their use in colloid aggregation. *Carbohydrate Polymers*, 103:187-192.

Lima, M.M.D. and Borsali, R. (2004). Rodlike cellulose microcrystals: structure, properties, and applications. *Macromolecular Rapid Communications*, 25:771-787.

Liu, C. and Wayman, C.E. (2003). The effect of flow rate of compressed hot water on xylan, lignin, and total mass removal from corn stover. *Industrial and Engineering Chemistry Research*, 42:5409-5416.

Liu, H., Zhang, J., Bao, N., Cheng, C., Ren, L. and Zhang, C. (2012). Textural properties and surface chemistry of lotus stalk-derived activated carbons prepared using different phosphorus oxyacids: adsorption of trimethoprim. *Journal of Hazardous Materials*, 235:367-375.

Lotti, M., Gregersen, O.W., Moe, S. and Lenes, M. (2011). Rheological studies of microfibrillar cellulose water dispersions. *Journal of Polymers and the Environment*, 19:137-145.

Lu, X. and Saka, S. (2010). Hydrolysis of Japanese beech by batch and semi-flow water under subcritical temperatures and pressures. *Biomass and Bioenergy*, 34:1089-1097.

Lynd, L.R., Cushman, J.H., Nichols, R.J. and Wyman, C.E. (1991). Fuel ethanol from cellulosic biomass. *Science*, 251:1318-1323.

Madani, A., Kiiskinen, H., Olson, J.A. and Martinez, M.D. (2011). Fractionation of microfibrillated cellulose and its effects on tensile index and elongation of paper. *Nordic Pulp & Paper Research Journal*, 26:306-311.

Mandal, A. and Chakrabarty, D. (2011). Isolation of nanocellulose from waste sugarcane bagasse (SCB) and its characterization. *Carbohydrate Polymers*, 86:1291-1299.

Manfredi, B.L., Rodrigue, E.S., Wladyka, P.M. and Vazquez, A. (2006). Thermal degradation and fire resistance of unsaturated polyester modified acrylic resins

and their composites with natural fibers. *Polymer Degradation and Stability*, 91:255-261.

Marjo, P., Vapaavuori, J., Silvennoinen, R., Kosonen, H., Ankerfors, M., Lindström, T., Berglund, L.A. and Ikkala, O. (2008). Long and entangled native cellulose I nanofibers allow flexible aerogels and hierarchically templates for functionalities. *Soft Matter*, 4:2492-2499.

Mason, T. J. (2000). Sonochemistry, *Oxford Chemistry Primers*. Oxford, OX, United Kingdom, 1-2

McMillan, J.D. (1994). Pretreatment of lignocellulosic biomass. In: Himmel, M. E., Baker, J. O., Overend, R. P. (Eds.), *Enzymatic Conversion of Biomass for Fuels Production*. American Chemical Society, Washington.

Mehling, T., Smirnova, I., Guenther, U. and Neubert, R.H.H. (2009). Polysaccharide based aerogels as drug carriers. *Journal of Non-Crystalline Solids*, 355:2472-2479.

Meng, F., Schlup, M. R. and Fan, L. T. (1997). Fractal analysis of polymeric and particulate titania aerogels by adsorption. *Chemistry of Materials*, 9:2459-2463.

Mes-Hartree, M., Dale, B.E. and Craig, W.K. (1988). Comparison of steam and ammonia pretreatment for enzymatic hydrolysis of cellulose. *Applied Microbiology and Biotechnology*, 29:462-468.

Modenbach, A. (2013). Sodium hydroxide pretreatment of corn stover and subsequent enzymatic hydrolysis: An investigation of yields, kinetic modeling and glucose recovery, Ph.D. dissertation at the University of Kentucky, 147-191.

Mok, W.S.L. and Antal, M.J. (1992). Uncatalyzed solvolysis of whole biomass hemicellulose by hot compressed liquid water. *Industrial and Engineering Chemistry Research*, 31:1157-1161.

Moldes, A.B., Cruz, J.M., Domínguez, J.M. and Parajó, J.C. (2002). Production of a cellulosic substrate susceptible to enzymatic hydrolysis from prehydrolyzed barley husks. *Agricultural and Food Science Finland*, 11:51-58.

Moller, M., Nilges, P., Harnisch, F. and Schroder, U. (2011). Subcritical water as reaction environment: Fundamentals of hydrothermal biomass transformation. *ChemSusChem*, 4:566-579.

Mondal, S., Memmott, P., Wallis, L. and Martin, D. (2012). Physicothermal properties of spinifex resin bio-polymer. *Materials Chemistry and Physics*, 133:692-699.

Moon, R.J., Martini, A., Nairn, J., Simonsen, J., and Youngblood, J. (2011). Cellulose nanomaterials review: structure, properties and nanocomposites. *Chemical Society Reviews*, 40:3941-3994.

- Morrison, W. H. and Akin, D. E. (1990). Water soluble reaction products from ozonolysis of grasses. *Journal of Agricultural and Food Chemistry*, 38:678-681.
- Mosier, N.S., Sarikaya, A., Ladisch, C.M. and Ladisch, M.R. (2001). Characterization of dicarboxylic acids for cellulose hydrolysis. *Biotechnology Progress*, 17:474-480.
- Mosier, N.S., Wyman, C., Dale, B., Elander, R., Lee, Y.Y., Holtzapple, M. and Ladisch, M.R. (2005). Features of promising technologies for pretreatment of lignocellulosic biomass. *Bioresource Technology*, 96:673-686.
- Murphy, D.M. and Koop, Q. (2005). Review of the vapour pressures of ice and supercooled water for atmospheric applications. *Royal Meteorological Society*, 131:1539-1565.
- Nakagaito, A. N. and Yanom H. (2005). Novel high-strength biocomposites based on microfibrillated cellulose having nano-order-unit web-like network structure. *Applied Physics A*, 80:155-159.
- Nakagaito, A.N. and Yano, H. (2004). The effect of morphological changes from pulp fiber towards nano-scale fibrillated cellulose on the mechanical properties of high-strength plant fiber based composites. *Applied Physics A: Materials Science and Processing*, 78:547-552.
- Nakagaito, A.N., Nogi, M. and Yano, H. (2010). Displays from transparent films of natural nanofibers. *MRS Bulletin*, 35:214-218.
- National Institute of Standards and Technology (NIST) Chemistry Webbook, accessed on June 2014. Available from: <http://webbook.nist.gov>.
- Neely, W. C. (1984). Factors affecting the pretreatment of biomass with gaseous ozone. *Biotechnology and Bioengineering*, 26:59-65.
- Nguyen, M. H. and Dao, L. H. (1998). Effects of processing variable on melamine-formaldehyde aerogel formation. *Journal of Non-Crystalline Solids*, 225:51-57.
- Nguyen, Q.A., Tucker, M.P., Keller, F.A. and Eddy, F.P. (2000). Two-stage dilute-acid pretreatment of softwoods. *Applied Biochemistry and Biotechnology*, 84-86:561-576.
- Nishiyama, Y. (2009). Structure and properties of the cellulose microfibril. *Journal of Wood Science*, 55:241-249.
- Nishiyama, Y., Langan, P. and Chanzy, H. (2002). Crystal structure and hydrogen bonding system in cellulose I $\beta$  from synchrotron X-ray and neutron fiber
- Nogi, M. and Yano, H. (2008). Transparent nanocomposites based on cellulose produced by bacteria offer potential innovation in the electronics device industry. *Advanced Materials*, 20:1849-1852.

- Nystrom, G., Mihranyan, A., Razaq, A., Lindstrom, T., Nyholm, L. and Strømme, M. (2010). A nanocellulose polypyrrole composite based on microfibrillated cellulose from wood. *Journal of Physical Chemistry B*, 114:4178-4182.
- O' Sullivan, A.C. (1997). Cellulose: the structure slowly unravels, *Cellulose*, 4:173-207.
- Okahisa, Y., Yoshida, A., Miyaguchi, S. and Yano, H. (2009). Optically transparent wood-cellulose nanocomposite as a base substrate for flexible organic light-emitting diode displays. *Composites Science and Technology*, 69:1958-1961.
- Oksman, K., Mathew, A.P. and Sain, M. (2009). Novel bionanocomposites: processing, properties and potential applications. *Plastics, Rubber and Composites*, 38:396-405.
- Olsson, R.T., Azizi, Samir., M.A.S., Salazar-Alvarez, G., Belova, L., Ström, V., Berglund, L.A., Ikkala, O., Nogues, J. and Gedde, U.W. (2010). Making flexible magnetic aerogels and stiff magnetic nanopaper using cellulose nanofibrils as templates. *Nature Nanotechnology*, 5:584-588.
- Osong, S.H., Norgren, S. and Engstrand, P. (2015). Processing of wood-based microfibrillated cellulose and nanofibrillated cellulose, and applications relating to papermaking: a review. *Cellulose*, 23:93-123.
- Oujai, S. and Shanks, R.A. (2005). Composition, structure and thermal degradation of hemp cellulose after chemical treatments. *Polymer Degradation and Stability*, 89:327-335.
- Ozturk, I., Irmak, S., Hesenov, A. and Erbatur, O. (2010). Hydrolysis of kenaf (*Hibiscus cannabinus* L.) stems by catalytical thermal treatment in subcritical water. *Biomass and Bioenergy*, 34:1578-1585.
- Pääkkö, M., Ankerfors, M., Kosonen, H., Nykanen, A., Ahola, S., Osterberg, M., Ruokolainen, J., Laine, J., Larsson, P.T., Ikkala, O. and Lindström, T. (2007). Enzymatic hydrolysis combined with mechanical shearing and high-pressure homogenization for nanoscale cellulose fibrils and strong gels. *Biomacromolecules*, 8:1934-1941.
- Pääkkö, M., Vapaavuori, J., Silvennoinen, R., Kosonen, H., Ankerfors, M., Lindström, T., Berglund, L.A. and Ikkala, O. (2008). Long and entangled native cellulose I nanofibers allow flexible aerogels and hierarchically porous templates
- Pan, X., Xie, D. and Kang, K.Y. (2007). Effect of organosolv ethanol pretreatment variables on physical characteristics of hybrid poplar substrates. *Applied Biochemistry and Biotechnology*, 140:367-377.
- Parajó, J.C., Domínguez, H. and Domínguez, J.M. (1996). Xylitol from wood: Study of some operational strategies. *Food Chemistry*, 57:531-535.

- Paralikar, S.A., Simonsen, J. and Lombardi, J. (2008). Poly(vinyl alcohol)/cellulose nanocrystal barrier membranes. *Journal of Membrane Science*, 320:248-258.
- Pedersen M. and Meyer, A.S. (2009). Influence of substrate particle size and wet oxidation on physical surface structures and enzymatic hydrolysis of wheat straw. *Biotechnology Progress*, 25:399-408.
- Peng, Y., Gardner, D. J. and Han, Y. (2012). Drying cellulose nanofibrils: in search of a suitable method. *Cellulose*, 19:91-102.
- Perez, J., Muñoz-Dorado, J., De-la-Rubia, T. and Martínez, J. (2002). Biodegradation and biological treatments of cellulose, hemicellulose and lignin: An overview. *International Microbiology*, 5:53-63.
- Pérez, J.A., Ballesteros, I., Ballesteros, M., Sáez, F., Negro, M.J. and Manzanares, P. (2008). Optimizing liquid hot water pretreatment conditions to enhance sugar recovery from wheat straw for fuel-ethanol production. *Fuel*, 87:3640-3647.
- Perez, S. and Samain, D. (2010). Structure and engineering of celluloses. *Advances in Carbohydrate Chemistry and Biochemistry*, 64:5-116.
- Phaiboonsilpa, N. and Saka, S. (2011). Effect of acetic acid addition on chemical conversion of woods as treated by semi-flow hot-compressed water. *Holzforschung*, 65:667-672.
- Pierre, A., Begag, R. and Pajonk, G. (1999). Structure and texture of alumina aerogel monoliths made by complexation with ethyl acetoacetate. *Journal of Material Science*, 34:4937-4944.
- Pierre, A.C. and Pajonk, G.M. (2002) Chemistry of aerogels and their applications. *Chemistry Reviews*, 102:4243-4266.
- Pierre, A.C. and Pajonk, G.M. (2002). Chemistry of aerogels and their applications. *Chemical Reviews*, 102:4243-4266.
- Prasad, S., Singh, A., Joshi, H.C. (2007). Ethanol as an alternative fuel from agricultural, industrial and urban residues. *Resources, Conservation and Recycling*, 50:1-39.
- Pronyk, C. and Mazza, G. (2010). Kinetic modeling of hemicellulose hydrolysis from triticale straw in a pressurized low polarity water flow-through reactor. *Industrial and Engineering Chemistry Research*, 49:6367-6375.
- Pronyk, C. and Mazza, G. (2011). Optimization of processing conditions for the fractionation of triticale straw using pressurized low polarity water. *Bioresource Technology*, 102:2016-2025.
- Pronyk, C. and Mazza, G. (2012). Fractionation of triticale, wheat, barley, oats, canola, and mustard straws for the production of carbohydrates and lignins. *Bioresource Technology*, 106:117-124.

- Pu1, Y., Hu, F., Huang, F. and Ragauskas, A. J. (2015). Lignin structural alterations in thermochemical pretreatments with limited delignification. *Bioenergy Research*, 8:992-1003.
- Quievy, N., Jacquet, N., Selavons, M, Deroanne, C., Paquot, M. and Devaux, J. (2010). Influence of homogenization and drying on the thermal stability of microfibrillated cellulose. *Polymer Degradation and Stability*, 95:306-314.
- Rambabua, N., Panthapulakkalb, S., Sain, M. and Dalai, A.K. (2016). Production of nanocellulose fibers from pinecone biomass: Evaluation and optimization of chemical and mechanical treatment conditions on mechanical properties of nanocellulose films. *Industrial Crops and Products*, 83:746-754.
- Ramos, L.P. (2003). The chemistry involved in the steam treatment of lignocellulosic materials. *Quimica Nova*, 26: 863-871.
- Ratanakhanokchai, K., Waeonukul, R., Pason, P., Tachaapaikoon, C., Kyu, K.L., Sakka, K., Kosugi, A. and Mori, Y. (2013). Paenibacillus curdlanolyticus strain B-6 multienzyme complex: A novel system for biomass utilization. In: Matovic, M.D. (Ed.), Biomass Now - Cultivation and Utilization. In-Tech Education and Publishing, Austria.
- Ray, D., Sarkar, B.K., Basak, R.K and Rana, A.K. (2002). Study of the thermal behavior of alkali-treated jute fibers. *Journal of Applied Polymer Science*, 85:2594-2599.
- Reddy, N. and Yang, Y. (2005). Structure and properties of high quality natural cellulose fibers from cornstalks. *Polymer*, 46:5494-5500.
- Revol, J., Dietrich, A. and Goring, D. (1987). Effect of mercerization on the crystallite size and crystallinity index in cellulose from different sources. *Canadian Journal of Chemistry*, 65:1724-1725.
- Robitzer, M., Renzo, F.D. and Quignard, F. (2011). Natural materials with high surface area. Physisorption methods for the characterization of the texture and surface of polysaccharide aerogels. *Microporous and Mesoporous Materials*, 140:9-16.
- Rowell, M.R. (1992). Emerging technologies for material and chemicals from biomass. Proceedings of Symposium. American Chemical Society, Washington, DC, pp. 26-31.
- Ruangudomsakul, W., Ruksakulpiwat, C. and Ruksakulpiwat, Y. (2015). Preparation and characterization of cellulose nanofibers from cassava pulp. *Macromolecular Symposia*, 354:170-176.
- Ruiz, E., Cara, C., Ballesteros, M., Manzanares, P., Ballesteros, I. and Castro, E. (2006). Ethanol production from pretreated olive tree wood and sunflower stalks by an SSF process. *Applied Biochemistry and Biotechnology*, 129:631-643.

- Saha, B.C. (2003). Hemicellulose bioconversion. *Journal of Industrial Microbiology and Biotechnology*, 30:279-291.
- Saito, T., Kimura, S., Nishiyama, Y. and Isogai, A. (2007). Cellulose nanofibers prepared by TEMPO-mediated oxidation of native cellulose. *Biomacromolecules*, 8:2485-2491.
- Saito, T., Nishiyama, Y., Putaux, J.L., Vignon, M. and Isogai, A. (2006). Homogeneous suspensions of individualized microfibrils from TEMPO-catalyzed oxidation of native cellulose. *Biomacromolecules*, 7:1687-1691.
- Saito, T., Uematsu, T., Kimura, S., Enomae, T. and Isogai, A. (2011). Self-aligned integration of native cellulose nanofibrils towards producing diverse bulk materials.
- Sakurada, I., Nukushina, Y. and Ito, T. (1962). Experimental determination of elastic modulus of crystalline regions in oriented polymers. *Journal of Polymer Science*, 57:651-660.
- Saldaña, M.D.A. and Valdivieso-Ramirez, C.S. (2015) Pressurized Fluid Systems: Phytochemical Production from Biomass. *The Journal of Supercritical Fluids*, 96:228-244.
- Salmon, D.F., Mergoum, M. and Gómez-Macpherson, H. (2004). Triticale production and management. In: Mergoum, M., Gómez-Macpherson, H. (Eds.), *Triticale Improvement and Production*, Food and Agriculture Organization of the United Nations, Rome.
- Sánchez, C. (2009). Lignocellulosic residues: Biodegradation and bioconversion by fungi. *Biotechnology Advances*, 27:85-194.
- Sarah, P., Rushing, T.S., Landis, E.N. and Cummins, T.K. (2010). Nanocellulose and microcellulose fibers for concrete. *Nanotechnology in Cement and Concrete*, 2:25-28.
- Segal, L., Creely, L., Martin, A. E. and Conrad, C. M. (1959). An empirical method for estimating the degree of crystallinity of native cellulose using X-ray diffractometer. *Textile Research Journal*, 29:786-794.
- Sehaqui, H., Salajkova, M., Zhou, Q. and Berglund, L. A. (2010). Mechanical performance tailoring of tough ultra-high porosity foams prepared from cellulose I nanofiber suspensions. *Soft Matter*, 6:1824-1832.
- Sehaqui, H., Zhou, Q. and Berglund, L.A. (2011). High-porosity aerogels of high specific surface area prepared from nanofibrillated cellulose (NFC). *Composites Science and Technology*, 71:1593-1599.
- Selig, M.J., Viamajala, S., Decker, S.R., Tucker, M.P., Himmel, M.P. and Vinzant, T.B. (2007). Deposition of lignin droplets produced during dilute acid pretreatment of maize stems retards enzymatic hydrolysis of cellulose. *Biotechnology Progress*, 23:1333-1339.

- Shevchenko, S.M., Beatson, R.P. and Saddler, J.N. (1999). The nature of lignin from steam explosion/enzymatic hydrolysis of softwood. *Applied Biochemistry and Biotechnology*, 9:867-876.
- Shuai, L., Yang, Q., Zhu, J.Y., Lu, F.C., Weimer, P.J. and Ralph, J. (2010). Comparative study of SPORL and dilute-acid pretreatments of spruce for cellulosic ethanol production. *Bioresource Technology*, 101:3106-3114.
- Silverstein, R.A., Chen, Y., Sharma-Shivappa, R.R., Boyette, M.D. and Osborne, J. (2007). A comparison of chemical pretreatment methods for improving saccharification of cotton stalks. *Bioresource Technology*, 98:3000-3011.
- Singh, P.P, Saldaña, M.D.A., 2011. Subcritical water extraction of phenolic compounds from potato peel. *Food Research International*, 44:2452-2458.
- Singleton, V.L. and Rossi, J.A. Jr. (1965). Colorimetric of total phenolics with phosphomolybdic-phosphotungstic acid reagents. *American Journal of Enology and Viticulture*, 16:144-58.
- Siro, I. and Plackett, D. (2010). Microfibrillated cellulose and new nanocomposite materials: a review. *Cellulose* 17:459-494.
- Sirtori, C.R., Lovati, M.R., Manzoni, C., Castiglioni, S., Duranti, M., Magni, C., Morandi, S., D'Agostina, A. and Arnoldi A. (2004). Proteins of white lupin seed, a naturally isoflavone-poor legume, reduce cholesterolemia in rats and increase LDL receptor activity in HepG2 cells. *Journal of Nutrition*, 134:18-23.
- Sivers, M.V. and Zacchi, G.A. (1995). Techno-economical comparison of three processes for the production of ethanol from pine. *Bioresource Technology*, 51:43-52.
- Sjöström, E. (1981). Wood chemistry: Fundamentals and applications, Academic Press, New York.
- Sluiter, A., Hames, B., Ruiz, R., Scarlata, C., Sluiter, J. and Templeton, D. (2006). Determination of sugars, byproducts, and degradation products in liquid fraction process samples; Laboratory Analytical Procedure (LAP). NREL/TP-510-42623. National Renewable Laboratory, Golden, CO.
- Sluiter, A., Hames, B., Ruiz, R., Scarlata, C., Sluiter, J., Templeton, D. and Crocker, D. (2008). Determination of structural carbohydrates and lignin in biomass; Laboratory Analytical Procedure (LAP). NREL/TP-510-42618. National Renewable Laboratory, Golden, CO.
- Smichi, N., Yosra, M., Ksouri, R., Abdelly, C. and Gargouri, M. (2014). Pretreatment and enzymatic saccharification of new phytoresource for bioethanol production from halophyte species. *Renewable Energy*, 63:544-549.

- Sorrentino, A, Gorrasi, G. and Vittoria, V. (2007). Potential perspectives of bionanocomposites for food packaging applications. *Trends in Food Science and Technology*, 18:84-95.
- Stenberg, K. and Tengborg, C. (1998). Optimisation of steam pretreatment of SO<sub>2</sub>-impregnated mixed softwoods for ethanol production. *Journal of Chemical Technology and Biotechnology*, 71:299-308.
- Sun, R., Lawther, J.M. and Banks, W.B. (1995). Influence of alkaline pretreatments on the cell wall components of wheat straw. *Industrial Crops and Products*, 4:127-145.
- Sun, X. F., Xu, F., Sun, R. C., Fowler P. and Baird, M. S. (2005). Characteristics of degraded cellulose obtained from steam-exploded wheat straw. *Carbohydrate Research*, 340:97-106.
- Sun, Y. and Cheng, J. (2002). Hydrolysis of lignocellulosic materials for ethanol production: a review. *Bioresource Technology*, 83:1-11.
- Sun, Y.E. and Cheng, J.J. (2002). Hydrolysis of lignocellulosic materials for ethanol production: A review. *Bioresource Technology*, 83:1-11.
- Sun, Y.E. and Cheng, J.J. (2005). Dilute acid pretreatment of rye straw and Bermuda grass for ethanol production. *Bioresource Technology*, 96:1599-1606.
- Svagan, A.J., Samir, M.A.S.A. and Berglund, L.A. (2007). Biomimetic polysaccharide nanocomposites of high cellulose content and high toughness. *Biomacromolecules*, 8:2556-2563.
- Syverud, K. and Stenius, P. (2009). Strength and barrier properties of MFC films. *Cellulose*, 16:75-85.
- Taherzadeh, M.J. and Karimi, K. (2008). Pretreatment of lignocellulosic wastes to improve ethanol and biogas production: A review. *International Journal of Molecular Sciences*, 9:1621-1651.
- Tajkarimi, M., Riemann, H.P., Hajmeer, M.N., Gomez, E.L., Rzaszilar, V. and Cliver, D.O. (2008). Ammonia disinfection of animal feeds-laboratory study. *International Journal of Food Microbiology*, 122:23-28.
- Tan, C.B., Fung, B.M., Newman, J.K. and Vu, C. (2001). Organic aerogels with very high impact strength. *Advanced Materials*, 13:644-646.
- Taniguchi, T. and Okamura, K. (1998). New films produced from microfibrillated natural fibres. *Polymer International*, 47:291-294.
- Tatsumi, D., Ishioka, S. Matsumoto, T. (2002). Effect of fiber concentration and axial ratio on the rheological properties of cellulose fiber suspensions. *Journal of the Society of Rheology Japan*, 30:27-32

- Tengerdy, R.P. and Szakacs, G. (2003). Bioconversion of lignocellulose in solid substrate fermentation. *Biochemical Engineering Journal*, 13:169-179.
- Teymouri, F., Laureano-Perez, L., Alizadeh, H. and Dale, B.E. (2005). Optimization of the ammonia fiber explosion (AFEX) treatment parameters for enzymatic hydrolysis of corn stover. *Bioresource Technology*, 96:2014-2018.
- Thring, R.W., Chorent, E. and Overend, R. (1990). Recovery of a solvolytic lignin: Effects of spent liquor/acid volume ratio, acid concentration and temperature. *Biomass*, 23:289-305.
- Tingaut, P., Zimmermann, T. and Sebe, G. (2012). Cellulose nanocrystals and microfibrillated cellulose as building blocks for the design of hierarchical functional materials. *Journal of Materials Chemistry*, 22:20105-20111.
- Toor, S.S., Rosendahl, L. and Rudolf, A. (2011). Hydrothermal liquefaction of biomass: A review of subcritical water technologies. *Energy*, 36:2328-2342.
- Tsiptsias, C., Michailof, C., Staurooulos, G. and Panayiotou, C. (2009). Chitin and carbon aerogels from chitin alcogels. *Carbohydrate Polymers*, 76:535-540.
- Turbak, A. F., Snyder, F. W. and Sandberg, K. R. (1983). Microfibrillated cellulose, a new cellulose product: properties, uses, and commercial potential. *Journal of Applied Polymer Science*, 37:815-827.
- Ubeyitogullari, A., Ciftci, O.N. (2016). Formation of nanoporous aerogels from wheat starch. *Carbohydrate Polymers*, 147:125-132.
- Uematsu, M. (1980). Static dielectric constant of water and steam. *Journal of Physical Chemical Reference Data*, 9:1291-1306.
- Um, B.H. and van Walsum, G.P. (2009). Acid hydrolysis of hemicellulose in green liquor pre-pulping extract of mixed northern hardwoods. *Applied Biochemistry and Biotechnology*, 153:157-183.
- Van Dongen, F.E.M., Van Eylen, D. and Kabel, M.A. (2011). Characterization of substituents in xylans from corn cobs and stover. *Carbohydrate Polymers*, 86:722-731.
- Varga, E., Reczey, K. and Zacchi, G. (2004). Optimization of steam pretreatment of corn stover to enhance the enzymatic digestibility. *Applied Biochemistry and Biotechnology*, 113:509-523.
- Vargas-Guerrero, B., Garcia-Lopez, P.M., Martinez-Ayala, A.L., Dominguez-Rosales, J.A. and Gurrola-Diaz, C.M. (2014). Administration of *Lupinus albus* gamma conglutin (c-gamma) to n5 STZ rats augmented Ins-1 gene expression and pancreatic insulin content. *Plant Foods for Human Nutrition*, 69:241-247.
- Vázquez, D., Lage, M.A., Parajó, J.C. and Vázquez, G. (1992). Fractionation of Eucalyptus wood in acetic acid media, *Bioresource Technology*, 40:131-136.

- Velásquez-Cocka, J., Gánán, P., Posadac, P., Castrod, C., Serpa, A., Gómez C. H., Putaux, J.-L. and Zuluaga, R. (2016). Influence of combined mechanical treatments on the morphology and structure of cellulose nanofibrils: Thermal and mechanical properties of the resulting films. *Industrial Crops and Products*, 85:1-10.
- Vidal, P.F. and Molinier, J. (1988). Ozonolysis of lignins improvement of in vitro digestibility of poplar sawdust. *Biomass*, 16:1-17.
- Voronova, M.I., Zakharov, A.G., Kuznetsov, O.Y. (2012). The effect of drying technique of nanocellulose dispersions on properties of dried materials. *Materials Letters*, 68:164-167.
- Vrije, T., Haas, G.G., Tan, G.G., Keijzers, E.R.P. and Claassen, P.A.M. (2002). *International Journal of Hydrogen Energy*, 27:1381-1390.
- Wågberg, L., Decher, G., Norgren, M., Lindström, T., Ankerfors, M. and Axnas, K. (2008). The build-up of polyelectrolyte multilayers of microfibrillated cellulose and cationic polyelectrolytes. *Langmuir*, 24:784-795.
- Wahyundiono; Kanetake, T., Sasaki, M. and Goto, M. (2007). Decomposition of a lignin model compound under hydrothermal conditions. *Chemical Engineering Technology*, 30:1113-1122.
- Wang, B., Sain, M. and Oksman, K. (2007). Study of structural morphology of hemp fiber from the micro to the nanoscale. *Applied Composite Materials*, 14:89-103.
- Wang, H., Wang, J., Fang, Z., Wang, X. and Bu, H. (2010). Enhanced bio-hydrogen production by anaerobic fermentation of apple pomace with enzyme hydrolysis. *International Journal of Hydrogen Energy*, 35:8303-8309.
- Wang, H., Zhang, X., Jiang, Z., Yu, Z. and Yu, Y. (2016). Isolating nanocellulose fibrils from bamboo parenchymal cells with high intensity ultrasonication. *Holzforschung*, 70:401-409.
- Wang, S. Q. and Cheng, Q. Z. (2009). A novel process to isolate fibrils from cellulose fibers by high-intensity ultrasonication, Part 1: Process optimization. *Journal of Applied Polymer Science*, 113:1270-1275.
- Watanabe, M., Sato, T., Inomata, H., Smith, R.L., Arai, K., Kruse, A. and Dinjus, E. (2004). Chemical reactions of C(1) compounds in near-critical and supercritical water. *Chemical Reviews*, 104:5803-5821.
- Weil, J.R., Sarikaya, A. and Rau, S.L. (1997). Pretreatment of yellow poplar sawdust by pressure cooking in water. *Applied Biochemistry and Biotechnology*, 68:21-40.
- Weingartner, H. and Franck, E.U. (2005). Supercritical water as a solvent. *Angewandte Chemie International Edition*, 44:2672-2692.

Weiqi, W., Shubin, W. and Ligu, L. (2013). Combination of liquid hot water pretreatment and wet disk milling to improve the efficiency of the enzymatic hydrolysis of eucalyptus. *Bioresource Technology*, 128:725-730.

Wyman, C.E., Dale, B.E., Elander, R.T., Holtzapple, M., Ladisch, and Lee, Y.Y. (2005). Coordinated development of leading biomass pretreatment technologies. *Bioresource Technology*, 96:1959-1966.

Xiao, B., Sun X. F. and Sun, R. (2001). Chemical, structural, and thermal characterizations of alkali-soluble lignins and hemicelluloses, and cellulose from maize stems, rye straw, and rice straw. *Polymer Degradation and Stabilization*, 74:307-319.

Xu, J., Thomsen, M.H., Thomsen, A.B. (2009). Pretreatment on corn stover with low concentration of formic acid. *Journal of Microbiology and Biotechnology*, 19:845-850.

Yamamoto, H. and Horii, F. (1993). CP MAS C-13 NMR analysis of the crystal transformation induced for valonia cellulose by annealing at high-temperatures. *Macromolecules*, 26:1313-7.

Yamamoto, H, Horii, F. and Odani, H. (1989). Structural-changes of native cellulose crystals induced by annealing in aqueous alkaline and acidic solutions at hightemperatures. *Macromolecules*, 22:4130-2.

Yang, H., Yan, R., Chen, H., Lee, D. H. and Zheng, C. (2007). Characteristics of hemicellulose, cellulose, and lignin pyrolysis. *Fuel*, 86:1781-1788.

Yang, H.P., Yan, R., Chen, H.P., Zhen, C.G., Lee, D.H. and Liang, D.T. (2006). In-depth investigation of biomass pyrolysis based on three major components: hemicellulose, cellulose and lignin. *Energy and Fuels*, 20:388-393.

Yano, H. and Nakahara, S. (2004). Bio-composites produced from plant microfiber bundles with a nanometer unit web-like network. *Journal of Material Science*, 39:1635-1638.

Yano, H., Sugiyama, J., Nakagaito, A. N., Nogi, M., Matsuura, T., Hikita, M. and Handa, K. (2005). Optically transparent composites reinforced with networks of bacterial nanofibers. *Advanced Materials*, 17:153-155.

Yiying, Y., Han, J., Han, G., Zhang, Q., French, A.D. and Wu, Q. (2015). Characterization of cellulose I/II hybrid fibers isolated from energy cane bagasse during the delignification process: Morphology, crystallinity and percentage estimation. *Carbohydrate Polymers*, 133:438-447.

Yousefi, H. (2009). Canola straw as a bio-waste resource for medium density fiberboard (MDF) manufacture. *Waste Management*, 29:2644-2648.

- Yu, Q., Zhuang, X., Yuan, Z., Qi, W., Wang, W., Wang, Q. and Tan, X. (2013). Pretreatment of sugarcane bagasse with liquid hot water and aqueous ammonia. *Bioresource Technology*, 144:210-215.
- Zhang, J., Song, H., Lin, L., Zhuang, J., Pang, C. and Liu, S. (2012). Microfibrillated cellulose from bamboo pulp and its properties. *Biomass and Bioenergy*, 39:78-83.
- Zhang, Y.H.P., Ding, S.Y., Mielenz, J.R., Cui, J.B., Elander, R.T. and Laser, M. (2007). Fractionating recalcitrant lignocellulose at modest reaction conditions. *Biotechnology and Bioengineering*, 97:214-223.
- Zheng, Y., Pan, Z. and Zhang, R. (2009). Overview of biomass pretreatment for cellulosic ethanol production. *International Journal of Agricultural and Biological Engineering*, 2:51-68.
- Zimbardi, F. and Viola, E. (2007). Acid impregnation and steam explosion of corn stover in batch processes. *Industrial Crops and Products*, 26:195-206.
- Zimmerman, T., Pohler, E. and Geiger, T. (2004). Cellulose fibrils for polymer reinforcement. *Advanced Engineering Materials*, 6:754-761.
- Zimmermann, T., Bordeanu, N. and Strub, E. (2010). Properties of nanofibrillated cellulose from different raw materials and its reinforcement potential. *Carbohydrate Polymers*, 79:1086-1093.
- Zuluaga, R., Putaux, J. L., Cruz, J., Velez, J., Mondragon, I. and Ganan, P. (2009). Cellulose microfibrils from banana rachis: effect of alkaline treatments on structural and morphological features. *Carbohydrate Polymers*, 76:51-59.

## APPENDIX A

**Figure A.1.** Flow chart for experimental design of Chapter 3.

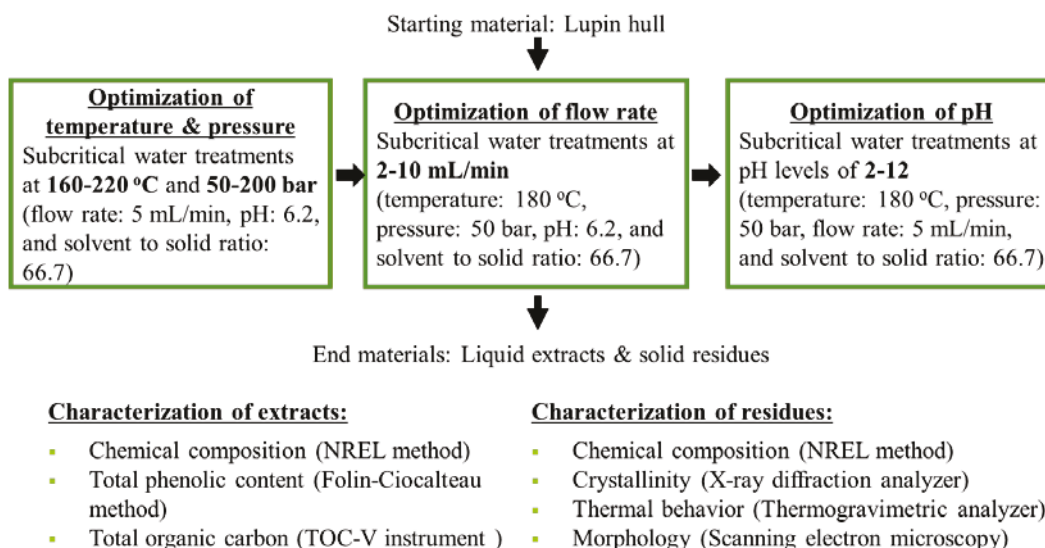


**Table A.1.** Effect of temperature and pressure on total hemicellulosic sugar yield (sum of xylose, galactose, arabinose, and mannose) in the extracts (5 mL/min and pH 6.2).

| Temperature (°C) | Pressure (bar) |          |          |          |
|------------------|----------------|----------|----------|----------|
|                  | 50             | 100      | 150      | 200      |
| 160              | 64.0±1.2       | 63.9±1.6 | 64.2±0.7 | 60.8±3.9 |
| 180              | 85.5±2.3       | 84.4±3.2 | 85.3±1.1 | 81.5±1.8 |
| 200              | 79.5±0.9       | 79.2±2.4 | 79.5±1.7 | 76.5±3.7 |
| 220              | 72.9±0.5       | 73.0±0.4 | 72.9±2.2 | 70.7±3.4 |

**Table A.2.** Effect of flow rate on total hemicellulosic sugar yield (sum of xylose, galactose, arabinose, and mannose) in the extracts (180 °C, 50 bar, and pH 6.2).

| Flow rate (ml/min) | Yield (%) |
|--------------------|-----------|
| 2.5                | 81.3±3.1  |
| 5.0                | 85.5±2.3  |
| 7.5                | 79.4±0.9  |
| 10.0               | 78.4±1.4  |

**Table A.3.** Effect of pH on total hemicellulosic sugar yield (sum of xylose, galactose, arabinose, and mannose) in the extracts (180 °C, 50 bar, 5 mL/min).

| pH   | Yield (%) |
|------|-----------|
| 2.6  | 84.5±0.6  |
| 6.2  | 85.5±2.3  |
| 8.5  | 80.7±1.1  |
| 11.7 | 79.2±0.4  |

**Table A.4.** Effect of temperature on cellulose and lignin contents of the solid residues (50 bar, 5 mL/min, and pH 6.2).

| Temperature (°C) | Cellulose (wt.%) | Lignin (wt.%) |
|------------------|------------------|---------------|
| 160              | 61.4±4.7         | 25.6±2.1      |
| 180              | 78.8±5.6         | 15.4±1.3      |
| 200              | 84.6±2.5         | 11.4±1.9      |
| 220              | 86.8±3.2         | 5.7±1.4       |

**Table A.5.** Effect of flow rate on cellulose and lignin contents of the solid residues (180 °C, 50 bar, and pH 6.2).

| <b>Flow rate (ml/min)</b> | <b>Cellulose (wt.%)</b> | <b>Lignin (wt.%)</b> |
|---------------------------|-------------------------|----------------------|
| 2.5                       | 75.3±4.9                | 14.0±1.4             |
| 5.0                       | 78.8±5.1                | 15.4±1.3             |
| 7.5                       | 74.1±3.9                | 11.6±1.1             |
| 10.0                      | 70.2±2.7                | 9.5±1.5              |

**Table A.6.** Effect of pH on cellulose and lignin contents of the solid residues (180 °C, 50 bar, and 5 mL/min).

| <b>pH</b> | <b>Cellulose (wt.%)</b> | <b>Lignin (wt.%)</b> |
|-----------|-------------------------|----------------------|
| 2.6       | 76.5±4.2                | 13.9±1.1             |
| 6.2       | 78.8±3.8                | 15.4±1.5             |
| 8.5       | 72.3±2.6                | 13.4±1.4             |
| 11.7      | 70.6±3.6                | 11.5±1.1             |

**Table A.7.** Effect of temperature and pressure on total phenolic content of lupin hulls.

| Temperature<br>(°C) | Pressure (bar) |                           |                           |            |
|---------------------|----------------|---------------------------|---------------------------|------------|
|                     | 50             | 100                       | 150                       | 200        |
| 160                 | 0.08±0.011     | 0.30±0.014                | 0.51±2.711e <sup>-4</sup> | 0.68±0.018 |
| 180                 | 0.08±0.014     | 0.37±0.010                | 0.50±0.014                | 0.69±0.015 |
| 200                 | 0.06±0.019     | 0.34±5.693e <sup>-3</sup> | 0.55±0.011                | 0.65±0.036 |
| 220                 | 0.07±0.017     | 0.35±2.711e <sup>-4</sup> | 0.55±0.025                | 0.72±0.010 |

## APPENDIX B

**Figure B.1.** Flow chart for experimental design of Chapter 4.

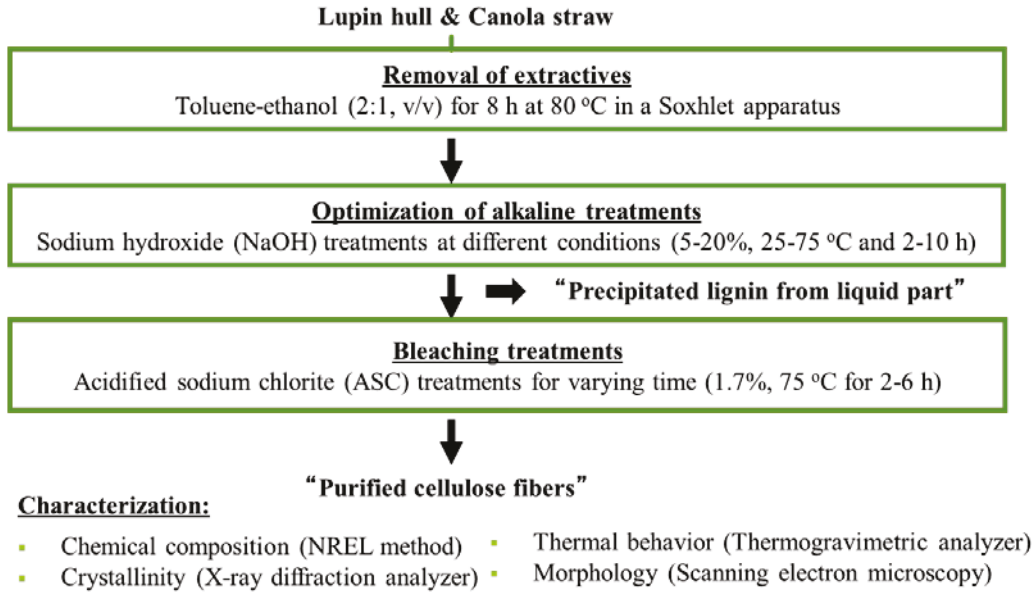


**Table B.1.** Effect of NaOH concentration and temperature on hemicellulose and lignin removal of (a, b) lupin hull, and (c, d) canola straw.

a)

| Temperature<br>(°C) | NaOH (%) |      |      |      |
|---------------------|----------|------|------|------|
|                     | 5        | 10   | 15   | 20   |
| 25                  | 28±3     | 60±5 | 74±3 | 74±4 |
| 50                  | 40±5     | 64±3 | 78±3 | 78±2 |
| 75                  | 56±5     | 70±3 | 80±6 | 81±4 |

b)

| Temperature<br>(°C) | NaOH (%) |      |      |      |
|---------------------|----------|------|------|------|
|                     | 5        | 10   | 15   | 20   |
| 25                  | 26±4     | 41±3 | 51±3 | 52±5 |
| 50                  | 31±4     | 45±5 | 55±2 | 55±3 |
| 75                  | 37±5     | 49±4 | 58±2 | 59±2 |

c)

| Temperature<br>(°C) | NaOH (%) |      |      |      |
|---------------------|----------|------|------|------|
|                     | 5        | 10   | 15   | 20   |
| 25                  | 30±9     | 52±3 | 65±2 | 65±2 |
| 50                  | 39±5     | 55±4 | 66±3 | 68±4 |
| 75                  | 48±5     | 58±4 | 71±4 | 71±3 |

d)

| Temperature<br>(°C) | NaOH (%) |      |      |      |
|---------------------|----------|------|------|------|
|                     | 5        | 10   | 15   | 20   |
| 25                  | 26±3     | 39±3 | 52±2 | 54±3 |
| 50                  | 30±1     | 43±2 | 53±4 | 57±2 |
| 75                  | 37±4     | 47±2 | 57±3 | 60±3 |

**Table B.2.** Effect of acidified sodium chlorite treatment (1.7%/75 °C) time (2, 4 and 6 h) on cellulose, hemicellulose, and lignin recovery of (a) lupin hull and (b) canola straw treated at optimum NaOH conditions (15% NaOH/99 °C/6h).

a)

| <b>Biomass fraction (wt.%)</b> | <b>Time (h)</b> |          |              |
|--------------------------------|-----------------|----------|--------------|
|                                | <b>2</b>        | <b>4</b> | <b>6</b>     |
| Cellulose                      | 94±2            | 94±2     | 87±1         |
| Hemicellulose                  | 12±1            | 8±1      | Not detected |
| Lignin                         | 17±1            | 9±0      | 5±0          |

b)

| <b>Biomass fraction (wt.%)</b> | <b>Time (h)</b> |          |          |
|--------------------------------|-----------------|----------|----------|
|                                | <b>2</b>        | <b>4</b> | <b>6</b> |
| Cellulose                      | 93±2            | 93±2     | 92±2     |
| Hemicellulose                  | 21±1            | 20±2     | 19±2     |
| Lignin                         | 23±1            | 18±1     | 16±1     |

## APPENDIX C

**Figure C.1.** Flow chart for experimental design of Chapter 5.

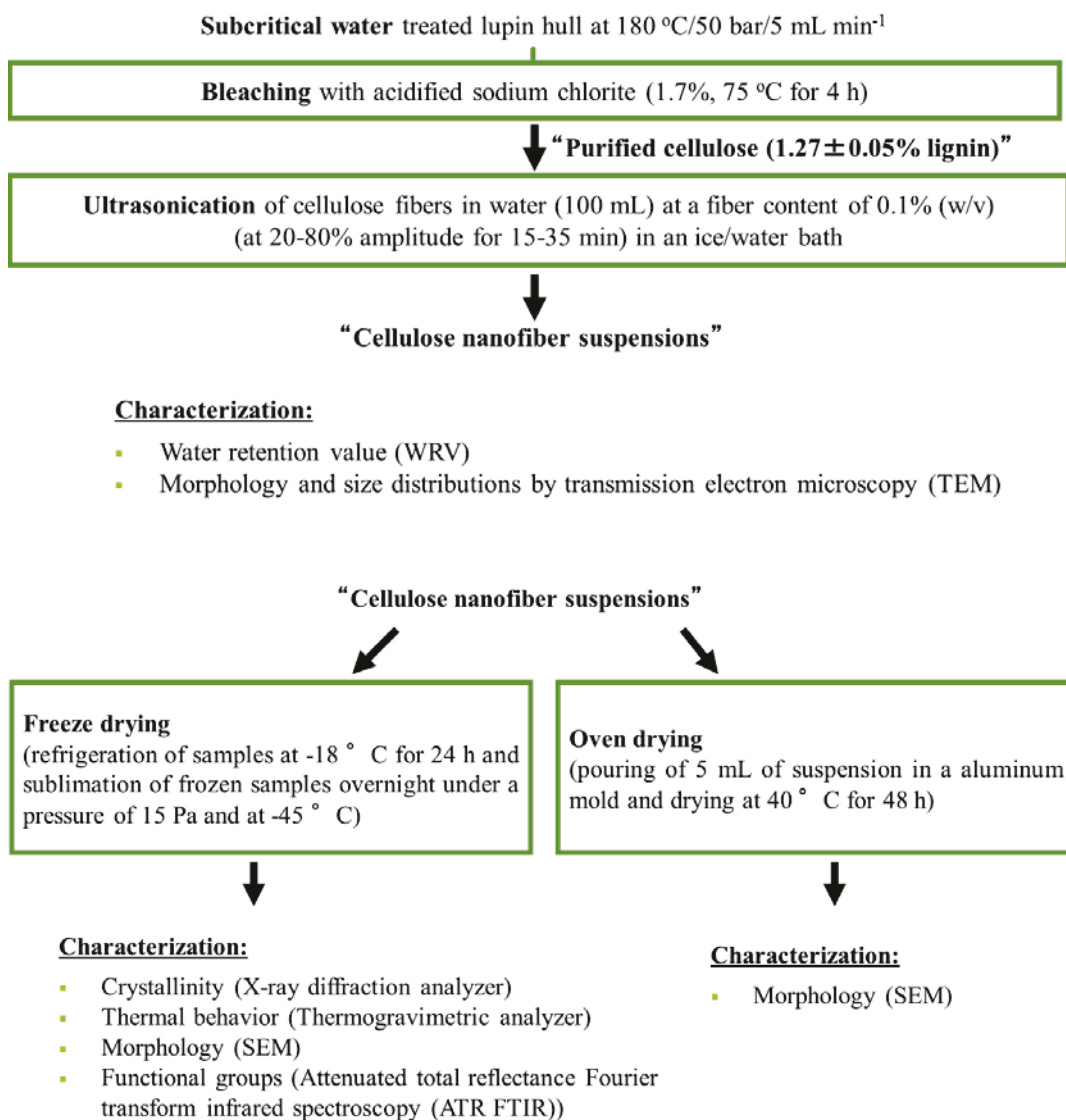


**Table C.1.** Water retention value (WRV) of untreated and ultrasonicated lupin hull cellulose at different amplitudes (20, 50 and 80%) for varying time (15, 25 and 35 min).

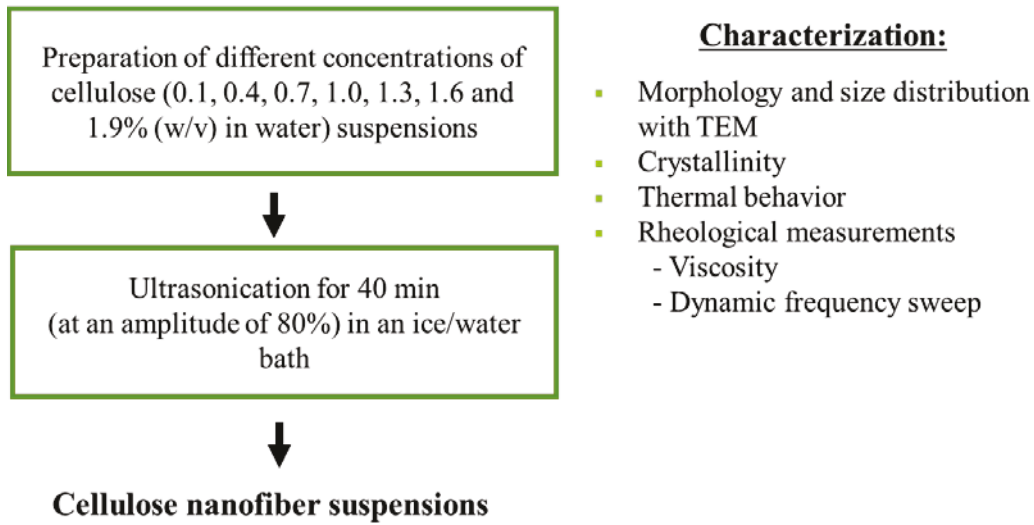
| <b>Amplitude (%)</b> | <b>Time (min)</b> | <b>WRV (%)</b> |
|----------------------|-------------------|----------------|
| 0                    | 0                 | 157±3          |
| 30                   | 15                | 161±3          |
| 30                   | 25                | 166±2          |
| 30                   | 35                | 167±3          |
| 60                   | 15                | 194±3          |
| 60                   | 25                | 246±2          |
| 60                   | 35                | 263±1          |
| 90                   | 15                | 207±2          |
| 90                   | 25                | 287±1          |
| 90                   | 35                | 305±5          |

**Table C.2.** Effect of water retention value (WRV) on average cellulose nanofiber diameter.

| <b>Amplitude (%)</b> | <b>Time (min)</b> | <b>WRV (%)</b> | <b>Average diameter (nm)</b> |
|----------------------|-------------------|----------------|------------------------------|
| 60                   | 35                | 246±1          | 46                           |
| 90                   | 15                | 263±2          | 32                           |
| 90                   | 25                | 287±1          | 19                           |
| 90                   | 35                | 305±5          | 15                           |

## APPENDIX D

**Figure D.1.** Flow chart for experimental design of Chapter 6.



## APPENDIX E

**Figure E.1.** Flow chart for experimental design of Chapter 7.

